NASA CONTRACTOR REPORT

NASA CR-370

AN ACOUSTICAL STUDY OF THE KIWI B NUCLEAR ROCKET

by J. Kenneth Manhart, C. M. Ailman, S. R. Lane, and A. H. Marsh

Prepared under Contract No. NASw-596 *by*
DOUGLAS MISSILE & SPACE SYSTEMS DIVISION
Santa Monica, Calif.
for

NATIONAL AERONAUTICS AND SPACE ADMINISTRATION • WASHINGTON, D. C. • JANUARY 1966

NASA CR-370

AN ACOUSTICAL STUDY OF THE KIWI B NUCLEAR ROCKET

By J. Kenneth Manhart, C. M. Ailman,
S. R. Lane, and A. H. Marsh

Prepared under Contract No. NASw-596 by
DOUGLAS MISSILE & SPACE SYSTEMS DIVISION
Santa Monica, Calif.

for

NATIONAL AERONAUTICS AND SPACE ADMINISTRATION

For sale by the Clearinghouse for Federal Scientific and Technical Information
Springfield, Virginia 22151 – Price $4.00

ACKNOWLEDGEMENT

The acoustical research reported in this document was partially supported by the Atomic Energy Commission through the joint AEC-NASA Space Nuclear Propulsion Office in Germantown, Maryland; and by the United States Air Force, Biodynamics and Bionics Division, Biophysics Laboratory, 6570th Aerospace Medical Research Laboratories, Wright Patterson Air Force Base, Ohio.

CONTENTS

Page

AN ACOUSTICAL STUDY OF THE KIWI B NUCLEAR ROCKET

By J. Kenneth Manhart, C. M. Ailman,
S. R. Lane, and A. H. Marsh

SUMMARY

Sound pressures generated by the exhaust of the KIWI B nuclear rocket engine have been measured and the data analyzed. The characteristics of the radiated sound field that were identified include the:

- Distribution of sound pressures with frequency
- Distribution of radiated sound power with frequency and total radiated sound power
- Directivity characteristics
- Conversion efficiency of exhaust mechanical stream power to sound power
- Space-time correlation of sound pressures in the near field
- Probability distribution of instantaneous peak pressures.

These characteristics have been related to the flow parameters of the KIWI B exhaust and, where relevant, to acoustical data and flow parameters of chemical rocket engines.

A new method of normalizing the sound power spectra is introduced because the conventional methods did not satisfactorily relate the acoustical data from the KIWI B and chemical rocket engines. On the basis of two data sets from power runs of the KIWI B reactor, the acoustical conversion efficiency of the KIWI B exhaust is shown to be lower than for chemical rockets. In the near-field, the distribution of instantaneous peak pressures was found to be approximately Gaussian.

In addition, the response of simple structures to the KIWI B sound field was studied. Comparisons of measured and analytically derived response were made.

INTRODUCTION

This study resulted from an unsolicited proposal directed to the National Aeronautics and Space Administration on 17 April 1962. The duration of the study was 21 months and commenced on 1 March 1963. The study was funded jointly by the National Aeronautics and Space Administration, the Atomic Energy Commission and the United States Air Force.

Prior to submitting the proposal, a Douglas-funded acoustical study of the KIWI A-3 reactor revealed the following problems peculiar to the measurement of sound pressure levels around a nuclear reactor, see ref. 1: (a) the need for reliable remote operation, (b) nuclear radiation effects on instrumentation microphones (ref. 2), and the importance of working the acoustical activities into the precise schedule of the reactor operations. The results of these qualification tests were incorporated into the Douglas proposal to perform a large-scale acoustical study of the KIWI B nuclear rocket. The earlier efforts were essential to make a suitable selection of instrumentation and a reasonably good estimate of the scope of the effort required.

Objectives of the Investigation

The purpose of the study was to conduct an experimental and analytical scientific investigation of the acoustical characteristics of the KIWI B nuclear rocket engine. The initial objectives were to:

- Define the acoustic field radiated by the jet exhaust of a propulsive type of nuclear engine and assess the contribution of the noise field generated by burning hydrogen
- Relate the data analytically to the flow parameters of the KIWI B and to other acoustical data from turbojets and chemical rockets
- Modify the current methods, where necessary, for predicting the sound pressure levels in the acoustic near- far-field of a nuclear engine
- Investigate experimentally and analytically the relation of acoustic loading and the dynamic response of a simple flat test panel in the acoustic near-field of the reactor.

In July 1964, the initial objectives of the study were supplemented to obtain additional engineering data that would be useful for design applications. Authorization was received to acquire more near-field acoustical and structural response data and to make space-time correlation plots for two locations in the near-field.

The principal activities of the study were divided into the following phases:

- The design, fabrication, installation, and calibration of acoustical and vibration data acquisition systems at the Nuclear Reactor Development Station (NRDS), Nevada Test Site (NTS), Mercury, Nevada
- Participation in experimental KIWI B test activities in cooperation with personnel of the Los Alamos Scientific Laboratories (LASL)
- Conduct of data reduction and analysis
- Reporting and liaison.

Uniqueness of the Study

During the last decade, there has been a significant quantity of acoustical data acquired from measurements of turbojet and chemical rocket engine exhausts. For the most part, with the exception of some model studies, the exhaust gases from these sources had comparable molecular weights and the range of velocities and temperatures has been within a factor of 2 or 3. The data have been generalized, and empirically derived constants were evolved that have been used for predictive purposes.

The exhaust of the KIWI B nuclear rocket is directed upwards and is an uncooled, unreflected, freely expanding supersonic flow of hydrogen with an exhaust velocity of approximately 20 000 feet per second and a molecular weight of 2. The operation of this rocket engine offered the opportunity to obtain new and unique acoustical data that cannot be obtained from any other existing source. It was anticipated that the data would extend our present knowledge of the dependence of many characteristics of a radiated sound field on the exhaust flow parameters and could modify or tend to confirm existing theories or hypotheses which are used to define the sound field radiated from a jet source.

The nominal performance figures for the KIWI B reactor studied here are: 1000 megawatts of thermal power, or approximately 50 000 pounds of thrust with a specific impulse of 700 lb/lb/sec.

SYMBOLS AND SPECIAL TERMINOLOGY

Some of the terminology used in this study requires definition. We refer to terms used in Los Alamos reactor operations and, consequently, adopted for this report. A brief explanation of the terms and their meaning follows.

Hot Firing or Power Run.- A flow of propellant to which heat is transferred as it passes through the core while it is critical.

Cold Flow Test (CFT).- A flow of propellant that has no heat transferred to it as it passes through an unloaded* or non-radioactive core.

Simulated Nozzle Test.- In this type of test, the propellant does not flow through the reactor core, but instead flows into a manifold which is installed on the nozzle attachment flange downstream of the exit plenum. See Fig. 1. The propellant exhausts upwards through a small hole in a flat plate. A simulated nozzle test is used when the objective is to check out some part of the propellant transfer system that does not involve the reactor core. The orifice diameter was 2.910 inches for liquid flows and 1.840 inches for gaseous flows.

Engineering Plan (EP).- An Engineering Plan consists of a series of gas or liquid flows which have common test objectives. A single gas flow could be considered a test, but it is subordinated to an overall objective that an

*No uranium, but with a geometrically similar graphite configuration.

Engineering Plan was designed to achieve. Frequently, an Engineering Plan had a duration of two weeks.

Dewar.- A cryogenic, vacuum insulated tank to store liquid hydrogen (LH_2).

The symbols used in this report are defined as they are introduced.

DESCRIPTION OF ACOUSTICAL TEST FACILITIES

Description of the Test Site

The field work for this study was performed at the Nuclear Reactor Development Station (NRDS) at the Nevada Test Site (NTS). The isolated station, located at Jackass Flats, Nevada, about 90 miles northwest of Las Vegas, is the facilities center for ground tests of all nuclear reactors, engines, and stages that will be used in this nation's space program.

The topography of the test site is typical of the southern Nevada desert. The NRDS facilities lie in a desert valley at an altitude of 3800 feet and, generally, have a very low relative humidity, varying between 6 and 15 per cent during the summer months. The reactor tests are conducted during daylight hours when the wind speeds are between 5 and 15 knots.

All of the field activities for this study were conducted at Test Cell C (Fig. 2). A remotely-controlled electric locomotive moves the reactor to and from the test cell. The reactor is oriented in a non-flyable nozzle-up position (hence the designation KIWI). This convenient orientation has many operational advantages and minimizes radiation and explosive hazards. The reactor is enclosed in the sheet metal shed shown to the right of the picture. This shed, which provides a secure area when all final adjustments to the reactor have been made, is mounted on railroad tracks. In the morning of the day for reactor operations the shed is withdrawn and all personnel vacate the test cell. Because of the hazards from high radiation levels, the entire reactor operation is controlled and monitored at the control point 2 miles distant, and the test cell and surrounding area is closed to personnel during the test. This situation requires a very reliable remote control for the acoustical data acquisition system.

Tower and Balloon Microphone Installation

Since the exhaust of the KIWI B nuclear rocket is directed upward, the measurement of sound pressures necessary to define the radiated sound field required a tall vertical array of microphones so that the directivity characteristics and radiated sound power could be determined accurately.

The towers and a balloon were used to support the microphone arrays. The location of the towers and balloon relative to the reactor at Test Cell C may be seen in Figs.2 and 3. The short tower is 120 feet high and placed 100 feet from the reactor. With this tower, near-field data could be obtained up to 100 feet above the exit plane of the nozzle which was 20 feet above the concrete pad. The tall tower is 420 feet high and located 260 feet (approximately

100 nozzle diameters) from the reactor. This tower was used to support microphones measuring sound pressure levels which were estimated to be in the far-field. However, since the KIWI B exhaust had such a high velocity, implying either an extended region of sound power generation or a localized source very far downstream, it was not certain that the source would appear as a point source to the microphones on the 420-foot tower. Thus, to determine whether the 420-foot tower was in the acoustic far-field (at all frequencies) the 10 000 cubic foot helium filled balloon was used during EP IV to support the third array of microphones. The balloon was flown to a height of 600 feet and the cable was anchored at a point 520 feet from the reactor (twice the distance of the 420-foot tower). Spherical divergence (6 dB loss in pressure with doubling the distance) between comparable points on the two microphone arrays was to be the criterion to conclude whether the 420-foot tower was in the far-field.

A channel and trolley assembly was installed on each tower on the side facing the reactor to guide the array of microphones while they were raised or lowered. This arrangement allowed all pre- and post-calibrations to be made at ground level. Fig. 4 shows the channel on the 420-foot tower.

Instrumentation

A discussion of the instrumentation system that was used is presented in Appendix A. Details are given on the nuclear radiation tests on equipment, and a description is given of the microphone and accelerometer signal and power circuits.

Microphone System.- The selection of microphones for the KIWI B acoustical study was based on an evaluation of their performance in a nuclear radiation field and consideration of their technical specifications. The microphones were mounted on microphone distribution boxes which, in turn, were bolted to trolleys that were supported in the channel by a flexible steel cable as shown in Fig. 5. The microphones on the towers and the concrete pad were positioned horizontally so that the sound radiating from any point along the jet exhaust would strike the microphone diaphragm at grazing incidence. Thus, corrections for microphone directional characteristics were negligible. Nose cones were used on all microphones.

Both electrical calibrations, to measure frequency response, and acoustical calibrations, to establish a sensitivity reference level, were made on all microphone channels before and after each test except that post-calibrations could not be made on the microphones used for the balloon array. The electrical calibrations were recorded on tape by applying 1 volt to the cathode followers at the frequencies designated in Table I. The acoustical calibrations were made by placing a Pistonphone over the microphone cartridge and applying a known sound pressure level to the diaphragm (124 dB less the correction for barometric pressure). The sensitivity, frequency response, and location for each microphone installed for the tests reported here are listed in Tables II through V.

At the beginning and conclusion of the study, the microphone cartridges that remained undamaged, or that were not radioactive, had their pressure

frequency response measured using an electrostatic actuator. The sensitivity of the cartridges was also checked and found to be unchanged.

Accelerometer System.- Measurements were made of the vibratory response of three structures: the external shell of the LH_2 Dewar nearest the reactor, and two flat rectangular panels placed 30 feet and 130 feet from the reactor. An analysis of the vibration data from the accelerometers mounted on the Dewar and the panels is given in the section of Structural Studies.

The Dewar shell response was measured with an Endevco Model 2215C. A microdot cable, wrapped with aluminum foil, connected the accelerometer to a battery powered transistorized charge amplifier which was protected from nuclear and thermal radiation by a thick concrete wall.

The flat rectangular panels were much closer to the reactor, and radiation resistant Statham strain gage accelerometers, Model TC A514, were used. The responses of the Dewar and panel are discussed in the section on Structural Studies and the location of the accelerometers are shown below.

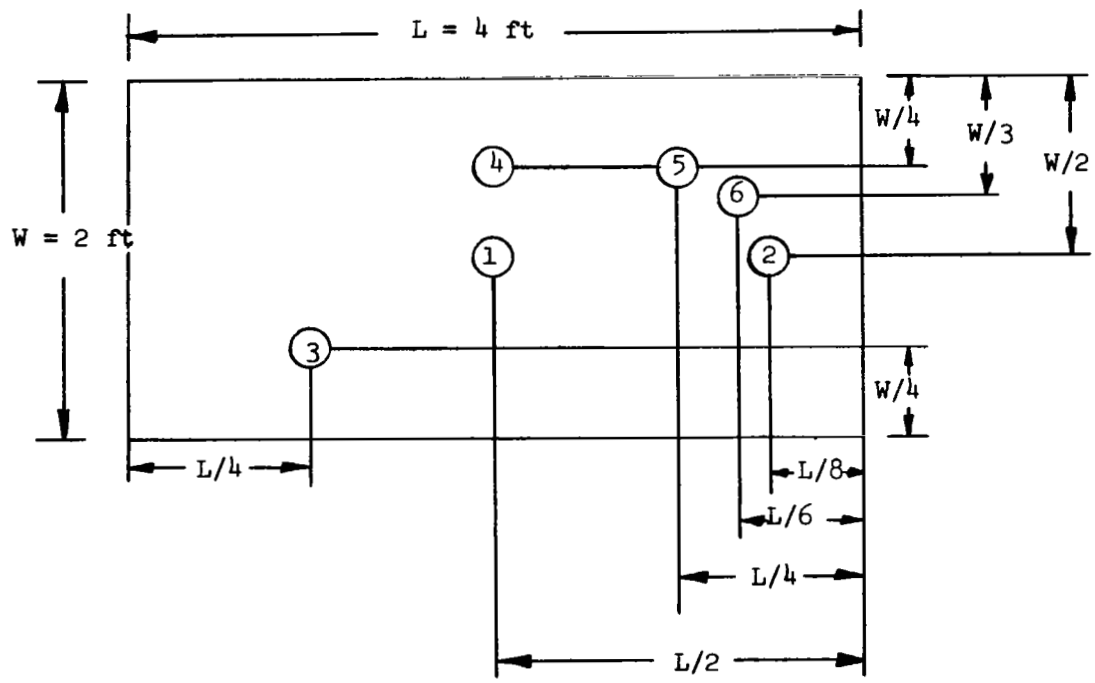

Recording System.- The tape recorders used during this study were:

Ampex CP-100's in the direct and FM record modes
Ampex PR-10's in the direct record mode.

The performance characteristics of the units are listed below.

Model	Record Mode	Tape Speed	Frequency Response	Signal to Noise
Ampex CP-100	FM	30 ips	20 cps - 10 kc*	44 dB
Ampex CP-100	Direct	30 ips	200-25 000* cps	30 dB
Ampex PR-10	Direct	7 1/2 ips	40-20 000* cps	50 dB

ips = inches per second

* = frequency range used in the study

The tape recorders were operated simultaneously by remote control in the basement of the Command Post, 2 miles distant. A remotely controlled television camera was installed in the basement of Test Cell C to provide a view of the equipment rack (which contained 14 monitor oscilloscopes and the plate and filament power supplies for the microphones) and the tape recorders. See Fig. 6. In addition, two audio channels were used to monitor the recorded signal at the remote control point. Thus, both visual and aural methods were available to monitor the status of the equipment and the signal during the power run. The monitor facility gave a means of estimating signal level during the recording and was helpful in determining whether to continue to record or to stop and wait for a "hold" that would allow re-entry to the test cell, or to wait for a later flow.

Playback System.- The data reduction systems used in the study are indicated in Fig. 7. The oscillograph was used to make visual examination of the data, and the Sanborn system was used to make time history plots (either overall or in one-third octave bands). The B & K system employed a tape loop (usually 10 seconds long) that was selected from the most stable portion of the full power run. This reduction resulted in overall SPL's and 1/1 or 1/3 octave band plots of SPL. All SPL's are referenced to 0.0002 dynes/cm^2.

PERSONNEL INVOLVED IN THE STUDY

The Project Manager of the study was Mr. J. K. Manhart. He was responsible for coordinating the study requirements with NASA and Los Alamos personnel and for assigning and reviewing the technical work undertaken by Douglas personnel.

Four engineers from Douglas contributed greatly to the study: Mr. Carroll M. Ailman, Mr. James E. Apple, Mr. Samuel R. Lane and Mr. Alan H. Marsh. Mr. Ailman was responsible for much of the analytical analysis and for the panel response and correlation studies that could be accommodated within the authorization of this contract. Mr. Lane was responsible for most of the data reduction and analysis and for an excellent study of the flow conditions of the KIWI B nozzle. Mr. Apple was responsible for the instrumentation and the field operations. Mr. Marsh was responsible to the Project Manager for special studies and acted as a consultant whose trenchant criticisms were highly valued.

Professor Alan Powell, Engineering Department, University of California, Los Angeles* was used as a consultant throughout this study. He participated actively in group discussions and offered valuable technical guidance.

Several oral reviews were also held with Mr. Harvey H. Hubbard, who was the NASA Technical Monitor for the study, and Mr. John N. Cole, of the Wright-Patterson Air Force Base.

Dr. Keith Boyer of the Los Alamos Scientific Laboratories, and Director of the KIWI B Nuclear Engine Development, was instrumental in having the acoustical study approved. The total support that he and his staff gave to Douglas at the test site was in a large measure responsible for the satisfactory accomplishment of the study objectives.

COMPARISON OF SOLID CORE NUCLEAR AND CHEMICAL ROCKET ENGINES

Understanding the need for making an acoustical study of the KIWI B solid core nuclear rocket engine requires some knowledge of the basic differences between the nuclear and chemical-powered rockets. Primarily, these differences involve the method to generate and transfer heat energy to the propellant that is required to produce useful thrust.

The energy for a chemical rocket (either liquid or solid) is derived from combustion of a propellant and an oxidizer must be supplied. The burning of the propellant releases a large quantity of gas which is accelerated in the nozzle and exhausted to produce thrust. In contrast, the propellant for the nuclear rocket provides no intrinsic energy itself but, as it passes through the core, it is heated by the energy released during the controlled fission processes within the core of a nuclear reactor. The heated (but not burning) propellant is then exhausted through the nozzle in a similar manner as the chemical rocket, and ignited and burned externally during ground tests.

To maximize the thrust produced for a given weight flow of propellant, the propellant discharged from a nozzle must have as high an exhaust velocity as possible. This can be achieved best by using a low molecular weight propellant heated to a high temperature. The lightest molecule, pure hydrogen, is used in the nuclear rocket for these reasons. No consideration need be given to its combustion characteristics and no oxidizer is needed.

A schematic of a solid core nuclear rocket is given in Fig. 8. Its principal components are the reactor, which consists of a uranium-loaded graphite core, a neutron reflector, a pressure shell, a nozzle, and a propellant-feed turbopump which pumps the liquid hydrogen from a cryogenic vacuum-insulated storage tank (Dewar). The liquid hydrogen is pumped from the Dewar and ducted to the nozzle manifold through the double walls to regeneratively cool the nozzle and the reflector. The hydrogen next flows through the many tube-like passages of the

*Now with the David Taylor Model Basin, Washington, D.C.

reactor core where it is heated to a very high temperature and then accelerated through the nozzle to produce thrust. A hot-bleed cycle extracts a small amount of heated hydrogen to drive a turbine which, in turn, drives the liquid hydrogen turbopump.

Thus, in comparing the performance of nuclear rockets to chemical rockets, we see, for the nuclear rocket, that the exhaust velocity of the propellant is much higher and the molecular weight is much lower and, thus, the specific impulse is much greater than any chemical rocket can ever achieve. Also, the propellant is ignited and burned externally during tests in the atmosphere. Since so many characteristics of the radiated sound field are velocity and/or density dependent, a study of the noise generated by a nuclear rocket exhaust should contribute materially to studies of jet exhaust noise.

DISCUSSION OF THE EXPERIMENTAL ACCOMPLISHMENTS

The data presented in this study are from two power runs (EP IV and EP V) and four reactor cold flow tests. While every reasonable effort was made to obtain valid acoustical data, the study was conducted in the field as a secondary objective to the development of an operable reactor, and some restrictions of the acoustical study were necessary. With these limitations, the study will report on the:

- Design, installation, and operation of an instrumentation system to measure near- and far-field sound pressure levels (SPL's) generated by the KIWI B exhaust
- Description of the flow parameters of the KIWI B exhaust
- Calculation of the radiated sound power
- Distribution of sound sources along the jet
- Directional characteristics in the far-field as a function of frequency
- Relation of the acoustical characteristics to the flow parameters of the KIWI B exhaust and to other jet sources
- Calculation of the conversion efficiency from mechanical stream power to radiated sound power
- Estimation of the contribution of the noise generated by burning hydrogen to the radiated sound field
- Distribution of instantaneous peak pressures in the near-field.
- Space-time cross correlation characteristics of the acoustic near-field.

DATA REDUCTION

This section discusses the various data reduction techniques used during this study.

For each EP and the high flow test (one of the CF tests), two tapes were obtained from each tape recorder; one contained pre- and post-calibration signals, and the other the data signals. The calibration tape provided a means to determine the frequency response and sensitivity of each data analysis channel. Comparison of the pre- and post-calibrations, plus the qualification tests of the microphones and microphone boxes in an environment of nuclear radiation, gave some assurance that the sensitivity of the recording system did not change throughout the test. Thus, the frequency response, sensitivity, and stability were established for each data channel from the microphone to the meter or graphic level recorder of the data reduction system. The data reduction systems are shown in Fig. 7 and the techniques used are described below.

Visual Evaluation of the Data

Oscillograph traces were made of the overall signal versus time for each recorded channel so that data quality could be assessed. Such conditions as dropouts, electrical noise, overdriving (peak clipping), or system failure could be observed by examination of these traces.

Sound Power Levels

A computer program was used to obtain sound power levels from the sound pressure levels. The sound field was assumed to be hemispherical and symmetrical about the axis of the jet exhaust. The measured SPL's were corrected for distance to a hemisphere having a radius of 350 feet and centered at the nozzle.

The corrected SPL's are converted to an intensity which is multiplied by the area of the appropriate zone (see Appendix B) to give the sound power radiated through that zone. The total radiated sound power in watts is the sum of the power passing through all of the zones.

Power Spectral Density Plots

Some digital power spectral density (PSD) plots were made during the study. These plots indicate the amount of power in a 1 cycle per second band at any frequency within the limits of the system, and are useful for structural analyses. Each PSD was obtained by taking the Fourier transform of the autocorrelation of the pressure function (see correlation calculations section below for a description of the statistical time averaging technique--assuming the function to be both stationary and ergodic--by which the autocorrelation is calculated).

Hence, a PSD, or $\phi(\omega)$, is defined as

$$\phi(\omega) = \frac{1}{2\pi} \int_{-\infty}^{+\infty} \psi(t) e^{-j\omega t} dt$$

where $\psi(t)$ = the autocorrelation of the pressure function

and $j = \sqrt{-1}$

Reactor Data and Field Support

For each gas flow, LASL provided Douglas with strip charts showing time histories of such engine parameters as propellant flow rates, temperatures, pressures, flow profiles, etc. In addition, environmental data, timing signals, and photographic coverage were also obtained. Table VI lists the wind conditions, air temperature, and relative humidity for each test.

Vibration Data

The reduction of measured acceleration levels used both oscillograph display (to observe data quality) and digital PSD techniques as discussed above.

Correlation Calculations

The measured near-field acoustical data resulting from the firing of the KIWI B nuclear engine was processed digitally to provide space-time correlation information. The cross-correlation between two stationary random signals $f_1(t)$ and $f_2(t)$ is expressed as:

$$\psi_{12}(\tau) = \lim_{T \to \infty} \frac{1}{2T} \int_{-T}^{T} f_1(t) \cdot f_2(t + \tau) dt$$

Similarly, the auto-correlation for either of these two functions is:

$$\psi_{11}(\tau) = \lim_{T \to \infty} \frac{1}{2T} \int_{-T}^{T} f_1(t) \cdot f_1(t + \tau) dt$$

The computer program used to produce these ψ functions performs the following operations:

1. Delay the signal by a known time difference equal to τ (the lag time)

2. Multiply the amplitude of the two signals together and

3. Average the instantaneous amplitude products over the sampling time.

As the procedure is repeated for various values of τ, the cross-correlation values, as a function of time, result. By means of the following Fourier transform pairs, cross-power spectral densities of the two random signals are obtained:

$$\phi_{12}(\omega) = \frac{1}{2\pi} \int_{-\infty}^{\infty} \psi_{12}(\tau) e^{-j\omega\tau} d\tau \qquad \text{or conversely} \qquad \psi_{12}(\tau) = \int_{-\infty}^{\infty} \phi_{12}(\omega) e^{j\omega\tau} d\omega$$

In the KIWI B study, the cross-power spectral density (a complex number) is presented in terms of $\phi_{12}(\omega) = |\phi_{12}| e^{j\theta}$ where the absolute value of ϕ_{12} equals the square root of the sum of the squares of the real and imaginary parts $|\phi_{12}| = \left[Re_{12}^{\ 2} + I_{12}^{\ 2}\right]^{1/2}$ and θ is equal to the arc tangent of the ratio of the imaginary part over the real part (θ = arc tan I_{12}/Re_{12}).

Because the relative phase difference should be negligible between channels used to obtain correlation data, calibration signals at closely spaced frequency intervals (Table I) were applied simultaneously to channels intended for cross-correlation studies. The signal was applied directly to the cathode followers of each correlation group. Thus, the phase shift of the complete data acquisition and data reduction system could be measured. The phase shift of the 1/4-inch B and K microphone was not included in this calibration, but laboratory measurements show the phase shift of the cartridge below 2000 cps to be small. The results of the calibrations between channels used in cross-correlations in this study (while not ideal, i.e., zero phase shift at all frequencies), are considered tolerable for the accuracy involved here.

DISCUSSION OF EXHAUST FLOW VELOCITY

The KIWI B exhaust nozzle had a convergent-divergent optimized bell-shaped contour with a nominal expansion ratio (nozzle exit area to throat area) of 12. The area ratio selected compromised the most efficient expansion ratio to obtain adequate regenerative cooling of the nozzle throat. For a weight flow required for design thrust, the exhaust will be overexpanded (i.e., the static pressure at the exit is less than the ambient pressure of 12.7 psia at 3800 feet elevation).

On leaving the nozzle, the static pressure in the exhaust stream increases to a pressure approaching the ambient pressure and the flow velocity decreases accordingly. In the flow (downstream of the nozzle exit) where ambient pressure is reached, the flow velocity is designated V_{eq} (the equivalent velocity) and the thrust developed is the product of the mass flow ($\dot{w}/g$) and V_{eq}.

The mechanical power of the exhaust flow is obtained from the relation

$$\text{Mechanical Power } (W_m) = 0.678\ FV \text{ (watts)}$$

where V (the exhaust velocity) should be specified as V_{eq}, rather than V_{exit} (the velocity at the nozzle exit plane), since V_{eq} is proportional to the thrust F.

A value for V_{eq} was computed for each maximum stabilized gas flow. The data required for calculating V_{eq} were supplied by LASL, and included the gas flow rate, the plenum pressure and temperature data. This information is summarized in Table VII and the classified appendix to this report. These data were used with the standard equations for one-dimensional compressible flow to calculate flow parameters across the nozzle throat and the exit. In addition, since the flow conditions at the exit can be described in terms of one-dimensional and three-dimensional flow regions, the exit flow parameters for the three-dimensional condition were also calculated using estimates for the three-dimensional nozzle pressure ratio and nozzle wall separation pressure ratio supplied by the nozzle designer*. Thus, values for V_{eq} were calculated for both one-dimensional and three-dimensional flow conditions. The accuracy of the value of V_{eq}, based upon the flow data provided by LASL, is $\pm$ 10 percent.

A description of the method used to calculate equivalent exhaust velocities is given in Appendix C.

SUMMARY OF ACOUSTICAL TEST ACTIVITIES

Corrected acoustical data from EP's I, II, III, a special high-flow gas test, and EP's IV and V are presented in Tables Xa through Xj. The first three EP's were cold flows of gaseous nitrogen (GN_2), gaseous hydrogen (GH_2) and liquid hydrogen (LH_2) at various weight flows. The high flow test used gaseous hydrogen and gaseous helium (GHe). EP's IV and V used LH_2 as the propellant.

For EP's I, II and III, and the part-power holds of EP IV and V the gas flows generally were too low to calculate exit velocities accurately and, therefore, only a few direct comparisons can be made of the acoustical data. However, the acoustical data from the two hot tests (EP's IV and V) showed good repeatability for the full-power portion of the runs.

On 8 August 1963, simulated nozzle tests were conducted. See Fig. 1. On 21 August 1963, the propellant flowed through both an unloaded core and a nozzle. For these two 1963 tests, the propellant flows were programmed for stepped and/or ramp flow time histories as indicated below (only data from the

*Private communication from Mr. Stassinos of Rocketdyne.

two highest flows of the step or ramp profile were analyzed for acoustical data).

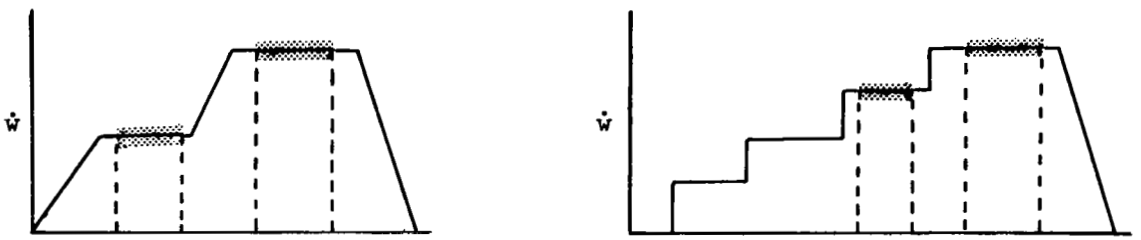

▒▒▒ Interval selected for data analysis

$\dot{w}$ = Propellant weight flow

t = Time

On 9 January 1964, LASL conducted a special gas flow for the acoustical study. The pressure shell and piping were modified to reduce flow resistance as much as possible to ensure maximum GH_2 and GHe gas flows through the nozzle. It was planned to have high flows of gaseous hydrogen with and without ignition downstream to provide data indicating the contribution of burning to the noise field. However, the flow of unburned hydrogen caused a severe vibration that affected all instrumentation channels, and spontaneous detonation of the exhaust occurred after approximately 8 seconds of flow. All instrumentation channels were disabled for that test.

Acoustical data were taken for all EP's , and vibration data were recorded for two of the tests. A tabulation of the pressure and acceleration sensors used during each test, and their identification, is given in Tables II to V (see Fig. 9 for geometrical location of each sensor). All measured data were corrected for recording-channel frequency response, attenuator settings, and data reduction filter corrections. The data also were averaged over short-time intervals during selected periods of the run where the data appeared to be stationary. Therefore, only corrected data are presented, and the sound pressure levels (in dB re 0.0002 dynes/cm^2) and acceleration levels are accurate for the designated positions in space for the flow conditions specified.

A summary of the acoustical activities is presented below and the measured SPL's are given in Table X.

EP or Test	Date	Flow Condition	Propellant	Flow Rate lb/sec	Gas Exit Velocity ft/sec	Thrust in lbs
I	8-8-63	Cold	GN_2/LH_2	85 & 69 / 35	Not Calculated	Not Calculated
II, III	8-21-63	Cold	GH_2/GN_2	24 / 43 & 52	Not Calculated	Not Calculated
High Flow Test	1-9-64	Cold	GH_2/GHe	100 / 130	7600 / 4950	16 600 / 12 400
IV	5-13-64	Hot	LH_2	69	20 600	38 300
V	8-28-64	Hot	LH_2	69	22 100	41 750

DISCUSSION OF MEASURED ACOUSTICAL DATA

Comparison of Gaseous Nitrogen Flows

Gaseous nitrogen was expelled through a simulated nozzle (EP-I) and the bell nozzle (EP-II) at comparable weight flows. Though it is difficult to calculate the two exhaust velocities or other flow parameters, the overall SPL's have been compared in Fig. 10. The overall SPL's from the simulated nozzles are slightly higher. The cause(s) of the difference(s) have not been established.

Comparison of Spectra from Helium and Hydrogen Cold Flow Tests

Fig. 11 compares the sound spectra at the same microphone locations for differing exhaust velocities, engine conditions, gas, and core conditions. As can be seen, the octave band spectra tend to be broad and flat for all gases except helium which peaks in the third octave band and generally shows less high frequency energy. This is probably due to the lower exhaust velocities for the helium flow. For all the hydrogen gas tests (except the unburned hydrogen flow), ignition of the gas was accomplished by a propane torch placed downstream of the nozzle exit plane. Thus, the turbulent combustion is itself a source of noise, and the question must be considered whether the combustion noise significantly contributed to the overall sound field generated by the jet exhaust.

To investigate this, the SPL's (Fig. 11) and the PWL's (Fig. 15) from the helium and hydrogen flows have been examined. The overall sound power level (OAPWL) generated by the helium flow was slightly greater than the OAPWL for the hydrogen flow. This would seem to be unusual since (although the weight flow of the two gases were comparable) the velocity, thrust and mechanical stream power were significantly less for the helium test and this would ordinarily result in a lower sound power level. However, the density of the hydrogen exhaust (refer

to Table VII) was less than half that of the helium exhaust. This indicates that the efficiency in generating sound power is less for hydrogen than for the helium exhaust having higher density.

On the other hand, since the exhaust velocity of the helium flow was lower, the helium sound pressure levels should have been lower (assuming a sound power dependence on velocity raised to some positive exponent). The hydrogen SPL's should also have been higher if the combustion of the hydrogen gas contributed materially to the sound field. However the hydrogen SPL's were only higher below 150 cps.

The data acquired during this study are insufficient to make any firm conclusions, but tentative suggestions are:

- The burning process in the hydrogen exhaust contributed significantly to the radiated sound field only below 150 cps, and
- The conversion efficiency in generating sound energy is lower for a hydrogen exhaust than for other higher density exhausts.

Determination of Near- and Far-Field Limit

To determine the limit of the acoustic near- and far-field of the KIWI B engine, three vertical arrays of microphones were used during the 13 May 1964 hot firing. The array farthest from the reactor had to be particularly high so that an appreciable portion of the radiated sound field could be covered. For that reason, the balloon was flown to an altitude of 600 feet. Though the position of the balloon was very stable during the power run, the data from the balloon microphones showed considerable fluctuation ($\pm$ 5 dB). No relation has been established between fluctuations in wind velocity (speed or direction) and data fluctuations since the wind fluctuations had a period of about one minute and the data variations had a period of approximately four seconds. However, this may be due to the slow response of the wind measuring system (the higher frequency fluctuations not being recorded). An indication that it was heat-generated turbulence is given by the magnitude of the SPL fluctuations versus microphone elevation. Those microphones at the extremities of the cable (close to the ground or balloon) showed the least amount of disturbance (being farthest from the center of burning) whereas those microphone positions near the center of the cable showed the greatest pressure fluctuations.

The SPL's measured during EP IV on the three microphone arrays were examined to define the sound field; i.e., the near-field, where the fluctuating pressures are caused by sound waves, but a simple source cannot be assumed and spherical divergence losses are not yet in effect; and the far-field where the source appears to be localized in space and pressure falls off inversely with the radius. The KIWI B acoustical data indicated that the near-field extends to about 250 feet from the engine. The large extent of the near-field may be partially due to the heat associated with the burning hydrogen which increases the speed of sound and causes refraction.

Fig. 12 compares the OASPL's to indicate whether the large tower can be considered in the far field. Distribution of SPL's along the microphone arrays were made and the difference between two points along a given radius has been compared with the value of 20 log S_1/S_2 where S_1 is the distance from the source to the balloon microphone and S_1 is the slant distance to the 420-foot tower.

The approximate 6 dB loss in sound pressure between the 420-foot tower and balloon arrays gives reasonable assurance that the large tower is in the far-field. A discussion, presented in the section on Discussion of KIWI B Acoustical Characteristics (Space-Time Correlation Calculations) indicates that the generalized origin of the sound source is estimated to be 40 feet downstream of the nozzle exit plane. The illustration (Fig. 12) uses this point for the origin of the radii.

Discussion of Contours of Equal Sound Pressure Levels

Contours of equal SPL's are presented in Figs. 13a to 13h to show the distribution of sound pressures around the KIWI B during a power run. The contours indicate that the region of maximum sound radiation in frequency intervals shifts closer to the nozzle as the frequency increases. Also, the wind currents and/or turbulence generated by the heat from the exhaust appear to influence the pressure field in the high frequencies.

Observation of motion pictures showing the burning exhaust reveals a wildly fluctuating random motion of pockets of burning hydrogen gas in the upper half of the plume. This phenomenon offers a plausible explanation of some of the anomalies seen in the directivity patterns and in the fluctuations in pressure at some microphone positions.

Discussion of Probable Error

The SPL's utilized for discussions and calculations in this report are subject to the following estimated errors: Electrical calibrations of each channel are accurate to $\pm$ 0.2 dB. The visual interpretation of most of the data amplitude is accurate to $\pm$ 1.0 dB except in instances of time averaging (which are discussed elsewhere) and low frequency data. Data reduction corrections are only read to the nearest dB so the error is probably close to $\pm$ 0.75 dB. The acoustical calibration is corrected for barometric pressure (altitude other than sea level) and introduced $\pm$ 0.2 dB error. Rounding off SPL values results in another $\pm$ 0.5 dB.

The probable error is, therefore, taken to be

$$\epsilon = \sqrt{0.04 + 1.0 + 0.56 + 0.04 + 0.25}$$

$$\doteq \pm 1.5 \text{ dB}$$

for all frequency bands above 100 cycles per second. Below that, the instability of the data increases the probable error to $\pm$ 2 dB.

Photographic Coverage

Motion pictures and still photographic coverage were furnished by LASL throughout this study. Both color and infrared films were found to be useful to obtain details of the exhaust structure. Fig. 14 is an infrared photograph taken during the full-power portion of the KIWI B-4E (EP V).

The infrared film has approximately a linear relation between image brightness and the heat radiated from a source. Fig. 14 shows that the temperature of the propellant increases due to combustion downstream of the nozzle and the maximum temperature and largest area of turbulent combustion occur about 150 feet downstream. One would expect this region to be the source of greatest generation of sound energy due to combustion (i.e., below 150 cps).

The extended length of the exhaust is also quite apparent and the burning exhaust extends to approximately 250 feet (giving an L/d ratio of approximately 100).

Where

L = length of plume

d = exit diameter of nozzle

DISCUSSION OF KIWI B ACOUSTICAL CHARACTERISTICS

This section discusses the calculations made with the measured sound pressures, describes the results obtained, and relates them to the flow parameters of the KIWI B exhaust and of other rocket data. The acoustical characteristics discussed in the following sections include overall sound power, sound power spectra, efficiency of conversion from mechanical stream power to sound power, directivity of the radiation sound field, and plots of the space-time correlation of the sound field.

Sound Power Levels

The sound power spectrum and the overall sound power are important acoustical characteristics of any noise source. In the study of the noise generated by the exhaust from the KIWI B nuclear rocket engine (during both cold- and hot-flow tests), the sound power levels were calculated in one-third octave bands using the sound pressure levels measured at the microphone positions on the 420-foot tower and balloon arrays. The 1/3 octave band sound power levels were summed to obtain octave band power levels. These data are presented in Fig. 15 and indicate the distribution of sound power over the frequency range of 20-10 000 cps during the maximum steady state flow conditions.

For purposes of comparison with the KIWI B data, the overall sound power levels and octave band sound power levels for other rocket engines in the thrust range of 250 to 100 000 pounds are also presented in Fig. 15. Since the evaluation of differences in sound power levels and spectra require consideration

of related engine performance parameters, items such as thrust, nozzle diameter, weight flow, velocity, and density of the respective propellants used by the KIWI B and chemical rocket engines are listed in Table VII. The plenum temperatures, pressures, and other restricted data are contained in a classified appendix.

Comparison of Spectra for Hot and Cold Hydrogen Flows.- KIWI B hot and cold-flow acoustical data were used to make the following comparisons and evaluations. The two hot flow tests (EP IV and V used liquid hydrogen for a propellant) had approximately the same weight flow and exhaust temperature, and resulted in almost identical overall sound power levels and octave band power spectra, except for the 6 dB difference in the eighth octave band.* The octave band spectra from both of these indicate that most of the sound power generated during the KIWI B hot tests was equally distributed in the third through the sixth octave bands (the frequency range from 150 to 2400 cps). There is a decrease of 3 to 4 decibels per octave below the third octave band, and a 3 to 6 decibel decrease per octave from bands 6 to 8.

The acoustical data from cold-flow tests using hydrogen gas indicated an octave band power spectrum that was similar to that from the hot-flow hydrogen tests. The overall sound power and octave band power levels were proportionately lower for the cold-flow hydrogen test since the thrust and exhaust gas velocity and, consequently, the exhaust stream mechanical power, were less than for the hot-flow hydrogen tests.

Comparison with Acoustical Data from Chemical Rockets.- Comparisons between the generalized chemical rocket engine sound power spectra have been made so that trends may be compared with the KIWI B sound spectra. The chemical rocket data were selected from ref. 3 because this reference contains the flow parameters necessary to make a good comparison. Two rockets, E and F, were in the same thrust range (40 000 pounds) as the KIWI B during power runs. The model rocket, ref. 4, using heated helium as a propellant, had a nozzle exit diameter of 1.47 inches and generated 250 pounds of thrust. The model rocket data were included because the propellant had a low molecular weight to compare with the KIWI B helium exhaust.

The octave band sound power spectra for the chemical rocket engines indicate that, as nozzle diameter and thrust increase, the peak sound power generated shifts toward the lower octave bands. The peak sound power levels for rocket H (5000 pounds thrust) were in octave bands 4 and 5; and for

---

* The SPL's from microphone no. 7 from EP IV appear to be too high in the eighth octave band and were responsible for the higher sound power level in that octave band.

rockets E and F (48 000 and 34 000 pounds thrust, respectively) the spectrum peaked in octave bands 3 and 4; and for rocket C (100 000 pounds thrust) the spectrum peaked in octave bands 1 and 2. The model rocket generated predominantly high frequency noise with the maximum sound powers occurring in octave bands 6 and 7 which include the frequency range 1200 to 4800 cps. The overall sound power radiated by rockets H to C increase in proportion to the exhaust mechanical power. The GHe model rocket, however, seems to be an unusual case since it generated about the same overall sound power levels as rocket H, which had much higher thrust and mechanical power (see Table VII).

The KIWI B sound power spectra of the two power runs (EP's IV and V) may be compared to the sound spectra for chemical rocket engines E and F, for comparable values of thrust. As indicated, the overall PWL's were approximately the same, however the difference in PWL's in some octave bands was as much as 5 dB. In general, the KIWI B PWL's were slightly lower in octave bands 1 through 4, and higher than the rocket E and F data in octave bands 5, 6 and 7. The reasons for the difference in spectra are not readily apparent, but it should be noted that the KIWI B hot-flow exhaust velocity was much greater than the exhaust velocity of rockets E and F and, therefore, the mechanical stream power of the exhaust during the KIWI B tests was higher than that for rockets E and F. On the other hand, the density of the hot hydrogen exhaust was much less than the exhaust density of the chemical engines (see Table VII). The comparisons offer more evidence that the hot hydrogen exhaust from the KIWI B rocket engine is less efficient than the chemical rocket engine exhaust in the generation of sound, which, in turn, may be due to the difference between the exhaust gas densities of the two types of rocket engines.

For comparable values of mechanical power, the acoustical data from the KIWI B hot-flow were compared with the acoustical data for rocket C, and the KIWI B cold-helium test data were compared with rocket H. As can be seen in Fig. 15, the sound power levels for the hot-flow hydrogen KIWI B tests were considerably less than those for rocket C: this, again, indicates that a hot hydrogen exhaust is less efficient than chemical rocket exhaust gases in the generation of sound energy.

The cold-flow helium generated considerably more sound power than that generated by rocket H, even though the velocity of the helium exhaust was about half the velocity of the chemical rocket exhaust. However, the thrust of the helium rocket was over twice the thrust of rocket H; thus, both exhausts had approximately the same mechanical stream power. This indicated that the exhaust from rocket H was less efficient in generating sound power than the KIWI B helium exhaust.

Fig. 15 also shows that KIWI B engine hot-flow generates approximately the same power as other rocket engines in the same thrust range. This is contrary to predictions of the radiated sound power based only upon the exhaust velocity raised to the third power or upon a sound power relation that has been deduced from other chemical rocket engine acoustical data. Additional discussion of the mechanism of sound power generation is presented in the section on Conversion Efficiency.

Generalized Sound Power Spectra

Conventional Normalizing Method.- The sound power spectrum of the noise generated by the KIWI B exhaust stream was normalized and examined in a generalized form. The purpose of this was to establish a basis for comparing the sound power spectra produced by the KIWI B engine and chemical rocket engines, and to establish a technique for combining the wide variety of rocket engine noise data with the KIWI B data in order to extend the method of predicting noise spectra.

The sound power spectra from the KIWI B tests were non-dimensionalized in the same fashion as other rocket noise data (see refs. 3 and 4) to yield the generalized power spectra curves shown in Fig. 16.

Generalized sound power spectra (based on the octave band sound power levels shown in Fig. 15) for the chemical rocket engines are also presented for comparison in Fig. 16.

The dimensionless parameters used are a Generalized Power Spectral Density (PSD) and the Strouhal Number. These terms are defined in the following ways:

$$\text{Generalized Power Spectral Density} = \frac{w_f}{W \div V_e/D_e}$$

where w_f is the sound power per unit frequency, and

W = Overall sound power (watts)

D_e = Nozzle exit diameter (ft)

V_e = Exhaust velocity at the nozzle exit plane (ft/sec).

The PSD was approximated as the average value for the power in some frequency band from the following relation (obviously the terms can also be derived in 1/3 octave bands):

$$w_f = \frac{\text{Octave Band Sound Power}}{\text{Octave Band Frequency Interval } (\Delta f_{OB})} \quad , \quad \frac{\text{watts}}{\text{cps}}$$

$$V_e/D_e = \frac{\text{Nozzle Exit Velocity}}{\text{Nozzle Exit Diameter}} \quad , \quad \frac{\text{ft/sec}}{\text{ft}}$$

Note $W \div V_e/D_e$ has units of watts/cps.

$$\text{Strouhal Number} = \frac{f}{V_e/D_e}$$

where f = octave band center frequency in cps.

The generalized power spectrum curve is also a normalized curve since the area under the curve is unity. That is,

$$\sum_{i=1}^{n} \frac{(w_f)_i}{W \div V_e/D_e} \cdot \frac{(\Delta f)_i}{V_e/D_e} = 1$$

The generalized power spectral density can be expressed in more commonly used terms by dividing w_f and W by the standard sound power level reference of 10^{-13} watts, and then taking the logarithm of the result to give the generalized power spectrum level (PSL).

$$\text{Generalized Power Spectrum Level} = 10 \log \frac{w_f/10^{-13}}{(W/10^{-13}) \div V_e/D_e}$$

$$\text{in dB re } \left(\frac{w_f}{\frac{W}{V_e/D_e}} \right) = 1$$

Thus, the

$$\text{Generalized Power Spectrum Level} = [(\text{OBPWL} - 10 \log_{10} \Delta f_{OB}) - (\text{OAPWL} - 10 \log_{10} V_e/D_e)].$$

The range of sound power spectra for the chemical rocket engines is indicated by the band shown in Fig. 16. Data points for rocket F and for the model rocket are also shown. The KIWI B spectra for the two hot-flow hydrogen tests are shown as a band rather than data points. In general, the KIWI B hot-flow noise spectra fall within the band of rocket data. At low frequencies, however, the KIWI B spectrum remains at a constant value while the chemical and model rocket spectra decrease in level. The generalized spectra for the cold-flow hydrogen tests compare reasonably well with the hot-flow hydrogen data over most of the frequency range; however, the cold-flow helium spectrum indicates much lower spectrum levels at low Strouhal Numbers than any of the other engines. In addition, the model rocket (which used heated helium as a propellant) has a significantly different normalized spectrum than that from the KIWI B cold flow helium tests.

The differences in normalized spectra are due to the variation in exhaust parameters, including jet density and temperature, which have not yet been systematically related. For the KIWI B tests, the burning hydrogen also contributes to the noise field in the first three octave bands. The discussion presented earlier in the section on sound power levels concerning these effects also apply to the normalized spectra. It appears from Fig. 16 that in the thrust level of 50 000 lbs, predictions of sound power spectra for nuclear rocket engines can be made with reasonable accuracy in the range of Strouhal Numbers from S = 0.01 to 3.

Effect of Exhaust Gas Density

Since it appeared as if the exhaust gas density (ρ_j) might be an important parameter to include in generalizing the sound power levels, the ratio of exhaust gas density to ambient air density (see Table VII) was used to modify the generalized power spectra and dimensionless frequency parameters as indicated in Fig. 17. The density ratio was included in both parameters so that the area under the power spectra curve would still be normalized to unity as in Fig. 16.

The results shown in Fig. 17 are unsatisfactory for empirically relating the KIWI B to the chemical rocket data. The data adjusted by the density ratio, (including the model jet) however, seem to follow a general trend, and the hot-and cold-flow KIWI B acoustical data points had been brought closer together. Thus, it appeared that the frequency distribution of sound energy from a rocket exhaust was also dependent on the exhaust gas density.

Introduction of a New Normalizing Technique

To obtain a better grouping of data points, another method of normalizing sound power data was attempted. This method introduced a parametric term which is called Relative Spectral Density. The frequency scale in this case was non-dimensionalized by dividing the geometrical mean frequency of the octave band by the frequency interval over which the total sound power was integrated.

The generalized parameters used are as follows:

$$\text{Relative Spectral Density} = \left[\frac{\left(\frac{\text{Octave Band Sound Power}}{\text{Octave Band Frequency Interval}} \right)}{\left(\frac{\text{Overall Sound Power}}{\text{Overall Frequency Interval}} \right)} \right]$$

or,

$$\text{Relative Spectral Density} = \frac{w_f}{W/\Delta f_{OA}}$$

where the

$$\text{Dimensionless Frequency} = f/\Delta f_{OA}$$

Thus, the Relative Spectral Density is the ratio of average sound power density in an octave band to the average sound power density for the frequency range of the overall sound power measurement. The result is also a normalized power spectrum since the area under the curve is unity:

$$\sum_{i=1}^{n} \frac{(w_f)_i}{W/\Delta f_{OA}} \cdot \frac{(\Delta f)_i}{(\Delta f)_{OA}} = 1$$

Again, as in the case of the generalized power spectra for the convenience of presentation, the relative spectral density values are expressed in decibels. The KIWI B and chemical rocket engine's acoustical data were treated in this fashion and the resultant relative spectral density levels are shown in Fig. 18. It is evident that a more orderly arrangement of the sound power spectra resulted from the relative spectral density type of normalization. The variation in spectral density levels is generally within $\pm$ 3 dB.

Discussion of Other Normalizing Techniques

During the study of the generalized power spectra, other combinations of engine flow parameters were investigated to observe their effect on the grouping of the power spectra data. In each case, terms were related to yield dimensionless power spectra. A description of four of the methods tried and the results that were obtained are given below:

Method I.- References 3 and 5 showed that a better relation could be obtained among rocket, turbojet, and model jet data by using the speed of sound in the exhaust gas at the nozzle exit (C_e) rather than the gas exit velocity (V_e) as a normalizing parameter.

With this approach, the power spectra parameters became:

$$10 \log \left[\frac{W_f/10^{-13}}{\frac{W/10^{-13}}{C_e/D_e}} \right] \quad \text{vs} \quad \frac{f}{C_e/D_e}$$

Using this relation, the acoustical data from the KIWI B did not compare well with chemical rocket data because of a 9 dB difference in the peak spectrum levels and a displacement by a factor of 30 in the spectral peak (for the KIWI B compared to chemical rockets) on the dimensionless frequency scale.

Method II.- In this attempt, the overall sound power (W) was normalized by the exhaust mechanical stream power (W_M) and the thrust (F). The density ratio (ρ_{eq}/ρ_a) was introduced as a modifying factor, and the nozzle diameter was used to normalize the frequency spectrum. The resulting dimensionless power spectra parameters were

$$10 \log \left[\frac{\left(W_f/10^{-13}\right)}{\left(\frac{W/10^{-13}}{\rho_{eq}{}^2 V_{eq}{}^3 D_e^2/F\rho_a}\right)} \right] \quad \text{vs} \quad \frac{f}{(V_{eq}/D_e)(\rho_{eq}/\rho_a)}$$

where ρ_{eq} and V_{eq} are the equivalent exhaust density and velocity respectively.

The term $\frac{W}{\left(\rho_{eq}{}^{2}V_{eq}{}^{3}D_e^{2}/F\rho_a\right)}$ was derived as follows:

To normalize W, divide by $\left(\frac{W_m'}{FD_e}\right)x\left(\frac{\rho_{eq}}{\rho_a}\right)$, using $W_m' = \rho_{eq}D_e{}^{2}V_{eq}{}^{3}$

Thus

$$\frac{W}{\frac{W_m'}{FD_e}(\rho_{eq}/\rho_a)} = \frac{W}{\rho_{eq}{}^{2}V_{eq}{}^{3}D_e/F\rho_a}$$

The terms used in the denominator of the generalized spectra are parameters related to both mechanical and sound power, and are used to obtain dimensionless power spectra. This method resulted in a close grouping of the various KIWI B power spectra. However, the grouping of the power spectra from the chemical rocket with those from the KIWI B was unsatisfactory and did not indicate systematic trends.

Method III.- This approach used the relative spectral density parameter (introduced earlier) with a Strouhal number (based upon V_{eq}) instead of the dimensionless frequency term $f/(\Delta f)_{OA}$. The power spectra parameters were related in the following way

$$10 \log \left[\frac{w_f/10^{-13}}{W/10^{-13}/\Delta f_{OA}}\right] \quad \text{vs} \quad \frac{f}{(V_{eq}/D_e)}$$

By this method, the sound spectra from the KIWI B hot hydrogen flow and chemical rockets grouped reasonably well. The average spectrum curve through these points had a spread of $\pm$ 4 dB. The KIWI B cold-flow hydrogen and helium sound spectra, however, were considerably displaced from the other data.

Method IV.- This approach also used the relative spectral density parameter and the Strouhal number, $f(D_e/V_{eq})$, introduced in Method III. In this procedure, the dimensionless frequency parameter (the Strouhal number) was generalized by the dimensionless term $\sqrt{RT_c/D_e}$, where R is the gas constant, and T_c is defined as: (a) the temperature of combustion for a chemical rocket engine, or (b) the plenum temperature for the KIWI B.

The power spectra parameters were related by

$$10 \log \left[\frac{(w_f/10^{-13})}{\left(\frac{W/10^{-13}}{\Delta f_{OA}}\right)}\right] \quad \text{vs} \quad f\left(\frac{D_e}{V_{eq}}\right) x \sqrt{\frac{RT_c}{D_e}}$$

These parameters result in generalized or dimensionless spectra but do not provide a normalized spectrum. The KIWI B and chemical rocket acoustical

data generalized by Method IV are shown in Fig. 19. The grouping of the spectral levels is somewhat similar to that obtained in Fig. 18, even though the frequency scales are non-dimensionalized on an entirely different basis. In general, the low frequency dispersion of spectrum levels is greater than at high frequencies and the lower spectrum levels are associated with small nozzle diameter or lower thrust engines. At higher frequencies, the KIWI B and model rocket acoustical data form the upper limit of the spectral band.

In comparing all the methods for generalizing sound power spectra discussed in this section, it appears that the normalized spectra using the relative spectral density level and the dimensionless frequency f/Δ_{OA}, shown in Fig. 18, provided an average spectrum with the least variation, and offered the most systematic comparison of the wide variety of engine exhaust conditions between the KIWI B and chemical rockets.

Conversion Efficiency

The ratio of total sound power generated by the exhaust flow to the mechanical stream power of the exhaust was calculated for the maximum flow condition of each 1964 KIWI B test, and is presented in the form of percent efficiency in the table below.

Test Date	Propellant	Acoustical Efficiency (%)
9 January 1964	Cold Flow GHe	0.52
9 January 1964	Cold Flow GH_2	0.16
13 May 1964	Hot Flow LH_2	0.24
28 August 1964	Hot Flow LH_2	0.19

There was a wide variation in values of exhaust gas density and velocity (see Table VII) between the hot- and cold-flow hydrogen tests, and between the hydrogen exhaust and chemical exhausts. The effect of independent variations of the velocity or density is difficult to evaluate. However, lower acoustical efficiencies were associated with the higher velocity and lower density hydrogen exhaust.

The overall sound power levels and mechanical power from which these values were computed are presented in Fig. 15 and Table VII, respectively.

To compare data and to establish trends, the associated sound power levels and mechanical power values for the KIWI B and other rocket engines are related graphically, as shown in Fig. 20. The mechanical stream power and overall sound power levels were obtained from ref. 3 for all the chemical rocket engines shown. It is evident that the cold and hot hydrogen exhaust during the KIWI B engine tests were not as efficient as the helium exhaust and most of the chemical

rocket engines in generating acoustic energy. The exhaust mechanical power of the hot-flow hydrogen test was about 8 times higher than for the cold-flow hydrogen test, and the difference in radiated sound power was approximately 10 dB. This indicates a nearly constant efficiency in conversion from mechanical power to sound power for increasing thrust with the hydrogen exhaust. Whether this conversion efficiency will remain constant for higher power (with higher weight flow and possible higher exhaust velocity) nuclear rocket engines has yet to be determined.

Directivity of the KIWI B Sound Field

Acoustical directivity patterns of the KIWI B exhaust were calculated for the far-field from hot- and cold-flow test data. The patterns were derived from the measured sound pressure levels by the following method:

$$\text{Space Average OASPL} = \text{OAPWL} - 10 \log_{10} (2\pi R^2)$$

$$\text{Directivity Index} = \text{OASPL} - \text{Space Average OASPL}$$

A comparison of the overall directivity pattern for the hot- and cold-flow tests is shown in Fig. 21. During the flow of gaseous helium, the peak occurred at an angle of 63° from the direction of the exhaust.

The data from the cold- and hot-flows of hydrogen peak generally at 71°. This is unusual since the exhaust velocity of the hot hydrogen flow was significantly higher than that of the cold hydrogen flow and the angle of maximum sound radiation was expected to increase with exhaust velocity. Some minor variations such as secondary peaks are superimposed, however, they are within $\pm$ 2 dB of the general trend and no significance is attributed to them.

A comparison of the directivity patterns for the balloon and two tower microphone arrays for the KIWI B-4D (EP IV on 13 May) is shown in Fig. 22. The 420-foot tower data show a peak at approximately 71°, as earlier gas flows indicated. The data from the 120-foot tower also shows a broad peak at about 70° despite the near-field character of the noise field and the fact that these microphone channels were calibrated for the frequency range from 300-20 000 cps to confirm that the spectrum continues to decrease between 10 000 and 20 000. The data from the balloon array does not permit a clear interpretation of whether the peak actually occurs at an angle greater than 71° or whether the data point (from the bottom of the microphone of the array) is unreliable.

Acoustical radiation patterns for selected 1/3 octave bands between 50 and 6300 cps are shown in Fig. 23. These directivity indices were computed from the sound pressure level measurements obtained during the 13 May hot-flow hydrogen test from the microphones on the 420-foot tower. The directivity patterns for the lower frequency ranges from 50 to 400 cps are almost identical to the overall directivity pattern. A greater variation in directivity is evident at the higher frequencies, particularly at 3150 cps and 6300 cps, where, although the index peaks at 71°, there is a sharper drop off on either side of the peak with a secondary peak at 34°. The directivity of acoustical radiation became

sharper with higher frequencies. However, the direction of maximum radiation remained 71° for all frequency ranges.

Space-Time Correlation Calculations

A rigorous mathematical description of structural response to acoustic pressure requires the knowledge of how the pressures are correlated in space and time in addition to their magnitude and the distribution of energy in the frequency range of interest. Unless measured data are used to calculate the space-time correlation of the pressure, assumptions must be made as to the shape of these functions. Thus, considerable error can be introduced through ignorance of the appropriate characteristics of the forcing function.

Certain aspects of the space-time correlations for the KIWI B acoustic field were within the scope of this study. These special tests included: (1) measurement of data suitable for space-time correlation calculations during both hot firings, and (2) calculation and graphical presentation of space-time correlation characteristics. These two tasks were done, and the results reported elsewhere*. A summary of the pertinent factors accumulated to date is included here. However, a complete analysis is not presented since the mathematical description of the correlation results was not within the authorization of this study.

The definition of the space-time correlation functions and how they are calculated was given in the section on Correlation Calculations. Repeated application of the mathematical manipulations (described for a group of near-field microphone locations: four microphones at 110 feet, and two at 50 feet) results in a description of the space-time correlation characteristics of the acoustic field at those locations. For the KIWI B tests, the normalized correlation in the two perpendicular directions to that of propagation is taken to be 1 (i.e., perfect correlation over the plane of the wave front). Though this is not entirely true, a check made during the 28 August 1964 firing (microphone number 28) indicated that, in the direction approximately parallel to an on-coming wave front (in the ground plane of the microphones), the time correlation essentially agrees with such an assumption but, in a distance of six feet, the spatial correlation shows a decrease of about 33%. This departure from the initial assumption of a perfectly correlated wave front in both space and time assumes significance only when considering the response of a large structure (with dimensions on the order of 15 to 20 feet).

Continuing on the basis then that the original assumptions are reasonable, a three-dimensional plot of the space-time correlation function for the acoustic near-field of the KIWI B nuclear engines is presented in Fig. 24. Such a plot indicates the general nature of the function. A more useful display of the contour characteristics is shown in Figs. 25 and 26 where projections of the space-time contour onto the time and space axes have been made respectively.

---

*The technical analysis was performed and supporting data transmitted under subcontract No. 24372-980-10 to the C. F. Braun Company.

By relocating the microphones for EP V (28 August) and performing cross-correlation calculations of narrow bands of data, several details were observed. The results, within the 20-2000 cps band, indicate that the pressures are correlated over an area of 2 square feet of the 8-square foot test panel (slightly less than one foot in the direction of propagation). The shape of the narrow-band cross-correlation resembles a damped cosine function. Also, the maxima of the cross correlation for a band of frequencies 330 cps wide with a geometrical mean of 1000 cps diminishes more rapidly in the space-time domain than does the maxima for a band of frequencies 33 cps wide with a geometrical mean of 100 cps. This difference is shown in Fig. 27.

The logarithm of the Fourier transform of the space-time correlation function (the relative cross power spectrum level) is shown in Fig. 28. It may be shown from either the cross-correlation or the cross-power-spectral function that a Delta function correlation is a very incomplete description of the field. However, for a modal analysis of large structures, or assuming a white noise forcing function (a flat power spectral density), a Delta correlation function approach (e.g., $\delta[x/v - \tau]$) might be a useful approximation, but the error involved in such an approximation has not been determined.

The mathematical description of the characteristics of the space-time correlation function for the KIWI B acoustic field would provide an analytical method to make an accurate prediction of the transfer efficiency of energy from the acoustic field to structure. However the work necessary to derive these analytical functions was beyond the authorization of this study.

Location of Generalized Sound Source

In addition to this basic question of structural response, the correlation calculations permit definition of other factors. From the data of EP IV (13 May 1964), a localized overall frequency source was calculated to be approximately 13 feet downstream of the nozzle exit plane. A sample computation using the data from EP IV (13 May 1964) is shown below. Note that the calculation indicates the speed of sound at the position of measurement to be 1220 ft/sec. The source height was calculated using the following approximations (assuming a plane wave at the microphone).

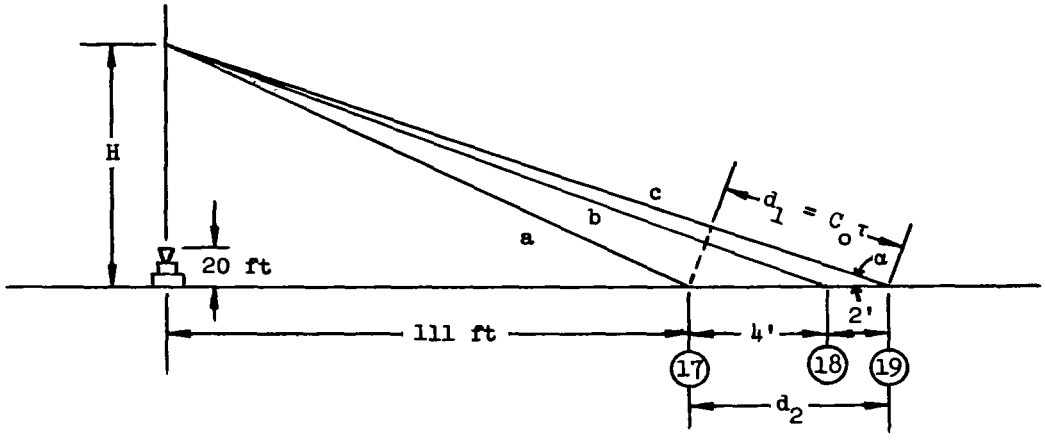

$$\text{Cos } \alpha = \frac{d_1}{d_2} = \frac{C_o \tau}{6}$$

$$H = 117 \tan \alpha$$

where C_o = speed of sound (ft/sec)

τ = time delay of correlation function maxima (sec)

From the maxima of the space-time correlation functions projected on the time axis (ref. Fig. 25) the time for the wave to travel along its directional paths are known to be 1.5 milliseconds from microphones 17 to 18, and 3.1 milliseconds from microphones 18 to 19. Hence:

$$b - a \doteq C_o[1.5 \times 10^{-3}]\text{ft and } c - b \doteq C_o[3.1 \times 10^{-3}]\text{ft}$$

$$a = \sqrt{111^2 + H^2} \qquad b = \sqrt{113^2 + H^2} \qquad c = \sqrt{117^2 + H^2}$$

By successive approximations, the two variables were found to be

$$H = 33 \text{ ft} \quad \text{and} \quad C_o = 1220 \text{ ft/sec}$$

Thus, the distance downstream from the nozzle exit was 13 feet.

Since this speed of sound is higher than that which would exist for ambient air temperatures, it was concluded that the air was heated by the thermal radiation from the exhaust of the KIWI B nuclear engine, c.f., Fig. 14.

During EP V (28 August 1964), a measurement of air temperature was made using a thermocouple near the microphones on the concrete pad at 110 feet (Fig. 32). The data indicate that the temperature of the air was 130°F during maximum power (the ambient air temperature was 80°F). Using this measured temperature, a speed of sound at the correlation microphone location was calculated to be 1191 ft/sec. With this speed of sound, and the time delays between microphone pairs 17-18, 17-19 and 18-19 obtained from the output of the 7090 computer (shown approximately in Fig. 25), a more accurate source location was determined. For the 28 August 1964 data, the localized overall source (20-2000 cps) was approximately 40 feet downstream of the nozzle exit plane.

Distribution of Instantaneous Pressure Peaks

The space-time correlation IBM program also provided a plot of the distribution of instantaneous pressure peaks. These peaks have approximately a Guassian distribution, as indicated by Fig. 29. An indication of sinusoidal influence is observable on some of the curves in the form of a small double peak, one on each side of the mean. This was attributed to a data reduction channel with a low-level 60 cycle per second noise.

Change in Correlation with Distance

Measurements were made during EP V (28 August 1964) to compare the correlation data at two distances from the reactor. Two Bruel and Kjaer 1/4" microphones were placed approximately 50 feet from the center line of the reactor (as near as possible without the microphones being influenced by the radiation effects) and six feet apart in the direction of propagation. The results indicate a much smaller correlation than that at 110 feet. Fig. 30 indicates the approximate difference in the correlation function projected on the time axis. This smaller degree of correlation is attributed to the much greater apparent spatial distribution of the sound source at the closer near-field measurements. The difference in time delay for maxima is due to the change in angle of incidence of the microphones with the source. However, it is not known whether the trend will continue as the reactor is approached.

STRUCTURAL STUDIES

Dewar Vibrational Response

During the 13 May test, a microphone and an accelerometer were mounted approximately 2 inches apart on one of the pie-shaped segments of the 60-foot diameter spherical Dewar. This section of the Dewar was in a direct, "line of sight" exposure to the acoustical source. The pie-shaped segments are butt welded, therefore, no appreciable individual panel response was expected. Hence, modal response of the sphere was most probable. An equation of motion for an evacuated 9/16-inch thick steel sphere was not available, so the fundamental resonance frequency could not be accurately predicted. Using the empirical data, a power transfer function (TF) was obtained by dividing the power spectral density of the acceleration response of the sphere wall by the power spectral density of the excitation. This transfer function, plotted in terms of dB, is:

$$TF = 10 \log_{10} \left[\frac{\text{acceleration of Dewar } (g^2/\text{cps})}{\text{impinging sound pressure } [(\text{lb/in}^2)^2/\text{cps}]} \right] \text{, in decibels}$$

$$\text{re } 5.00 \times 10^2 g^2/(\text{lb/in}^2)^2;$$

as shown in Fig. 31. The large response at 180 cps is due to a resonance of the sphere (using shallow shell theory, a fundamental resonance of a comparable ring stiffened hemisphere was calculated to be 173 cps).

Test Panel Response

During EP V, an attempt was made to measure the response of a simple structure to the KIWI B sound field. A simply supported, flat aluminum panel (2' x 4' x 3/16") was selected. The simple support was provided by a high temperature silicone rubber channel restrained by an angle iron frame. The panel assembly was mounted on four legs to raise the panel approximately one

foot off the ground. Surrounding the panel, but structurally separate from it, was a sheet metal baffle. The purpose of the baffle was to reduce back pressures due to diffraction. A 3-inch air gap around the base of the baffle vented the enclosure to avoid stiffening the enclosed air. The panel itself was canted to avoid standing waves between it and the concrete pad, and to achieve approximately normal incidence from the sound pressure radiated from the exhaust, see Fig. 32. Two identical panels, as described above, were placed on the concrete pad at approximately 30 feet and 130 feet from the center line of the reactor, see Figs. 33 and 34.

Prior to their field installation, laboratory tests indicated the fundamental resonance frequency, using both impulse and sinusoidal excitation, to be approximately 40 cps. The standard equation for a simply supported panel indicated a resonance frequency of 39 cps. This offered verification that the perimeter provided a simple support - at least for the lowest modes of vibration. Using a logarithmic decay of a sudden cessation of steady-state forcing function, the total damping of the plate and its edge effects was also measured in the laboratory. A curve is shown in Fig. 35 illustrating the results of the test.

Six strain-gage accelerometers were mounted on the rear of the panel for the field test: five accelerometers were placed in one quadrant at positions corresponding to the maximum displacements for the first major uncoupled modes; and the sixth accelerometer was placed in the diagonal quadrant to check symmetry of response. A theoretical prediction of the panel response was made using a Green's Function equation of motion (ref. 6) and Powell's joint acceptance approach (ref. 7) by assuming arithmetic approximations of the KIWI B exhaust correlation function. Only the Green's Function approach is reported upon. After integration, individual modal responses and total response were calculated (see Appendix D). The results of the theoretical analysis were compared with the laboratory and field test results which used sinusoidal excitation from a noise source having a different correlation function. Both the laboratory and the field tests compared favorably with the theoretical predictions. The test results are given in Table VIII.

To facilitate comparison between the theoretical predictions and the measured results, the total rms modal response in g's was found by taking the half power points of the power spectral density of the modal vibratory responses (in g^2/cps) and performing a graphical integration to get modal mean squared g's. The square root of this quantity compared to the theoretical rms g's is shown in Table IX.

The results of the comparison between predicted and measured values are somewhat disappointing in that the levels - though of the right magnitude (except at the higher frequencies where percent critical damping for the panel is difficult to measure) - are inconsistent. The measured response of the fundamental frequency of resonance is low compared to the predicted value. The next frequency at which a structural resonance occurred, falls in between two theoretical modal frequencies. One possible explanation for this is the resonance of the volume of air behind the baffle. When driven by sinusoidal excitation, the panel responded at 88 cps in the field installation (with

baffle), but did not do so in the laboratory installation (without baffle). The resonance frequency may, therefore, be somewhat shifted by some effect between the panel and the volume of air behind it. (It should be noted that the excitation spectrum from the KIWI exhaust is too flat in this frequency range to cause such a shift in modal response frequency.)

One consideration, the data reveals, is the relative magnitudes of modal response between the accelerometers located at the center of the two panels. The other accelerometers, located at comparable positions on the two panels, also showed consistency in this respect. Fig. 36 shows a power transfer function for the accelerometer located in the center of each of the panels (a transfer function similar to the one described previously for the Dewar). The figure clearly indicates the improved correlation of the pressures for the far panel as compared to the near one (predicted by comparing the space time correlation at 50 feet with that at 110 feet; see Fig. 30). The power TF also indicates a greater transfer of energy to the flat plate located 130 feet from the reactor than was evidenced by the spherical Dewar at approximately the same distance. This result is to be expected when considering the geometrical differences of the structures (i.e., stiffness, support, etc.).

Filter Effects in the Correlation Study

In addition to the wide-band correlation studies performed, narrow band analysis was done using filters in the playback system. Since it is known that filtering wide band data can influence the correlation calculations depending on the bandwidth of the filter, a special study was performed to obtain a more accurate definition of this dependency. Two random noise generators, operating independently, were recorded on two data tracks. Being completely uncorrelated, wide band correlation calculations should result in zero correlation at all times. The slight fluctuations in the correlation function can be considered the noise of the system. As the bandwidth of the data is narrowed, though the data remains uncorrelated, the effects of filtering appear in the results. The filters used were Bruel and Kjaer 1/3 and 1/1 octave band filters which have a relatively sharp cutoff (12 dB per 1/3 octave). The results of such a test are shown in Fig. 37 as an increase in the normalized correlation versus the number of cycles in a filter band.

CONCLUSIONS

Many characteristics of the sound field radiated from the exhaust of the KIWI B nuclear rocket have been defined and compared with those of chemical rockets. The far-field characteristics show the following:

1. The total sound power radiated by the exhaust of the KIWI B was less than that for chemical rockets of comparable mechanical power. The acoustical conversion efficiency for the nuclear rocket exhaust is approximately .2% which is lower than for chemical rocket exhausts.

2. A new method for normalizing sound power spectra introduces a relative spectral density level which successfully relates the acoustical data from a variety of jet noise sources and shows a systematic trend in the relation between the sound power and the engine flow parameters. The result is a new technique that may be used to make reasonably accurate predictions of sound spectra over a wide range of engine exhaust conditions.

3. The generalized sound source (20-2000 cps) was calculated to be 40 feet downstream of the nozzle exit plane which is equivalent to approximately 16 nozzle exit diameters.

4. The burning hydrogen exhaust appears to increase the relative spectral density levels at low frequencies indicating that the combustion radiates a substantial, but undefined amount of sound energy below 150 cps.

5. The shapes of the spectra for hot- and cold-hydrogen flows were similar although the SPL's were higher for the hot flows.

6. The maximum sound power radiated for both hot- and cold-flows of hydrogen is at an angle of 71° from the direction of the exhaust.

7. The tall tower at 260 feet (100 nozzle diameters) is considered to be in the far-field for a reactor of the power level of the KIWI B.

In the near-field, the following characteristics in the frequency range of 20-2000 cps were observed:

1. The instantaneous distribution of pressure peaks is approximately Gaussian.

2. At 110 feet, the pressures are well correlated over a distance less than 1 foot in the direction of propagation and approximately 12 feet in the horizontal direction transverse to the direction of propagation.

3. The correlation of pressures at 110 feet is substantially greater than correlation of pressures at 50 feet from the reactor.

4. The 1/3 octave band spectra of four microphone channels (the microphones on the 120 foot tower which had their frequency response extended to 25 000 cps) peaked below 2000 cps and did not show any rising characteristic from 5000 to 25 000 cps.

APPENDIX A

INSTRUMENTATION SYSTEMS

Nuclear Radiation Tests

The selection of microphones for the KIWI B acoustical study was based upon an evaluation of their performance in a field of intense nuclear radiation (ref. 2). Bruel and Kjaer Models 4131, 4134, and 4136 were used together with a cathode follower, Model 2615. These microphones showed no degradation of performance in a radiation field comparable to that which existed approximately 50 feet from the reactor operating at full power.

A similar nuclear radiation test was made to qualify the microphone distribution box and its plugs, sockets, and cables to the same radiation environment. The test was conducted as follows.

The cathode followers and their microphone boxes were placed close to the core of the 100 kilowatt Argonaut Research Reactor at UCLA. An electrical test was made using the voltage insert method to measure frequency response (30 to 8000 cps), gain, and signal-to-noise level. The reactor was brought to a power level of 50 KW where it dwelled for 10 minutes, then power was increased and remained at 100 KW for 30 minutes. The input and output voltages were monitored continuously during the irradiation. The air temperature in the reactor did not exceed 100°F. At maximum reactor power, the flux rate reached a steady level at:

1.56×10^{11} neutrons/cm^2/sec: Thermal

1.56×10^{11} neutrons/cm^2/sec: Epithermal

Total: 3.12×10^{11} neutrons/cm^2/sec.

The test results were:

Maximum change in sensitivity: $\pm$ 0.5 dB at 8000 cps.
Hum and noise did not increase from pre-exposure value.

Environmental Tests of Kaman Pressure Sensor

During EP V, a pressure gage was used instead of a B and K microphone to measure the sound pressures incident on the flat panel placed 30 feet from the reactor. The pressure gage was used because it had been radiation "hardened" (i.e., all meterials used in its construction had high tolerance to nuclear radiation) by the manufacturer. The equipment, manufactured by the Kaman Nuclear Corporation, was:

Item	Model	Serial Number
Pressure Transducer	K-1200	84
Oscillator-Demodulator	K-2000	A-84

Prior to EP V, an environmental test was conducted on the pressure transducer in the Douglas Dynamics Laboratory. The results of the test indicated that the unit had a frequency response (± 2 dB from 20 to 5000 cps), linearity (± 1 dB to 170 dB), and noise level satisfactory for its use as a microphone in a sound field in excess of 120 dB. However because of the sensitivity of the pressure sensor to longitudinal and lateral vibration, a very compliant mount was used to support it over the near panel.

Microphone Signal and Power Circuits

The microphone signal and power (plate and filament) circuits required a reliable power source that would be unaffected by the neutron and gamma flux around the reactor during hot firings. To accomplish this, the signal and power distribution system shown schematically in Fig. A-1 and A-2 was designed and fabricated. The design offered three advantages:

1. Only four regulated power supplies are required, one plate and one filament power supply for the near-field cathode followers; and another plate and filament supply for the far-field cathode followers.

2. The power supplies are located in the test cell basement where they are out of any significant nuclear radiation, high temperature environment, and weather.

3. Only one power cable was required for the plate and filament circuits for each array of microphones. This technique reduced the size of the cable bundle at the tower base and the weight of the cable bundle to be carried by the balloon.

This design parallels all of the cathode follower filaments in one circuit and all of the plates in another. Resistance was placed in series with each filament and each plate circuit so that the performance of any cathode follower is relatively independent of the others. For example, a shorted or open filament, or plate, in any microphone would have negligible effect upon the sensitivity of any other microphone.

Each power and signal cable on the balloon and tower arrays terminated in a microphone distribution box that is illustrated in Figs. 6 and A-2 and is described below. The other end of the cables terminated in a distribution box at the base of the tower. From this point, the power and signal cables were installed in a steel conduit approximately 4 feet below grade that terminated on one end at the tower distribution box (at the tower base) and on the other end at the entrance of the tunnel leading into the test cell. The signal cables continued through the tunnel into the test cell basement to the Douglas equipment racks and to the tape recorders.

The number and purpose of the cables installed are shown in Fig. A-3. The tower distribution box for the 120-foot tower contains barrier strips to connect all the signal cables for strain gage and accelerometer circuits and near-field microphones; the tower distribution box for the 420-foot tower contains barrier strips for the large tower and the balloon microphone arrays. The audio circuits were grounded to the Test Cell C instrumentation ground. The noise level of the microphone circuits were at least 60 dB below maximum output on each channel. All exposed cables located within 100 feet of the reactor were wrapped with aluminum foil to protect them against thermal radiation from the burning hydrogen.

Microphone Distribution Boxes

One end of all microphone signal and power circuits terminates in a 2 1/4" x 2 1/4" x 5" microphone distribution box. These enclosures include resistors to drop the 36-volt filament supply to 6.3 volts at the tube, a resistor in the plate circuit to offer a load if the plate should short circuit, and receptacles for the microphone and cable plugs (see Fig. A-2).

The boxes included at 10:1 step-down transformer for the signal circuits which reduced the cathode follower output impedance to 75 ohms. The lower impedance reduced the high frequency signal loss that results from the capacitance due to the long cable lengths between the microphone and the tape recorder. The impedance was stepped back up to 750 ohms by an identical transformer located at the input to the tape recorder.

Tape Recorders

The tape recorders used for the study were two Ampex CP-100's and two Ampex PR-10's. A summary of the recorder's performance has been given in the section "Description of Acoustical Test Facilities." Prior to each EP or test, the CP-100 recorder was checked out using the Ampex TC-10 FM calibration unit to set the center frequency, deviation, and gain of each channel. For each channel, the required gain was estimated so the recording would be made about 10 dB below the maximum record level for the highest flow conditions.

These operations preceded the voltage insert calibrations and the acoustical sensitivity checks.

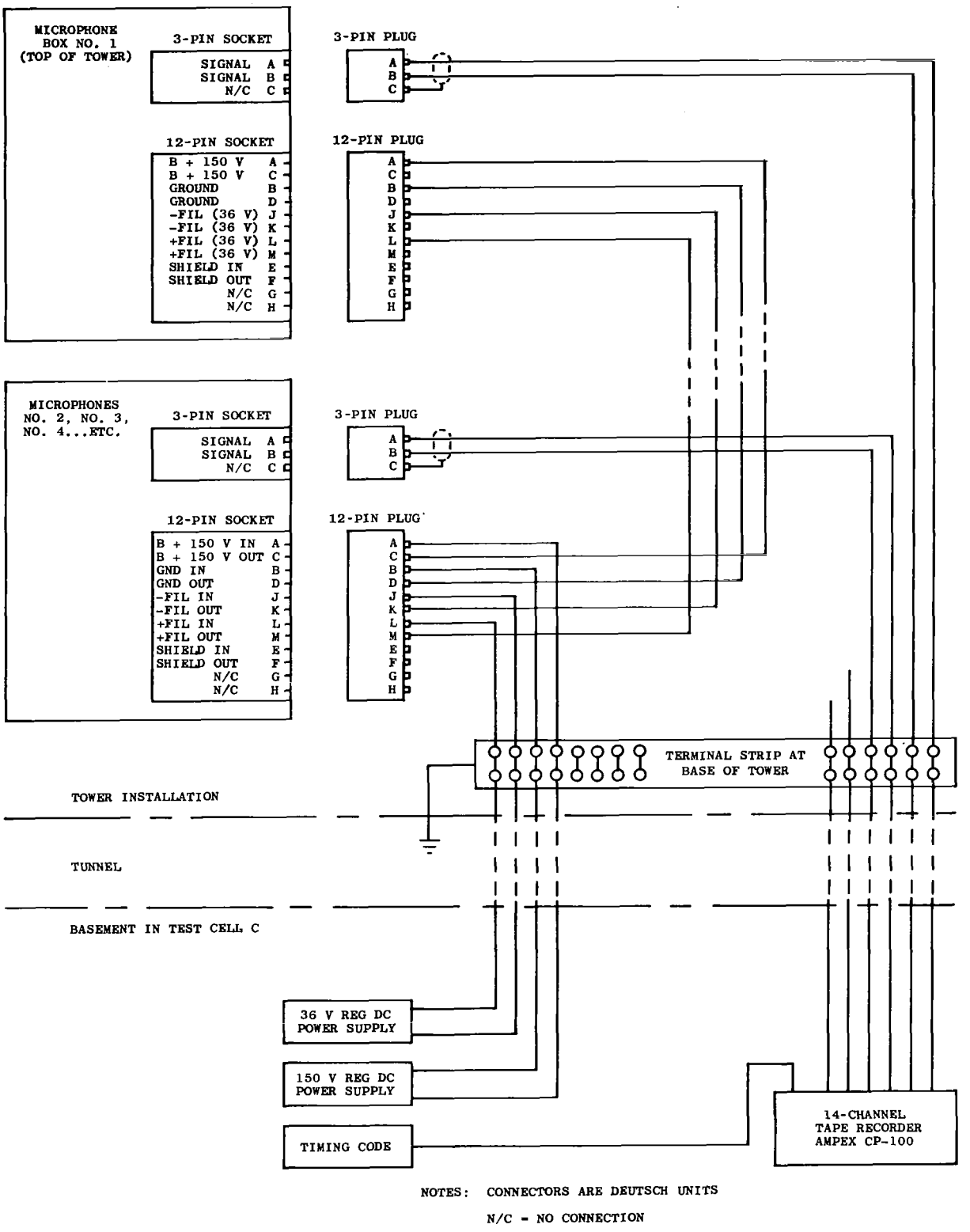

Figure A-1. Schematic of Signal and Power Distribution System

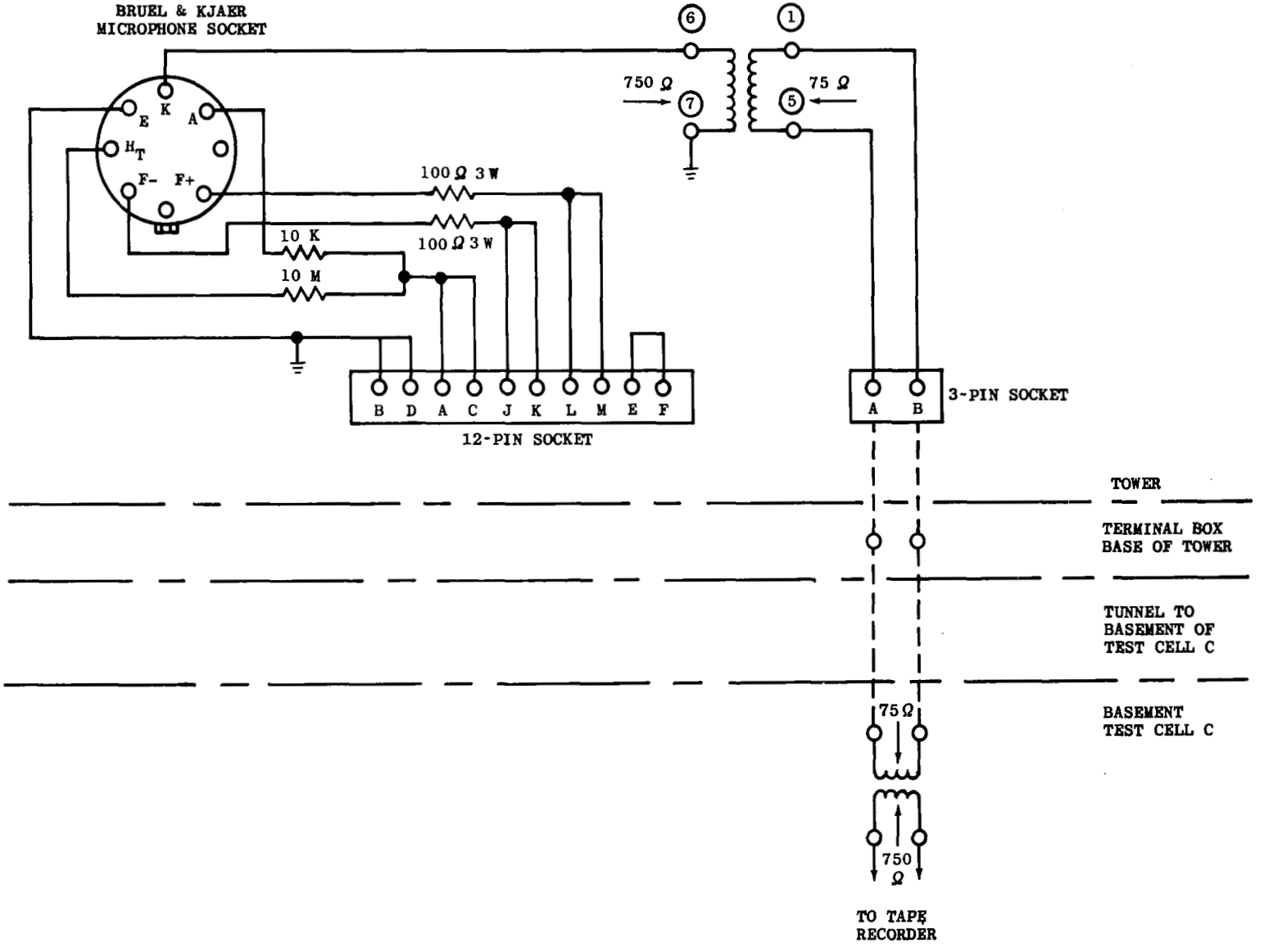

Figure A-2. Circuit Diagram of Microphone Box

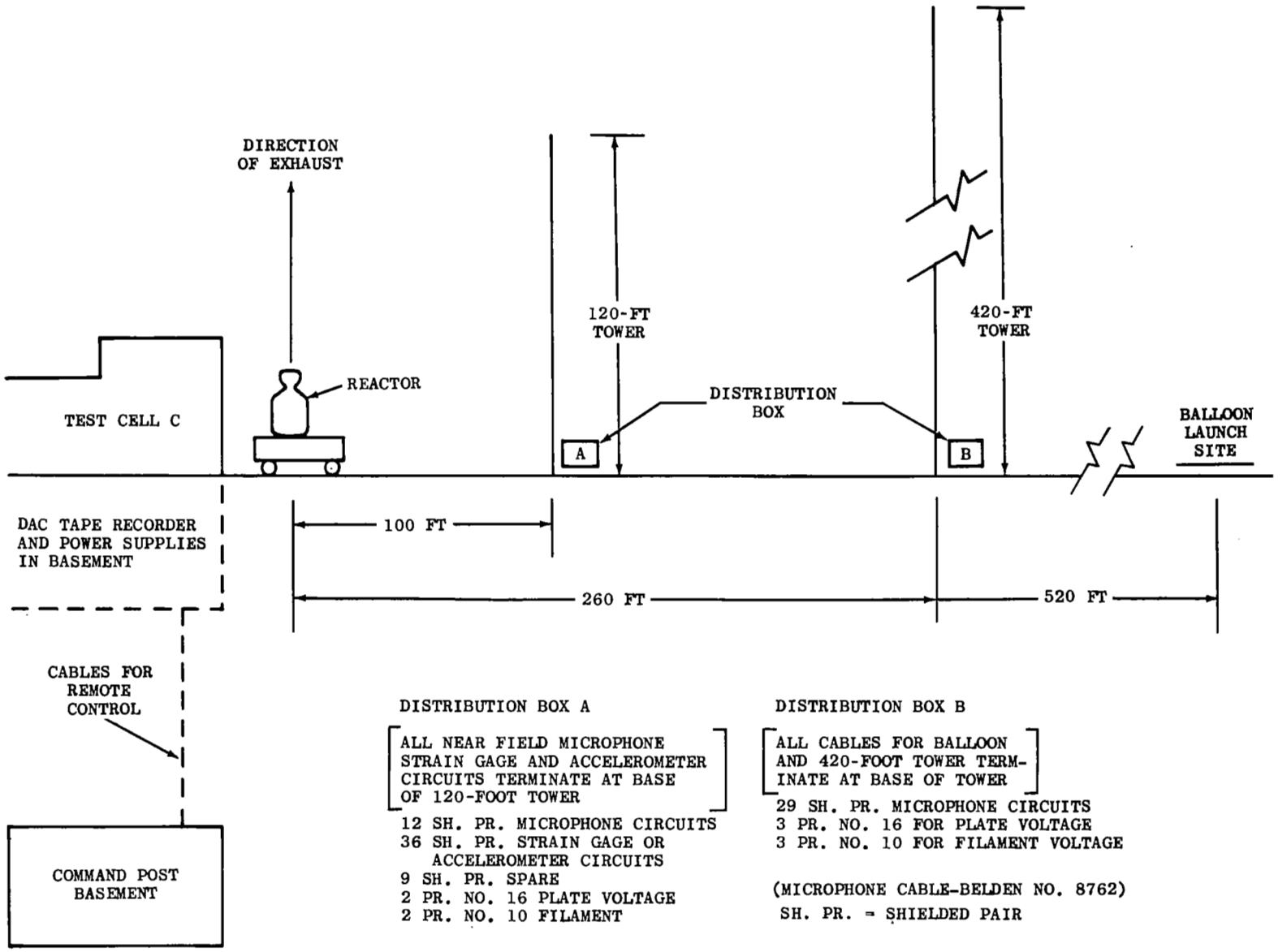

Figure A-3 Tower Signal and Power Cable Installation

APPENDIX B

METHOD USED TO CALCULATE SOUND POWER RADIATED FROM THE KIWI B EXHAUST

The sound power radiated from the jet exhaust was derived from the SPL's measured at each microphone position on the 420 foot tower. The measured SPL's were first corrected for distance to a hemisphere having a radius of 350 feet centered at the nozzle exit (see Fig. B-1). Next, the corrected SPL's were converted to an intensity level (IL see equation B-3) and multiplied by the area of the appropriate zone. The result was the sound power in watts passing through the zone. The total radiated sound power (in watts - see equation B-8) was the sum of the power passing through all of the zones. The sound power level (PWL) is given by equation B-9. Assuming that the SPL and the IL were approximately constant over the area of the zone, the sound power radiated out through zone i was

$$W_i = I_i A_i \quad \text{(watts)} \tag{B-1}$$

where I_i is the average sound intensity in watts/ft^2 of the i^{th} zone and A_i is the surface area of the i^{th} zone in ft^2.

The area of a zone of a hemisphere is given by

$$A_i = 2\pi R^2 (\cos \theta_j - \cos \theta_k) \quad (\text{ft}^2) \tag{B-2}$$

where R is the radius of the hemisphere and θ_j and θ_k are the limiting angles of the zone shown in Fig. B-1.

The intensity level IL was calculated by using the approximate identity

$$IL_i \doteq SPL_i \quad \text{(dB)} \tag{B-3}$$

where SPL_i = average sound pressure level over the i^{th} zone in dB re 0.0002 dynes/cm^2.

This relation is accurate to within 0.5 dB for most ambient conditions. By definition, the intensity level (IL_i) is:

$$IL_i = 10 \log_{10} \frac{I_i}{I_{ref}} \quad \text{(dB)} \tag{B-4}$$

where

$$I_{ref} = 10^{-16} \text{ watts/cm}^2 \doteq 10^{-13} \text{ watts/ft}^2 \tag{B-5}$$

therefore

$$I_i = 10^{\left(\frac{IL_i - 130}{10}\right)} \doteq 10^{\left(\frac{SPL_i - 130}{10}\right)} \text{ watts/ft}^2 \tag{B-6}$$

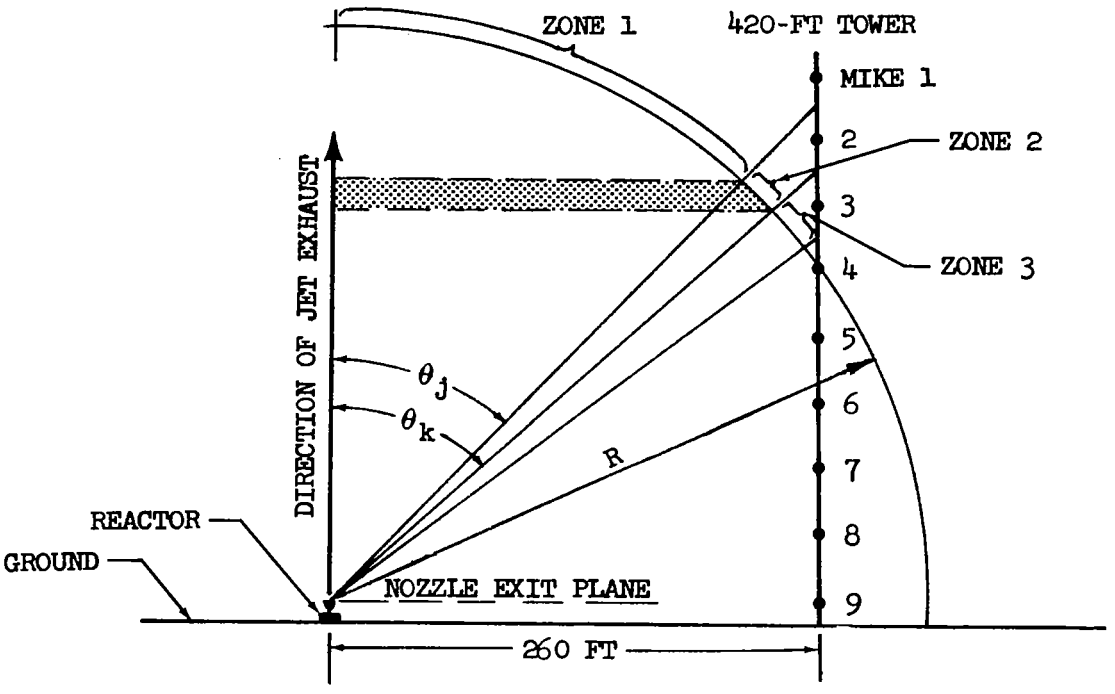

Figure B-1

and

$$W_i \doteq 10^{\left(\frac{SPL_i - 130}{10}\right)} 2\pi R^2 (\cos \theta_j - \cos \theta_k) \quad \text{(watts)} \tag{B-7}$$

The total sound power radiated through the hemisphere is:

$$W = \sum_{i=1}^{n} W_i \quad \text{(watts)} \tag{B-8}$$

where n is the number of microphone positions used for the calculation. The sound power level is given by

$$PWL = 10 \log_{10} \frac{W}{W_{ref}} = 10 \log_{10} \sum_{i=1}^{n} \frac{W_i}{W_{ref}} \quad \text{(dB)} \tag{B-9}$$

and $W_{ref} = 10^{-13}$ watts.

APPENDIX C

CALCULATIONS OF EQUIVALENT EXHAUST VELOCITIES

The equations and assumptions used in the method for calculating V_{eq} and a diagram of the KIWI B nozzle, with a list of associated parameters, are shown below:

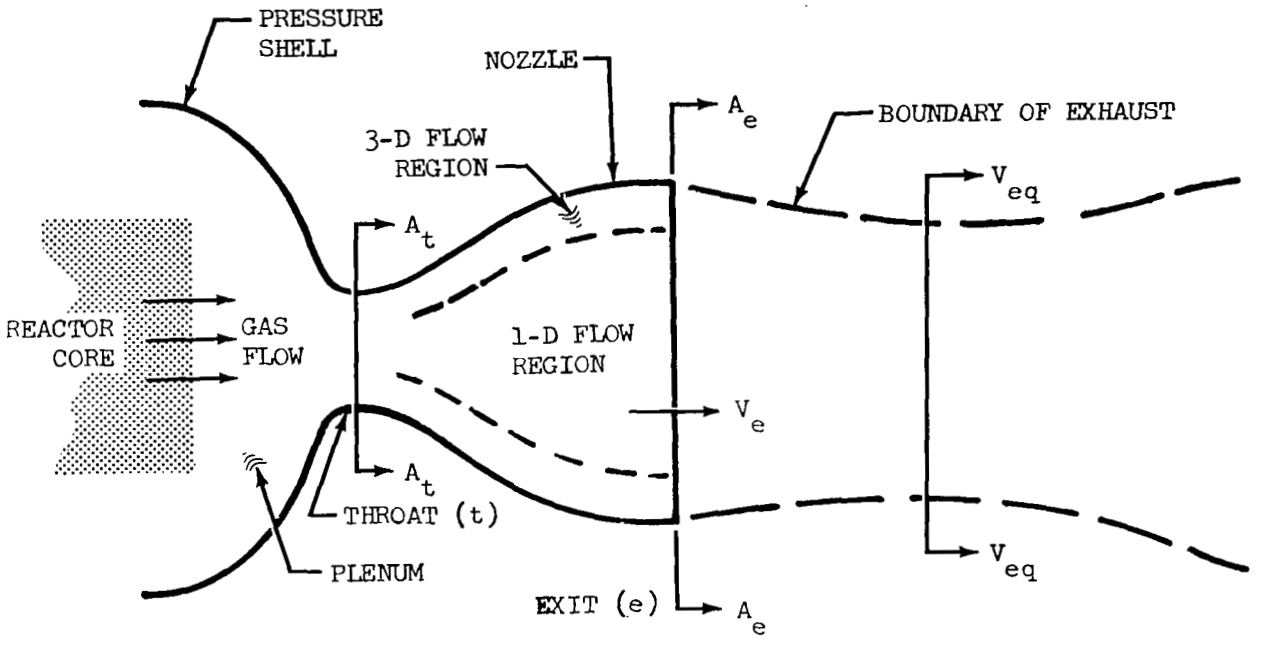

Measured Data:

$\dot{w}$	= gas weight flow	(lb/sec)
P	= pressure - plenum	(lb/in^2, absolute)
T	= gas temperature - plenum	($^\circ R$)
A_t	= nozzle throat area	(in^2)
A_e	= nozzle exit area	(in^2)

Gas Properties:

R	= gas constant	($ft\text{-}lb_f/lb_m\text{-}^\circ R$)
k	= ratio of specific heats	

Notes: k and R are assumed to have constant values. Static pressures and temperatures are designated by lower case letters. Total pressures and temperatures are designated by upper case letters.

The equations for one-dimensional compressible flow were obtained from ref. 9. It was assumed that there are no losses in total pressure and total temperature throughout the nozzle. First, calculations were made to ascertain that the nozzle throat was choked and, therefore, sonic flow conditions existed at the throat. The flow rate and gas temperature were used to calculate throat total pressure. For sonic flow at the throat (i.e., for a Mach number equal to unity), the general relation among the variables T, P, and A

$$\left(\frac{\dot{w}\sqrt{T}}{PA}\right)_t = \frac{\sqrt{\frac{kg}{R}\left(1 + \frac{k-1}{2}\right)}}{\left(1 + \frac{k-1}{2}\right)^{k/(k-1)}} = C_1 \text{ (constant for a specific k)} \quad (1)$$

Rearranging and solving for the pressure gives

$$P_t = \frac{\dot{w}_t\sqrt{T_t}}{C_1 A_t} \text{ (psia)} \quad (2)$$

The pressure ratio required for isentropic, one-dimensional expansion from the throat to the exit was obtained from the relation

$$\left(\frac{A_e}{A_t}\right)^2 = \frac{k-1}{2}\left[\frac{\left(\frac{2}{k+1}\right)^{(k+1)/(k-1)}}{\left(\frac{p_e}{P_t}\right)^{2/k}\left[1 - \left(\frac{p_e}{P_t}\right)^{(k-1)/k}\right]}\right] \quad (3)$$

by solving for p_e/P_t using $A_e/A_t = 11.85$. Note that this is the ratio of static pressure at the nozzle exit to the total pressure at the throat.

For the KIWI B nozzle, with a fixed area ratio and for a given value of k, we have $p_e/P_t = C_2$, and the static pressure in the one-dimensional flow region at the exit is $p_e = C_2 P_t$.

Having established the values for p_e/P_t using an iterative procedure, and for P_t from equation (2), the Mach number (M_e) and velocity at the exit (V_e) were obtained by the following equations:

$$M_e = \left(\frac{2}{k-1}\right)^{1/2}\left[\left(\frac{p_e}{P_t}\right)^{-(k-1)/k} - 1\right]^{1/2} \quad (4)$$

$$V_e = M_e c_e \quad (5)$$

where c_e is the speed of sound in the flow at the exit. This is related to the temperature of the gas by

$$c_e = \sqrt{kgRt_e} = \sqrt{kgRT_e \times \frac{t_e}{T_e}} \tag{6a}$$

Assuming that $T_e = T_t$, we have

$$c_e = \sqrt{kgRT_t}\ \sqrt{\frac{t_e}{T_t}} \tag{6b}$$

The relation between temperature and pressure is given by

$$\frac{t_e}{T_t} = \left(\frac{p_e}{P_t}\right)^{(k-1)/k} \tag{6c}$$

and equation (6b) becomes

$$c_e = \sqrt{kgRT_t}\ \sqrt{\left(\frac{p_e}{P_t}\right)^{(k-1)/k}} \tag{6d}$$

Solving for the pressure ratio in equation (4) and inserting this value into equation (6d), we obtain

$$V_e = \sqrt{kgRT_t}\ \sqrt{\frac{M_e^2}{1 + \left(\frac{k-1}{2}\right)M_e^2}} \tag{7}$$

For three-dimensional flow conditions, the nozzle design pressure ratio for complete expansion to the exit is

$$p_e/P_t = 0.0117 \tag{8}$$

and the separation pressure ratio is

$$p_s/p_a = 0.35 \tag{9}$$

where p_s is the static pressure measured at the nozzle wall where the flow separates, and p_a is ambient pressure. Since the nozzle will have an overexpanded flow at the test site, the flow static pressures at the exit (p_e) for the one-dimensional and three-dimensional regions were less than p_a. However, flow separation in the nozzle does not occur unless p_e is less than p_s. The effects of flow separation are discussed later and V_{eq} is calculated assuming the flow did not separate.

The pressure ratio for the three-dimensional flow was used in equation (4) to obtain the Mach number at the exit; the velocity at the exit for the three-

dimensional condition was then obtained from equation (7).

The ideal thrust of the engine in terms of nozzle exit parameters is given by

$$F_{ideal} = \frac{\dot{w}V_e}{g} + (p_e - p_a)A_e \quad \text{(lb)} \tag{10a}$$

or, in terms of equivalent velocity, by

$$F_{ideal} = \frac{\dot{w}V_{eq}}{g} \quad \text{(lb)} \tag{10b}$$

The exit velocity and pressure for unseparated, one-dimensional and three-dimensional flow conditions were inserted into equation (10a) to obtain a value of thrust for each condition. The corresponding equivalent exit velocities were then calculated by using first the thrust for the one-dimensional and then the three-dimensional values, using

$$V_{eq} = \frac{Fg}{w} \quad \text{(ft/sec)} \tag{11}$$

Thus, two values were obtained for V_{eq}. Since the values were very close and both flow regions existed in the nozzle, they were averaged to estimate the average diffused flow velocity for the conditions where flow static pressure was equal to ambient atmospheric pressure.

Flow Separation

A check for flow separation was made in each case by comparing the static pressure at the exit (p_e) (calculated using the three-dimensional pressure ratio) with the separation pressure (p_s), see equations (8) and (9). If p_e was less than p_s, separation occurred in the nozzle. The calculations, however, were made assuming that separation did not occur, and the exit parameters and V_{eq} were obtained from equations (4), (7), and (11).

Next, the ratio p_s/P_t was inserted into equation (4) to estimate a Mach number in the plane of separation in the nozzle.

The parameters for the separated flow were then inserted into equations (10) and (11) to estimate a value for V_{eq}. This is reasonable since the unknown value for the area of the separation plane, to be used in equation (10), would probably not be significantly less than A_e.

Finally, the value for V_{eq} estimated for the separated case and the V_{eq} value calculated for the unseparated, one-dimensional and three-dimensional flow conditions were averaged to obtain a representative V_{eq} for the exhaust flow (these three numbers are within 10 percent of each other). The estimated accuracy of the value V_{eq}, based on data measured during each test, is $\pm$ 10 percent.

Mechanical Stream Power of the Jet Exhaust

Using the values of V_{eq} and thrust F, as derived above, the mechanical power W_m was calculated using the relationship

$$W_m = 0.678\ FV_{eq}\ \text{(watts)}$$

Summary of Engine Flow Parameters

An unclassified summary of the exhaust flow parameters for maximum gas flows, including mechanical power and V_{eq} for the EP's of 8 and 21 August 1963, the 9 January 1964 CF Tests, and the power runs of 13 May and 28 August 1964, is presented in Table VII. A more complete tabulation is available in a classified appendix to this report. The August 1963 velocities have not been calculated since the flows were too low and separation occurred deep within the nozzle.

APPENDIX D

CALCULATION OF PANEL RESONANCE - DYER'S APPROACH

To analytically approximate the response of the flat plate placed in the acoustic field at 130 feet from the KIWI B engine, the equation of motion given by I. Dyer in ref. 8 was used. Laboratory measurements of the fundamental resonance of the plate indicated that the mounting provided simply supported boundary conditions of the edges. The following equations describe the plate displacement correlation as

$$\langle w(x, y, t)w^*(x', y', t')\rangle = p^2 \int_{-\infty}^{t} dt_o \int_{-\infty}^{t'} dt_o' \int_0^{L_x} dx_o \int_0^{L_x} dx_o' \int_0^{L_y} dy_o \int_0^{L_y} dy_o'$$

$$\cdot \sum_{m,n=1}^{\infty} \left\{ \frac{1}{\omega_{mn} M} \left[\frac{2}{(L_x L_y)^{1/2}} \sin \frac{m\pi x}{L_x} \sin \frac{n\pi y}{L_y} \right] \right.$$

$$\cdot \left[\frac{2}{(L_x L_y)^{1/2}} \sin \frac{m\pi x_o}{L_x} \sin \frac{n\pi y_o}{L_y} \right] e^{-a_{mn}(t-t_o)}$$

$$\left. \cdot \sin \left[\omega_{mn}(t - t_o)U(t - t_o) \right] \right\}$$

$$\cdot \sum_{p,q=1}^{\infty} \left\{ \frac{1}{\omega_{pq} M} \left[\frac{2}{(L_x L_y)^{1/2}} \sin \frac{p\pi x'}{L_x} \sin \frac{q\pi y'}{L_y} \right] \right.$$

$$\cdot \left[\frac{2}{(L_x L_y)^{1/2}} \sin \frac{p\pi x_o'}{L_x} \sin \frac{q\pi y_o'}{L_y} \right] e^{-a_{pq}(t'-t_o')}$$

$$\left. \cdot \sin \left[\omega_{pq}(t' - t_o')U(t' - t_o') \right] \right\}$$

$$\cdot \left\{ \Phi(x_o - x_o') e^{-\beta|t_o - t_o'|} \right\}$$

Here the unit functions U(t) are = 0 when $t < t_o$ or $t' < t_o'$

= 1 when $t > t_o$ or $t' > t_o'$

The other symbols are as follows:

$\langle \ldots \rangle$ = the time average

p = the mean squared pressure at the modal frequency for sinusoidal excitation or the power spectral density amplitude times the effective bandwidth for random excitation

$\langle w \cdot w^* \rangle$ = mean square displacement of the neutral plane of the plate

x, y = spatial locations of an arbitrary point on the plate

$*$ = complex conjugate

ω_{mn} or ω_{pq} = modal frequencies

M = mass per unit area

$L_x L_y$ = dimensions of the plate

m, n, p, q = modal subscripts

a_{mn} or a_{pq} = the modal damping coefficient including both viscous and hysteretic damping, related to the ratio of viscous damping to critical damping (C/C_c) by:

$$a_{mn} = \frac{2\pi C/C_c}{\sqrt{1 - (C/C_c)^2}}$$

$\Phi(x_o - x_o')$ = some spatial correlation function of the excitation in the x direction (assuming perfect correlation in the y direction)

β = the rate of decay of the maxima of the temporal correlation when the space time correlation function is projected on the time axis

Now if it is assumed that the modes are uncoupled and thereby independent ($m = p$ and $n = q$) and if we utilize the following equivalence:

$$B = \frac{16 \sin \frac{m\pi x}{L_x} \sin \frac{n\pi y}{L_y} \sin \frac{m\pi x'}{L_x} \sin \frac{n\pi y'}{L_y}}{M^2 L_x^2 L_y^2 \omega_{mn}^2}$$

and $\frac{m\pi}{L_x} = k_m$, $\frac{n\pi}{L_y} = k_n$, $X_o = x_o - x_o'$, $\tau_o = t_o - t_o'$, $\tau = t - t'$, $\gamma = (t' - t_o') - (t - t_o) = \tau_o - \tau$, and $\mu = (t' - t_o') + (t - t_o)$, the latter two after R. H. Lyon, (with the understanding that the summation and integration processes can be interchanged), we can therefore write for the modal response:

$$\langle w \cdot w^* \rangle_{mn} = B \left\{ \int_0^{L_y} dy_o \int_0^{L_y} dy_o' \sin k_n y_o \sin k_n y_o' \right.$$

$$\cdot \int_0^{L_x} dx_o' \int_{-x_o'}^{L_x - x_o'} dX_o \sin k_m (X_o + x_o') \sin k_m x_o' |\Phi(x_o - x_o')|$$

$$\left. \cdot \int_0^{\infty} \frac{1}{2} d\mu \int_{-\mu}^{+\mu} d\gamma \exp [- a_{mn}\mu - \beta|\gamma + \tau|] \frac{\cos \omega_{mn}\gamma - \cos \omega_{mn}\mu}{2} \right\}$$

Since the analysis necessary to identify the mathematical expression of the space-time correlation for the KIWI B sound field was not authorized by this study, the expression $|\Phi(x_o - x_o')|$ is approximated by an exponential $e^{-\alpha|X_o|}$, such a correlation function being applicable to a stationary field, and which lends itself to integration. The correlation function, which fits the data reasonably well represents a decreasing spectrum shape near the modal frequency. The error introduced by this approximation is small.

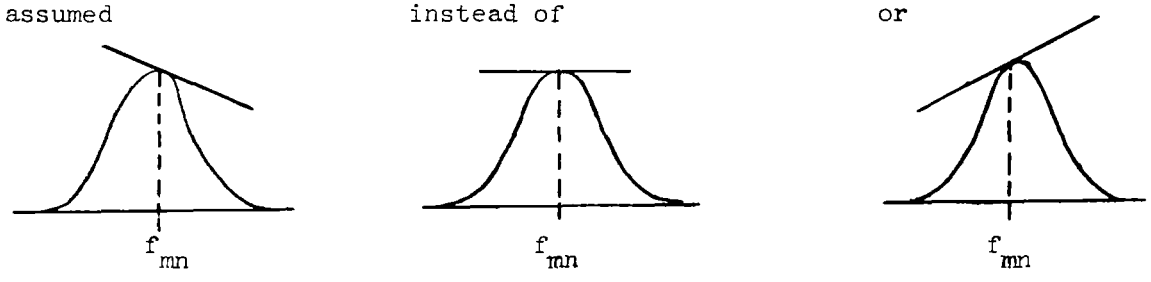

The first double integral becomes $[1 - (-1)^n]^2/k_n^2$ and thereby excludes the modes where n is even. The second integral can be written

$$I_2 = \int_0^{L_x} dx_o' \sin k_m x_o' \left\{ \cos k_m x_o' \int_{-x_o'}^{L_x - x_o'} dX_o \sin k_m X_o e^{-\alpha|X_o|} \right.$$

$$\left. + \sin k_m x_o' \int_{-x_o'}^{L_x - x_o'} dX_o \cos k_m X_o e^{-\alpha|X_o|} \right\}$$

because of the absolute value sign on X_o in the exponential, two additional terms

result. Expansion, integration and collection of terms yields

$$I_2\,(\alpha^2 + k_m^2) = k_m \int_0^{L_x} dx_o' e^{-\alpha x_o'} \sin k_m x_o' + 2\alpha \int_0^{L_x} \sin^2 k_m x_o'$$

$$- \int_0^{L_x} dx_o' e^{-\alpha x_o'} \sin k_m x_o' \left[\alpha e^{-\alpha L_x} \sin k_m L_x + k_m e^{-\alpha L_x} \cos k_m L_x \right]$$

with further integration, and $\sin k_m L_x = \sin m\pi = 0$,

$$I_2 = \frac{1}{(\alpha^2 + k_m^2)} \left\{ L_x \alpha + \frac{2k_m^2}{\alpha^2 + k_m^2} \left[1 - (-1)^m e^{-\alpha L_x} \right] \right\}$$

It is interesting to note that if a Delta function of the sort $\zeta(x_o - x_o')$ had been used instead of the exponential, the result would have been even simpler.

$$I_{2(\zeta)} = \frac{L_x}{2}$$

The third double integral (involving time), after integration, collection of terms, and simplification, can be shown to be the following:

$$4I_3 = \frac{e^{-a_{mn}\tau} \left\{ (-a_{mn} - \beta) \cos \omega_{mn} + \omega_{mn} \sin \omega_{mn}\tau \right\}}{(a_{mn} + \beta)^2 + \omega_{mn}^2} \left[-\frac{1}{\beta} + \frac{\beta}{\beta^2 + \omega_{mn}^2} \right]$$

$$- \frac{\omega_{mn} e^{-a_{mn}\tau}}{(\beta^2 + \omega_{mn}^2)} \left[\frac{(-a_{mn} - \beta) \sin \omega_{mn}\tau - \omega_{mn} \cos \omega_{mn}\tau}{(a_{mn} + \beta)^2 + \omega_{mn}^2} \right]$$

$$- \frac{\omega_{mn}^2 e^{-a_{mn}\tau}}{\beta(\beta^2 + \omega_{mn}^2)} \left[\frac{(-a_{mn} + \beta) \cos \omega_{mn}\tau + \omega_{mn} \sin \omega_{mn}\tau}{(-a_{mn} + \beta)^2 + \omega_{mn}^2} \right]$$

$$+ \frac{1}{(\beta^2 + \omega_{mn}^2)[(-a_{mn} + \beta)^2 + \omega_{mn}^2]} \left[\omega_{mn} e^{-a_{mn}\tau} \left\{ (-a_{mn} + \beta) \sin \omega_{mn}\tau \right.\right.$$

$$\left.\left. - \omega_{mn} \cos \omega_{mn}\tau \right\} + \omega_{mn}^2 e^{-\beta\tau} + \left(1 - \frac{a_{mn}}{\beta}\right)(\beta^2 + \omega_{mn}^2) + a_{mn}\beta e^{-\beta\tau} - \beta^2 e^{-\beta\tau} \right]$$

$$+ \frac{2e^{-a_{mn}\tau}\ \beta \cos \omega_{mn}\tau}{a_{mn}(\beta^2 + \omega_{mn}^2)} + \frac{1}{[(a_{mn} + \beta)^2 + \omega_{mn}^2]} \left[\frac{e^{-\beta\tau}}{\beta}(a_{mn} + \beta) + \frac{\omega_{mn}^2 e^{-\beta\tau}}{(\beta^2 + \omega_{mn}^2)} \right.$$

$$\left. - \frac{\beta e^{-\beta\tau}(a_{mn} + \beta)}{(\beta^2 + \omega_{mn}^2)} \right] + \frac{2e^{-a_{mn}\tau}}{\beta(a_{mn}^2 + \omega_{mn}^2)} \left[- a_{mn} \cos \omega_{mn}\tau + \omega_{mn} \sin \omega_{mn}\tau \right]$$

To get the mean squared displacement at a single position on the flat plate, $x = x'$ and $\tau = 0$. For this special case, the total mean squared displacement becomes

$$\langle w \cdot w^* \rangle = \sum_{m,n=1}^{\infty} \left[\frac{4p^2 \sin^2 k_m x \sin^2 k_n y}{M^2 L_x^2 L_y^2 \omega_{mn}^2} \left\{ \frac{[1 - (-1)^n]^2}{\left(\frac{n\pi}{L_y}\right)^2} \right\} \right.$$

$$\left\{ \frac{1}{\alpha^2 + \left(\frac{m\pi}{L_x}\right)^2} \left[L_x \alpha + \frac{2\left(\frac{m\pi}{L_x}\right)^2}{\alpha^2 + \left(\frac{m\pi}{L_x}\right)^2} \left(1 - \{-1\}^m e^{-\alpha L_x}\right) \right] \right\}$$

$$\left. \left\{ \frac{4\omega_{mn}^2 + 2\frac{a_{mn}\omega_{mn}^2}{\beta}}{(\beta^2 + \omega_{mn}^2)[(a_{mn} + \beta)^2 + \omega_{mn}^2]} + \frac{2\beta}{a_{mn}(\beta^2 + \omega_{mn}^2)} - \frac{2a_{mn}}{\beta(a_{mn}^2 + \omega_{mn}^2)} \right\} \right]$$

To compare with experimentally measured acceleration levels, values for all the variables were found experimentally and the mean squared displacement found for each accelerometer location for each mode. This was converted to a zero to peak acceleration by the relationship that

$$\text{Accel}_{grms} = \sqrt{\text{Displ}_{pk\text{-}pk}^2}\,(0.102\ f^2) \cdot \beta w_{eff} = 2.6 \times 10^{-3} \sqrt{\langle w \cdot w^* \rangle}\ \omega_{mn}^2 \beta w_{eff}$$

if $\langle w \cdot w^* \rangle$ is in feet squared and βw_{eff} is the effective bandwidth of the random excitation which is contributing to the modal response. βw_{eff} is given by

$$\beta w_{eff} = \frac{\pi}{2} \frac{\omega_{mn}}{Q} = \pi \omega_{mn} \frac{C}{C_c}$$

The calculated values for acceleration at the two locations on the plate are given in Table IX.

REFERENCES

1. Manhart, J. K., An Acoustical Study of the KIWI A-3 Engine, Report SM-37990, Douglas Aircraft Company, April 11, 1961 (C).

2. Manhart, J. K., Evaluation of Microphone Performance in a Field of Intense Nuclear Radiation, Engineering Paper 1356, Douglas Aircraft Company, May 23, 1962.

3. Cole, J. N., et al, "Noise Radiation from Fourteen Types of Rockets in the 1000 to 130 000 Pounds Thrust Range," WADC Report TR-57-354, 1957.

4. Morgan, W. V., and Kenneth J. Young, Studies of Rocket Noise Simulation with Substitute Gas Jets and the Effects of Vehicle Motion on Jet Noise, ASD-TDR-62-787, March 1963.

5. Howes, Walton L., "Similarity of Far Noise Fields of Jets," NASA Report TR-R-52, 1960.

6. Dyer, Ira, "Response of Plates to a Decaying and Convecting Random Pressure Field," Journal of Acoust. Soc. of Am., Vol. 31, No. 7, July 1959.

7. Powell, A., "On the Response of Structures to Random Pressures and to Jet Noise in Particular," Chapter 8 of Random Vibrations, edited by S. H. Crandall, Technology Press of MIT, 1958.

8. Shapiro, A. H., The Dynamics and Thermodynamics of Compressible Fluid Flow, Volume 1, Ronald Press Company, New York, 1953.

9. Bonney, E. A., Engineering Supersonic Aerodynamics, McGraw Hill Book Company, New York, 1950.

10. Mayes, W. H., and W. E. Lanford, Near Field and Far Field Noise Surveys of Solid Fuel Rocket Engines for a Range of Nozzle Exit Pressures, NASA TN D-21, August 1959.

TABLE I.- SCHEDULE OF ELECTRICAL CALIBRATIONS

DURATION OF CALIBRATION SIGNAL - 5 SECONDS AT EACH FREQUENCY

Engine	EP	Date	Microphone Positions	Type of Calibration
KIWI B-4B/CFT	I	8 August 1963	1-12	Calibration 10-10 K
KIWI B-4B/CFT	II, III	21 August 1963	1-12	Calibration 10-10 K
High Flow Acoustical Test		9 January 1964	1-10, 12-19	Calibration 10-10 K
KIWI B-4D-202	IV	13 May 1964	1-9, 15-20, 21-26,	
			11-14	Calibration 200-25 K
			17-19	Calibration 200-25 K
				Phase Calibration
KIWI B-4E-301	V	28 August 1964	2, 4, 5	Calibration 20-18 K
			6-9, 20	Calibration 10-10 K
			17-19, 28-30	Phase Calibration

Calibration Frequencies in cps

Calibration 30-18 K: 1 K, 30, 50, 100, 500, 1-2-4-6-10-15-18 K

Calibration 10-10 K: 1 K, 5, 10, 20, 50, 100, 500, 1-2-4-6-8-10-15 K

Calibration 200-25 K: 1 K, 200, 250, 300, 500, 1-2-4-6-10-15-20-25 K

Phase Calibration Applied to Groups of 2, 3, or 4 Microphones Simultaneously:
1 K, 10, 20, 50, 100, 150, 200--in 50 cps increments to 1 K, 1.1 K, 1.2 K--in 100 cps increments to 2 K, 2-3-6-8-10 K

TABLE II.- KIWI B-4D COLD FLOW TEST

GN_2 and GH_2

Test Dates: 8 and 21 August 1963

Recorder Channel	Microphone Number	Frequency Response in cps	Sensitivity for Maximum Record Level	Location	Height Above Ground in feet
1	1	10-10 K	141 dB	420 ft Tower	410
2	2	10-10 K	141 dB	420 ft Tower	360
3	3	10-10 K	141 dB	420 ft Tower	310
4	4	10-10 K	141 dB	420 ft Tower	260
5	5	10-10 K	141 dB	420 ft Tower	210
6	6	10-10 K	141 dB	420 ft Tower	160
7	7	10-10 K	141 dB	420 ft Tower	110
8	8	10-10 K	141 dB	420 ft Tower	60
9	9	10-10 K	141 dB	420 ft Tower	10
10	10	10-10 K	141 dB	500 ft on ground	1
11	11	10-10 K	151 dB	120 ft Tower	50
12	12	10-10 K	151 dB	120 ft Tower	25

TABLE III. - HIGH GAS FLOW ACOUSTICAL TEST

GH_2 and GHe

Test Date: 9 January 1964

	Recorder Channel	Microphone Number	Frequency Response in cps	Sensitivity for Maximum Record Level	Location	Height Above Ground in feet
Recorder A	1	Not Used				
	2	2	10-10 K	147 dB	420 ft Tower	360
	3	3	10-10 K	147 dB	420 ft Tower	310
	4	4	10-10 K	147 dB	420 ft Tower	260
	5	5	10-10 K	147 dB	420 ft Tower	210
	6	6	10-10 K	147 dB	420 ft Tower	160
	7	7	10-10 K	147 dB	420 ft Tower	110
	8	Spare				
	9	9	10-10 K	145 dB	420 ft Tower	10
	10	10	10-10 K	145 dB	520 ft from engine on ground	
	11	Timing Channel				
	12	12	10-10 K	161 dB	120 ft Tower	75
	13	13	10-10 K	161 dB	120 ft Tower	50
	14	14	10-10 K	161 dB	120 ft Tower	25
Recorder B	1	15	10-10 K	181 dB	Test Cell Face	
	2	Accelerometer No. 1				
	3	16	10-10 K	181 dB	3 ft below mike 15	
	4	8	10-10 K	147 dB	420 ft Tower	60
	5	Accelerometer No. 3				
	6	Accelerometer No. 4				
	7	Accelerometer No. 5				
	8	17	10-10 K	161 dB	Test Cell Pad	
	9	Accelerometer No. 6				
	10	18	10-10 K	161 dB	Test Cell Pad	
	11	Timing Channel				
	12	19	10-10 K	161 dB	Test Cell Pad	
	13	Spare				
	14	1	10-10 K	156 dB	420 ft Tower	410

TABLE IV.- KIWI B-4D FULL POWER RUN

Test Date: 13 May 1964

	Recorder Channel	Microphone Number	Frequency Response in cps	Sensitivity for Maximum Record Level	Location	Height Above Ground in feet
Recorder A	1	15	10-10 K	161 dB	Test Cell Face	
	2	21	10-10 K	141 dB	Top of Balloon Array	580
	3	Spare				
	4	22	10-10 K	141 dB	Balloon Array	480
	5	23	10-10 K	141 dB	Balloon Array	380
	6	24	10-10 K	141 dB	Balloon Array	280
	7	25	10-10 K	141 dB	Balloon Array	180
	8*	17	10-10 K	161 dB	Test Cell Pad	111
	9*	Accelerometer		3 g	LH_2 Dewar	
	10*	18	10-10 K	161 dB	Test Cell Pad	115
	11*	20	10-10 K	151 dB	Dewar Mike	
	12	19	10-10 K	161 dB	Test Cell Pad	117
	13*	26	10-10 K	141 dB	Balloon Array	80
	14*	Timing Channel				
Recorder B	1	1	10-10 K	141 dB	420 ft Tower	410
	2	2	10-10 K	141 dB	420 ft Tower	360
	3	3	10-10 K	141 dB	420 ft Tower	310
	4	4	10-10 K	141 dB	420 ft Tower	260
	5	5	10-10 K	151 dB	420 ft Tower	210
	6	6	10-10 K	151 dB	420 ft Tower	160
	7	7	10-10 K	151 dB	420 ft Tower	110
	8*	8	10-10 K	151 dB	420 ft Tower	60
	9*	9	10-10 K	151 dB	420 ft Tower	10
	10*	Timing Channel				
	11*	11	300-20 K	151 dB	120 ft Tower	100
	12*	12	300-20 K	151 dB	120 ft Tower	75
	13*	13	300-20 K	151 dB	120 ft Tower	50
	14*	14	300-20 K	151 dB	120 ft Tower	25

*Indicates recorder channels on monitor scopes.

TABLE V.- KIWI B-4E FULL POWER RUN

Test Date: 28 August 1964

	Recorder Channel	Microphone Number	Frequency Response in cps	Sensitivity for Maximum Record Level	Location	Height Above Ground in feet
Recorder A	1	29	10-10 K	161 dB	Pad - 50 ft from Reactor	
	2	20	10-10 K	161 dB	Over Panel at 130 ft	
	3	30	10-10 K	161 dB	Pad - 56 ft from Reactor	
	4	21	10-10 K	170 dB	Kaman Mike over Panel, 30 feet from Reactor	
	5	22	Microphone Evaluation Channel*	-----		
	6	6	10-10 K	141 dB	420 ft Tower	160
	7	7	10-10 K	151 dB	420 ft Tower	110
	8	17	10-10 K	161 dB	Pad - 110 ft from Reactor	
	9	9	10-10 K	141 dB	420 ft Tower	10
	10	18	10-10 K	161 dB	Pad - 110 ft 9 in from Reactor	
	11	8	10-10 K	151 dB	420 ft Tower	60
	12	19	10-10 K	161 dB	Pad - 120 ft from Reactor	
	13	Timing Channel (5-second Time Code)				
	14	28	10-10 K	161 dB	Pad - 4 ft from Mike 19	
Recorder B	A	2	30-18 K	141 dB	420 ft Tower	360
	B	4	30-18 K	141 dB	420 ft Tower	260
Recorder C	A	5	30-18 K	141 dB	420 ft Tower	210
	B	Microphone Evaluation Channel*				

*Denotes a test to evaluate radiation effects.

TABLE VI.- METEROLOGICAL DATA FOR KIWI B ACOUSTICAL TESTS

Activity and Date	Time of Day	Wind Conditions Speed (mph)	Direction	Outside Air Temperature °F	% Relative Humidity
EP I 8/8/63	0900	5 - 9	239°	100	19
	1000	7 - 12*	247°	102	18
	1100	9 - 23*	208°	104	18
	1200	12 - 21*	196°	104	17
	1300	11 - 21*	212°	106	17
	1400	8 - 22*	211°	106	17
EP II & III 8/21/63	0800	7.2	288°	80.6	16
	0900	4.9	246°	82.5	15
	1000	5.3	268°	86.9	13
	1100	8.9	199°	91.7	12
	1200	8.4	230°	93.2	11
KIWI B High Flow Acoustical Test 1/9/64	0900	0	---	30	20
	1000	2	360°	36	18
	1100	5	306°	40	16
	1200	6	255°	42	15
	1300	3	225°	42	15
	1400	4	221°	42	15
	1500	4	241°	40	15
EP IV 5/13/64	1000	13	225°	80	18
	1100	13	220°	80	16
EP V 8/28/64	1200	8	---	82	14
	1300	8	---	82	13

*Sporadic Gusts

TABLE VII

Comparison of Engine Performance Parameters

Rocket Engine	Thrust in lbs	Nozzle Diameter ft	Weight Flow lbs/sec	Equivalent Velocity ft/sec	Exhaust Density lbs/ft^3	Density Ratio (eff) ρ_{eff}/ρ_a	Gas Constant R ft-lb/lb-°R	Mech Stream Power watts	Sound Power Level PWL in dB	Mach No. M_e	Notes
KIWI B-4B/CF GN_2 8-8-63	--	.153	85 / 69	---	---	---	55	---	182 / 173	--	Simulated Nozzle
KIWI B-4B/CF GH_2/LH_2 8-8-63	--	.153 / .243	24 / 35	---	3.73×10^{-3}	.0545	772	---	179	--	Simulated Nozzle
KIWI B-4B/CFT GN_2 8-21-63	--	2.5	43 & 52	---	---	---	55	---	168		Gas Exit Temperature 490°R
KIWI B-4B/CFT GH_2 8-21-63	--	2.5	24	---	3.73×10^{-3}	.0545	772	---	176		Gas Exit Temperature 530°R
KIWI B High Flow Test GHe 1-9-64	12 400	2.5	130	3200	8.28×10^{-3}	0.1210	387	2.8×10^7	182	4.2	Gas Exit Temperature 465°R
KIWI B High Flow Test GH_2 1-9-64	16 600	2.5	100	5400	3.73×10^{-3}	.545	772	6.2×10^7	180	3.3	Gas Exit Temperature 533°R
KIWI B-4D Power Run 5-13-64	38 300	2.5	69	17 900	0.79×10^{-3}	0.0115	772	47×10^7	191	3.7	
KIWI B-4E Power Run 8-28-64	41 750	2.5	69	19 500	0.72×10^{-3}	.105	772	55×10^7	190	3.7	
Model Rocket* GHe (Hot)	250	.12	.965	8320	0.86×10^{-3}	0.1285	387	0.15×10^7	175	3.12	Plenum Temperature 1560°R
Rocket** C	100 000	x	x	x	38.7×10^{-3}	.5050	62	42×10^7	195		
E	48 400	x	x	x	15×10^{-3}	.1960	62	20.3×10^7	190		
F	34 000	x	x	x	14.6×10^{-3}	.1910	62	15.7×10^7	190		
H	5000	x	x	x	13×10^{-3}	.1690	62	2.2×10^7	176		

x Classified
* From Reference 4
** From Reference 3

TABLE VIII.- COMPARISON OF PREDICTED AND MEASURED PANEL RESPONSE TO SIMUSOIDAL EXCITATION

Data from Center of Panel Only

Measured Resonance Frequencies cycles/second	Incident Sound Pressures lb/ft^2	Measured Accelerations in Laboratory g's, 0-peak **unbaffled**	Measured Accelerations In Field g's, 0-peak **baffled**	Theoretical Mode Numbers	Predicted Resonance Frequencies cycles/second	Predicted Acceleration g's, 0-peak (for same incident pressure)
35	0.115		0.315			
40	0.15	0.916		1, 1	39	0.322
57	0.085	0.107		1, 2	62	Not Excitable
85 88	0.19 0.19		0.169 0.30	Not Predictable		
100	0.22		0.119	1, 3	101	0.095
190 207	0.26 0.44	0.44	0.34	2, 3 1, 5	194 226	Not Excitable 0.0625
330	0.30		0.295	3, 1	288	0.108

TABLE IX.- COMPARISON OF MEASURED AND PREDICTED RESPONSE OF TEST PANEL AT 130 FEET TO RANDOM EXCITATION

Accelerometer Location	Measured Frequency in cps	Predicted f_{mn} in cps	Measured Modal g's rms*	Predicted Modal g's rms Ref. Appendix D
1	35	39 (1, 1)	0.323	0.352
5	35	39 (1, 1)	0.177	0.176
5	54	62 (1, 2)	0.215	not excitable
1	84	101 (1, 3)	1.58	0.68
5	88	101 (1, 3)	0.78	0.345
1	190	226 (1, 5)	1.1	1.31
5	190	226 (1, 5)	0.6	0.655
1	280	288 (3, 1)	1.2	6.0
5	265	288 (3, 1)	1.06	3.0
1	380		0.71	
5	380		0.68	

*System corrections have been included to account for a roll off in system sensitivity versus frequency.

TABLE Xa.- SOUND PRESSURE LEVELS - KIWI B 4B/CF

Simulated Nozzle Test

EP I August 8, 1963 **Propellant:** Gaseous Nitrogen at 85 lbs/sec

Octave Band Center Frequency (cps)	Corrected Sound Pressure Levels - dB re 2 x 10^{-4} dynes/cm^2											
	Microphone Locations: 420' Tower										120' Tower	
	1	2	3	4	5	6	7	8	9	10*	11	12
63	100	103	103	107	108	110	109	108	112	106	115	119
125	102	104	107	110	110	112	112	112	112	106	120	121
250	103	105	107	108	110	112	113	115	108	105	121	126
500	104	107	107	108	111	115	116	117	116	108	125	128
1000	101	105	107	108	111	114	116	118	115	109	127	129
2000	100	105	108	108	110	113	116	116	116	103	124	124
4000	98	98	99	99	102	104	108	109	108	94	119	121
8000	---	---	---	---	95	98	100	101	100	89	116	117
10000	---	---	---	---	---	---	---	---	---	---	107	108
Overall SPL	110	113	115	116	118	121	122	123	122	114	132	134

*Located on ground in line with towers at 520 feet from nozzle center line.

TABLE Xb.- SOUND PRESSURE LEVELS - KIWI B 4B/CF

Simulated Nozzle Test

EP I August 8, 1963 Propellant: Gaseous Nitrogen at 69 lbs/sec

Octave Band Center Frequency (cps)	Corrected Sound Pressure Levels - dB re 2 x 10^{-4} dynes/cm^2											
	Microphone Locations: 420' Tower										120' Tower	
	1	2	3	4	5	6	7	8	9	10*	11	12
63	---	89	90	94	95	97	96	98	101	98	107	107
125	---	88	90	93	97	97	99	99	98	95	108	109
250	---	88	91	93	100	100	103	101	95	95	108	113
500	---	91	90	93	100	103	106	104	99	94	108	115
1000	---	91	93	96	102	106	111	109	102	95	113	119
2000	---	92	94	97	103	105	110	108	103	93	111	116
4000	---	---	---	90	93	94	97	96	91	80	103	109
8000	---	---	---	---	---	---	92	---	---	---	99	104
10000	---	---	---	---	---	---	---	---	---	---	---	---
Overall SPL	---	98	99	103	108	111	115	114	108	103	118	123

*Located on ground in line with towers at 520 feet from nozzle center line.

TABLE Xc.- SOUND PRESSURE LEVELS - KIWI B 4B/CF

Simulated Nozzle Test

EP I 8 August 1963 Propellant: Liquid Hydrogen at 35 lbs/sec

Octave Band Center Frequency (cps)	Corrected Sound Pressure Levels - dB re 2 x 10^{-4} dynes/cm^2											
	Microphone Locations: 420' Tower										120' Tower	
	1	2	3	4	5	6	7	8	9	10*	11	12
63	98	99	97	101	102	107	106	109	110	105	116	117
125	98	97	99	102	106	108	111	114	110	107	120	120
250	101	100	103	105	106	109	111	114	112	107	122	123
500	99	101	102	104	107	113	114	117	---	109	124	123
1000	98	100	103	104	107	112	114	119	116	107	126	125
2000	94	98	102	103	107	111	112	117	115	101	123	122
4000	90	91	93	93	97	100	102	109	106	90	119	119
8000	---	---	---	---	---	95	96	102	98	81	115	114
10000	---	---	---	---	---	---	---	---	---	---	---	---

*Located on ground in line with towers at 520 feet from nozzle center line.

TABLE Xd.- SOUND PRESSURE LEVELS - KIWI B-4B/CFT

(a) EP II 21 August 1963 Propellant: Gaseous Nitrogen at 43 lbs/sec

Octave Band Center Frequency cps	Corrected Sound Pressure Levels - dB re 2 x 10^{-4} dynes/cm^2											
	Microphone Locations			420' Tower							120' Tower	
	1	2	3	4	5	6	7	8	9	10*	11	12
63	---	---	---	89	---	---	---	89	86	81	94	95
125	95	96	96	93	93	94	94	95	94	89	102	105
250	94	100	100	96	96	95	95	97	92	91	105	106
500	100	99	102	97	98	99	98	100	99	92	107	108
1000	98	100	103	102	104	106	104	107	102	94	115	116
2000	96	100	103	98	104	107	107	109	107	94	114	115
4000	93	93	93	96	95	98	100	102	99	89	111	115
8000	---	---	---	---	---	---	93	96	92	75	107	110
10000	---	---	---	---	---	---	---	---	---	---	---	---
Overall SPL	104	106	109	106	108	110	113	112	109	100	119	121

*Located on ground in line with towers at 520 feet from nozzle center line.

TABLE Xe.- SOUND PRESSURE LEVELS - KIWI B-4B/CFT

(a) EP II August 21, 1963 Propellant: Gaseous Nitrogen at 52 lbs/sec

Octave Band Center Frequency (cps)	Corrected Sound Pressure Levels - dB re 2 x 10^{-4} dynes/cm^2											
	Microphone Locations:				420' Tower						120' Tower	
	1	2	3	4	5	6	7	8	9	10*	11	12
63	---	---	91	91	92	93	91	92	93	89	100	99
125	95	98	98	98	99	100	101	102	102	97	111	110
250	98	101	101	102	101	102	103	104	99	98	112	112
500	100	102	103	103	102	105	105	105	105	99	113	113
1000	101	102	104	107	103	108	108	108	103	98	115	117
2000	98	102	104	106	104	110	108	107	104	92	114	116
4000	96	93	98	99	97	101	101	103	98	88	113	115
8000	---	---	---	---	94	96	95	97	90	---	109	112
10000	---	---	---	---	---	---	---	---	---	---	---	---
Overall SPL	107	109	110	112	109	114	114	113	111	105	121	123

*Located on ground in line with towers at 520 feet from nozzle center line.

TABLE Xf.- SOUND PRESSURE LEVELS FOR KIWI B-4B/CFT

(b) EP II August 21, 1963 Propellant: Gaseous Hydrogen at 24 lbs/sec

Octave Band Center Frequency (cps)	Corrected Sound Pressure Levels - dB re 2 x 10^{-4} dynes/cm^2											
	Microphone Locations: 420' Tower										120' Tower	
	1	2	3	4	5	6	7	8	9	10*	11	12
63	101	103	103	106	108	110	109	107	113	107	115	118
125	100	105	108	109	111	111	112	113	111	107	122	122
250	102	105	107	109	110	112	114	115	108	106	121	126
500	103	107	107	108	111	115	117	118	116	108	125	128
1000	103	107	107	109	111	114	117	119	115	107	127	129
2000	100	107	107	109	111	114	116	117	115	102	124	124
4000	96	98	100	100	102	105	108	111	108	94	120	121
8000	---	---	---	---	96	99	101	102	101	90	117	117
10000	---	---	---	---	---	---	---	---	---	---	---	---
Overall SPL	110	114	115	117	119	121	123	124	122	114	132	134

*Located on ground in line with towers at 520 feet from nozzle center line.

TABLE Xg.- SOUND PRESSURE LEVELS FOR KIWI B HIGH FLOW ACOUSTICAL TEST

(a) January 9, 1964 Propellant: Gaseous Hydrogen at 100 lbs/sec

One-Third Octave Band Center Frequency (cps)	Corrected Sound Pressure Levels - dB re 2 x 10^{-4} dynes/cm^2															
	Microphone Locations: 420' Tower										120' Tower		Concrete Pad			
	1	2	3	4	5	6	7	8	9	10*	12	13	16	17	18	19
20	91	99	96	98	103	108	106	100	104	102	110	107	---	---	---	---
25	90	100	99	100	105	110	110	104	111	104	115	112	---	---	---	109
32	--	100	97	96	105	111	112	104	109	105	116	113	---	---	---	111
40	90	104	102	102	107	109	113	109	110	108	119	117	---	112	112	112
50	90	100	102	104	109	110	113	110	110	105	120	119	---	118	117	115
63	94	104	103	105	109	112	115	112	111	110	124	121	---	120	122	121
80	94	100	100	103	107	111	116	112	106	108	121	117	---	119	117	119
100	91	101	100	100	107	111	115	110	108	109	120	120	117	121	121	122
125	92	101	102	101	105	110	115	113	114	112	124	122	117	121	122	122
160	93	103	101	102	106	108	114	112	117	112	123	122	117	124	123	124
200	94	105	103	102	106	108	112	112	119	112	120	123	119	122	123	122
250	94	104	102	104	107	111	115	113	120	110	121	124	121	122	123	124
315	94	102	101	103	106	110	114	113	115	108	121	124	119	122	122	122
400	94	105	103	104	107	112	114	114	116	110	122	127	120	125	125	125
500	94	102	101	104	106	112	115	116	118	110	123	126	122	125	125	126
630	94	103	103	104	107	113	116	116	116	106	123	126	121	124	124	124
800	94	102	104	104	108	113	114	113	115	104	123	126	122	123	124	124
1000	94	103	104	106	110	113	115	114	114	102	124	128	125	125	125	125
1250	92	102	102	102	103	112	116	116	117	99	125	129	124	124	124	124
1600	92	103	103	104	108	114	115	111	116	95	124	126	127	122	123	123
2000	90	103	103	105	105	111	110	110	114	93	120	123	125	121	122	122
2500	--	98	99	100	101	105	106	103	109	94	117	119	123	120	119	120
3150	--	95	94	97	101	109	107	105	110	93	118	119	120	117	117	117
4000	--	---	96	99	98	106	106	109	108	94	118	119	119	117	117	114
5000	--	---	92	99	98	109	105	102	106	93	116	118	115	115	114	111
6300	--	---	94	99	94	109	102	100	107	92	116	116	110	111	111	108
8000	--	---	94	99	90	110	104	99	104	88	114	114	105	107	---	105
10000	--	---	---	---	---	---	---	---	---	---	---	---	---	---	---	---
Overall SPL	107	115	114	116	119	124	126	126	128	122	137	135	133	135	135	135

*Located on ground in line with towers at 520 feet from nozzle center line.

TABLE Xh.- SOUND PRESSURE LEVELS FOR KIWI B HIGH FLOW ACOUSTICAL TEST

(b) January 9, 1964 Propellant: Gaseous Helium at 130 lbs/sec

One Third Octave Band Center Frequency (cps)	Corrected Sound Pressure Levels - dB re 2×10^{-4} dynes/cm^2															
	Microphone Locations: 420' Tower										120' Tower		Concrete Pad			
	1	2	3	4	5	6	7	8	9	10*	12	13	16	17	18	19
20	---	---	89	87	89	88	87	83	85	---	---	---	---	---	---	---
25	95	---	96	94	95	92	91	90	90	86	99	---	---	---	---	---
32	95	---	98	98	98	97	94	89	92	88	100	---	---	---	---	---
40	101	100	105	103	104	103	100	94	95	93	105	103	---	101	---	---
50	104	104	108	106	107	106	103	96	97	95	107	105	---	105	---	107
63	107	105	111	109	111	109	106	98	100	99	112	111	---	108	109	110
80	106	107	112	112	114	112	108	101	96	103	114	110	---	114	---	112
100	109	113	112	114	116	114	111	101	98	100	116	111	110	110	112	111
125	110	115	112	113	116	117	113	106	105	104	119	114	111	114	114	114
160	112	115	114	114	116	117	115	108	109	104	120	116	113	115	115	116
200	110	114	112	112	116	118	116	109	110	104	121	116	113	113	113	113
250	113	115	113	115	117	117	117	110	112	100	123	117	115	115	115	116
315	109	112	110	112	115	117	116	110	109	98	122	118	114	116	117	117
400	107	112	110	111	116	117	114	111	111	101	124	121	116	118	118	118
500	105	110	108	111	114	118	117	114	112	100	125	121	117	117	118	119
630	106	109	109	111	113	118	117	113	111	102	126	122	116	117	119	118
800	105	109	108	110	113	116	115	112	110	98	125	121	117	118	119	119
1000	105	109	108	110	113	114	115	111	109	97	125	124	118	120	121	120
1250	101	104	103	104	108	115	117	116	114	99	128	125	120	119	119	119
1600	98	103	104	107	112	115	115	110	113	99	124	124	123	118	119	119
2000	98	105	105	107	106	112	109	109	112	101	120	120	122	118	118	118
2500	96	103	101	103	102	107	107	103	108	100	119	116	119	116	116	116
3150	93	97	94	101	104	109	105	105	108	97	118	116	117	113	114	114
4000	90	---	97	100	101	108	108	109	106	94	118	117	116	113	114	111
5000	---	---	94	102	100	109	107	103	104	93	115	116	112	112	111	107
6300	---	---	95	102	97	109	103	100	105	92	116	113	107	109	109	104
8000	---	---	96	101	93	110	106	100	104	91	114	113	---	106	---	102
10000	---	---	---	---	---	---	---	---	---	---	---	---	---	---	---	---
Overall SPL	119	123	121	123	125	128	126	123	122	114	137	131	129	129	129	128

*Located on ground in line with towers at 520 feet from nozzle center line.

TABLE Xi.- SOUND PRESSURE LEVELS - KIWI B-4D

EP IV May 13, 1964 Propellant: Liquid Hydrogen at 69 lbs/sec

One Third Octave Band Center Frequency (cps)	Corrected Sound Pressure Levels - dB re 2 x 10^{-4} dynes/cm^2																		
	Microphone Locations: 420' Tower									120' Tower				Balloon Cable					
	1	2	3	4	5	6	7	8	9	11	12	13	14	21	22	23	24	25	26
20	---	---	---	---	---	---	---	---	---	---	---	---	---	---	---	---	---	---	---
25	100	104	104	107	111	112	118	109	108	---	---	---	---	101	104	108	109	108	103
32	100	105	107	107	113	114	121	111	110	---	---	---	---	101	105	108	110	110	105
40	101	105	109	110	115	117	122	113	110	---	---	---	---	103	106	110	111	111	109
50	102	106	108	101	114	118	122	114	109	---	---	---	---	103	106	110	109	111	110
63	101	105	109	110	115	119	123	115	107	---	---	---	---	102	106	110	111	113	112
80	102	106	110	111	115	120	124	117	108	---	---	---	---	104	107	111	110	115	116
100	103	107	110	112	117	120	125	119	112	129	127	120	118	104	107	111	111	115	118
125	103	106	110	112	116	120	125	121	116	129	128	122	119	105	107	111	112	114	118
160	103	107	109	112	116	120	126	123	119	127	128	123	120	107	108	112	112	115	119
200	105	108	111	113	116	120	126	124	120	127	130	126	122	107	109	111	113	116	119
250	104	108	110	112	115	120	126	124	119	127	129	128	123	107	108	111	112	115	118
315	106	109	111	114	117	120	126	125	122	126	130	130	126	108	110	112	112	115	118
400	107	110	112	115	118	121	126	126	123	126	129	130	127	109	111	112	112	115	118
500	107	111	112	115	118	121	126	126	123	126	129	130	128	109	110	112	111	114	117
630	108	111	114	116	119	122	126	125	124	125	128	131	131	109	111	112	111	114	116
800	110	111	114	117	119	120	126	123	121	127	129	130	128	108	110	111	111	114	115
1000	110	113	114	118	118	120	125	124	120	123	125	128	129	108	109	110	110	112	115
1250	111	112	113	115	118	121	125	126	123	125	128	131	130	108	108	109	109	111	113
1600	109	111	112	113	118	121	125	123	121	124	125	127	130	106	107	108	107	109	112
2000	110	111	112	116	118	118	124	120	116	121	124	125	127	105	106	106	105	107	110
2500	110	110	110	114	113	112	123	115	115	118	120	122	123	103	104	104	102	105	109
3150	109	107	105	111	112	113	124	117	115	120	119	121	122	102	103	103	101	102	109
4000	105	103	103	108	112	115	124	120	118	118	121	125	124	99	102	101	98	98	107
5000	105	102	102	106	110	113	123	117	112	116	120	123	123	96	101	100	94	95	105
6300	105	101	101	105	109	110	123	113	109	114	117	118	120	93	100	97	92	92	102
8000	106	100	99	105	111	110	123	113	110	113	116	114	119	91	100	95	91	90	94
10000	106	99	100	105	115	112	125	114	112	110	115	117	117	93	99	95	94	93	93
12500	---	---	---	---	---	---	---	---	---	107	114	116	116	---	---	---	---	---	---
16000	---	---	---	---	---	---	---	---	---	107	114	115	115	---	---	---	---	---	---
20000	---	---	---	---	---	---	---	---	---	105	112	112	112	---	---	---	---	---	---
25000	---	---	---	---	---	---	---	---	---	104	111	109	110	---	---	---	---	---	---
Overall SPL	121	123	125	127	130	133	138	136	133	138	140	140	139	120	122	124	125	127	129

TABLE Xj.- SOUND PRESSURE LEVELS - KIWI B-4E

EP V August 28, 1964 Propellant: Liquid Hydrogen at 69 lbs/sec

One Third Octave Band Center Frequency (cps)	Corrected Sound Pressure Levels - dB re 2 x 10^{-4} dynes/cm^2															
	Microphone Locations: 420' Tower							Concrete Pad								Dewar*
	2	4	5	6	7	8	9	17	18	19	20	28	29	30	Kaman	
20	104	106	113	111	111	106	108	107	102	106	118	108	103	103	124	---
25	106	113	114	113	114	110	110	109	105	109	118	108	107	107	124	112
32	108	113	116	116	116	112	108	111	107	111	118	111	110	110	124	115
40	106	112	114	116	116	112	108	113	108	111	117	111	108	110	121	116
50	104	110	114	115	117	115	111	114	109	113	118	112	112	112	122	117
63	103	108	112	114	118	114	112	113	108	112	117	114	113	112	126	118
80	103	109	114	116	117	117	115	117	115	117	120	119	115	114	123	121
100	104	110	115	118	120	119	117	118	114	117	122	117	115	115	125	123
125	105	111	115	119	120	121	118	119	117	119	125	118	118	119	126	125
160	106	114	117	121	121	112	120	122	118	120	127	120	118	119	127	126
200	108	115	117	123	122	124	123	124	120	121	128	121	121	120	129	129
250	108	114	118	121	122	124	123	125	120	124	130	123	123	123	130	130
315	110	115	119	122	122	124	124	126	122	124	131	125	125	125	133	131
400	111	117	118	122	123	124	124	128	126	126	131	126	127	126	133	132
500	112	118	121	123	123	124	125	129	126	128	129	126	128	128	135	132
630	112	118	121	124	124	123	126	129	127	128	132	127	129	128	135	133
800	113	119	120	125	122	122	124	129	127	127	133	127	130	129	137	131
1000	113	119	120	122	122	123	124	128	126	126	133	125	129	130	137	132
1250	114	118	121	123	124	123	125	128	125	127	132	125	129	130	136	131
1600	112	115	122	123	122	122	123	128	124	125	131	124	129	130	136	128
2000	111	118	120	121	119	119	118	125	123	125	131	123	128	128	133	124
2500	113	118	115	115	113	114	115	124	121	123	128	122	127	126	132	122
3150	109	114	114	115	114	113	113	123	119	120	125	119	125	125	131	121
4000	105	112	114	117	117	117	117	122	119	120	123	118	124	124	133	119
5000	103	110	113	112	113	113	112	121	118	120	122	119	123	123	134	118
6300	99	107	111	110	109	108	108	120	116	118	120	117	120	120	133	119
8000	99	106	108	109	108	109	107	119	116	117	122	116	118	119	129	120
10000	100	105	110	104	105	107	104	115	115	113	121	116	114	118	---	120
Overall SPL	124	129	132	134	135	135	135	138	137	137	142	137	139	139	146	142

*Located on LH_2 Dewar 120 feet from KIWI B nozzle. This data obtained during the 5-13-64 test.

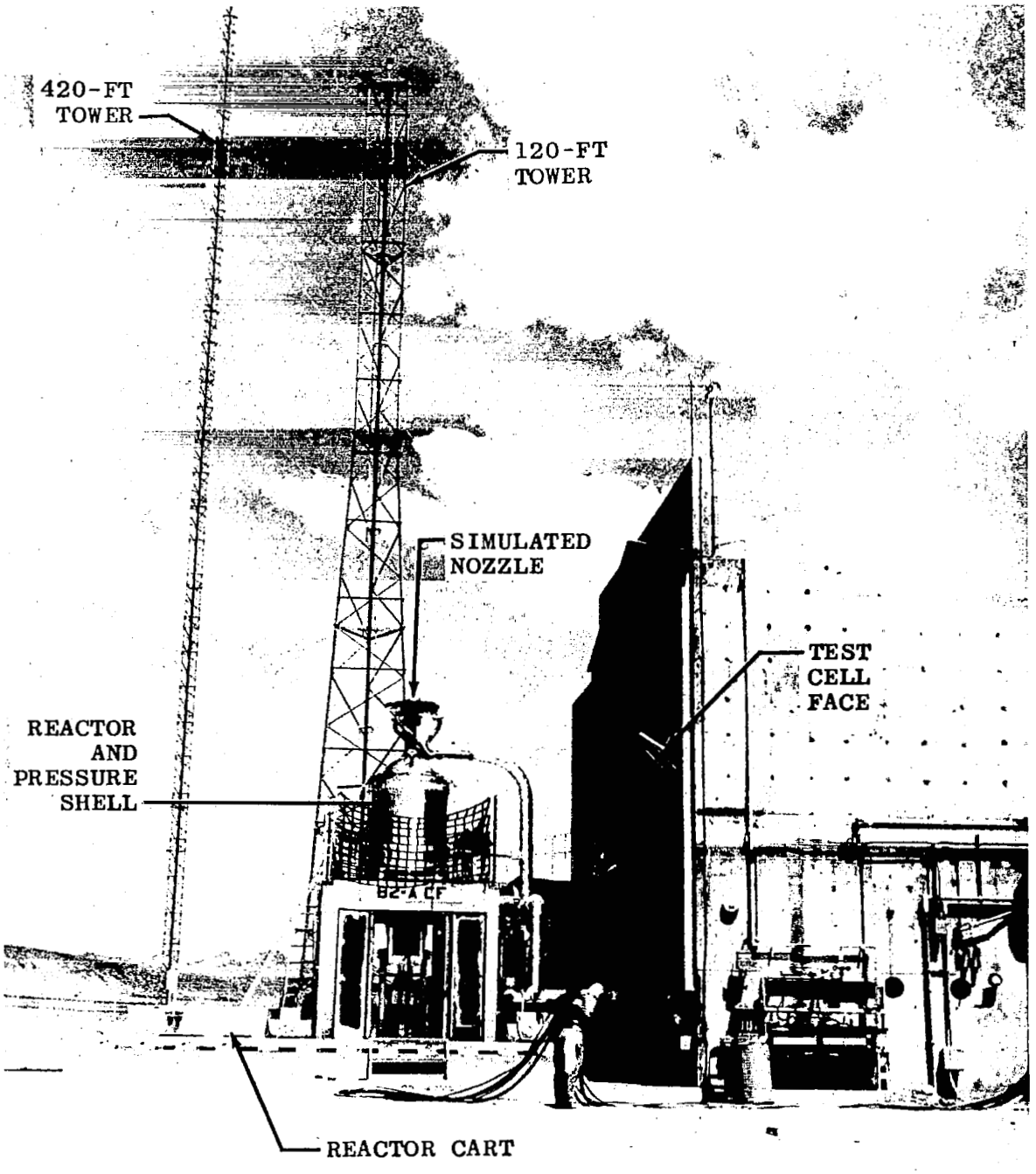

Figure 1. View of Test Site Showing Simulated Nozzle Assembly

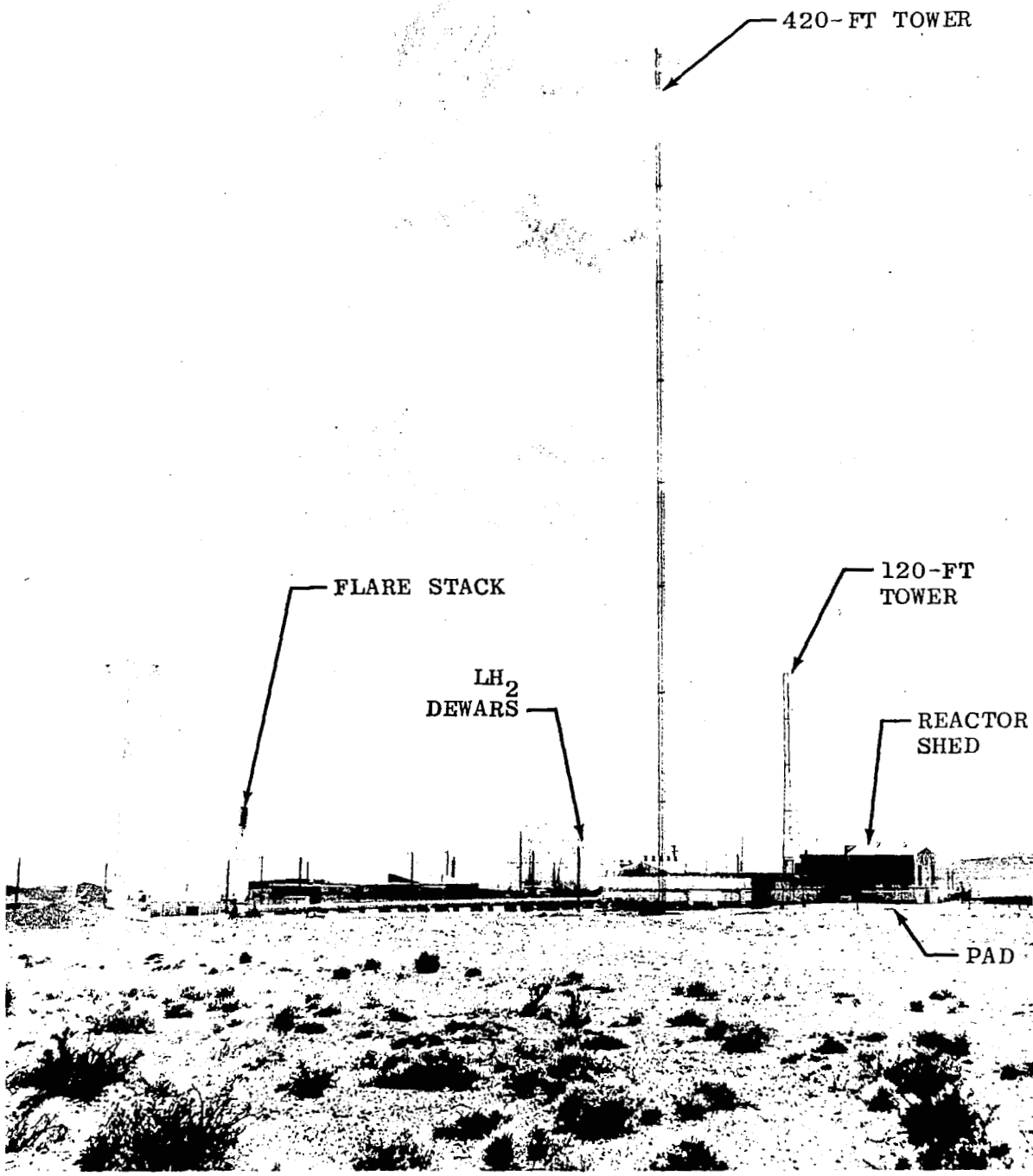

Figure 2. View of Test Cell C

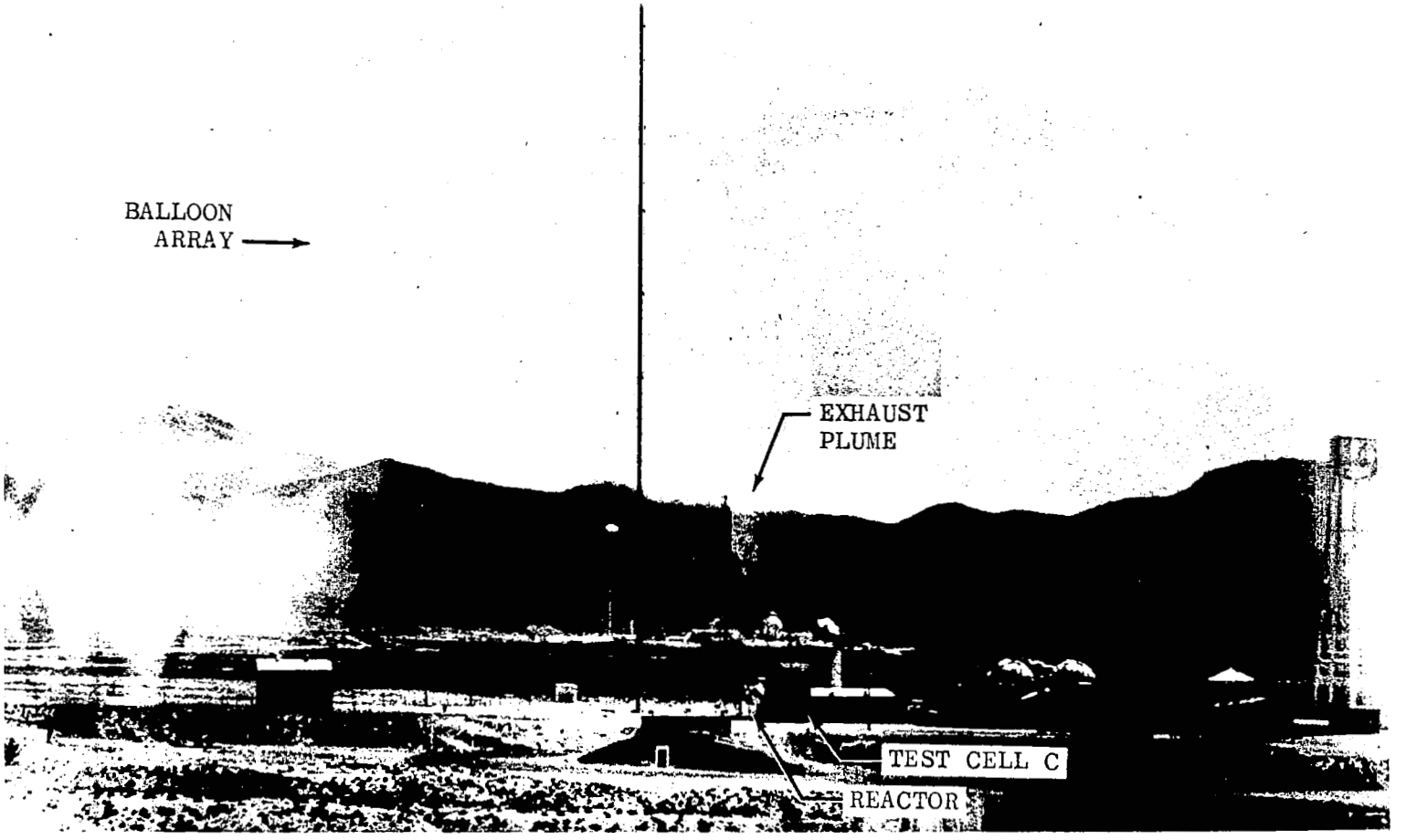

Figure 3. View of Test Cell C During Full Power Run of KIWI B-4D

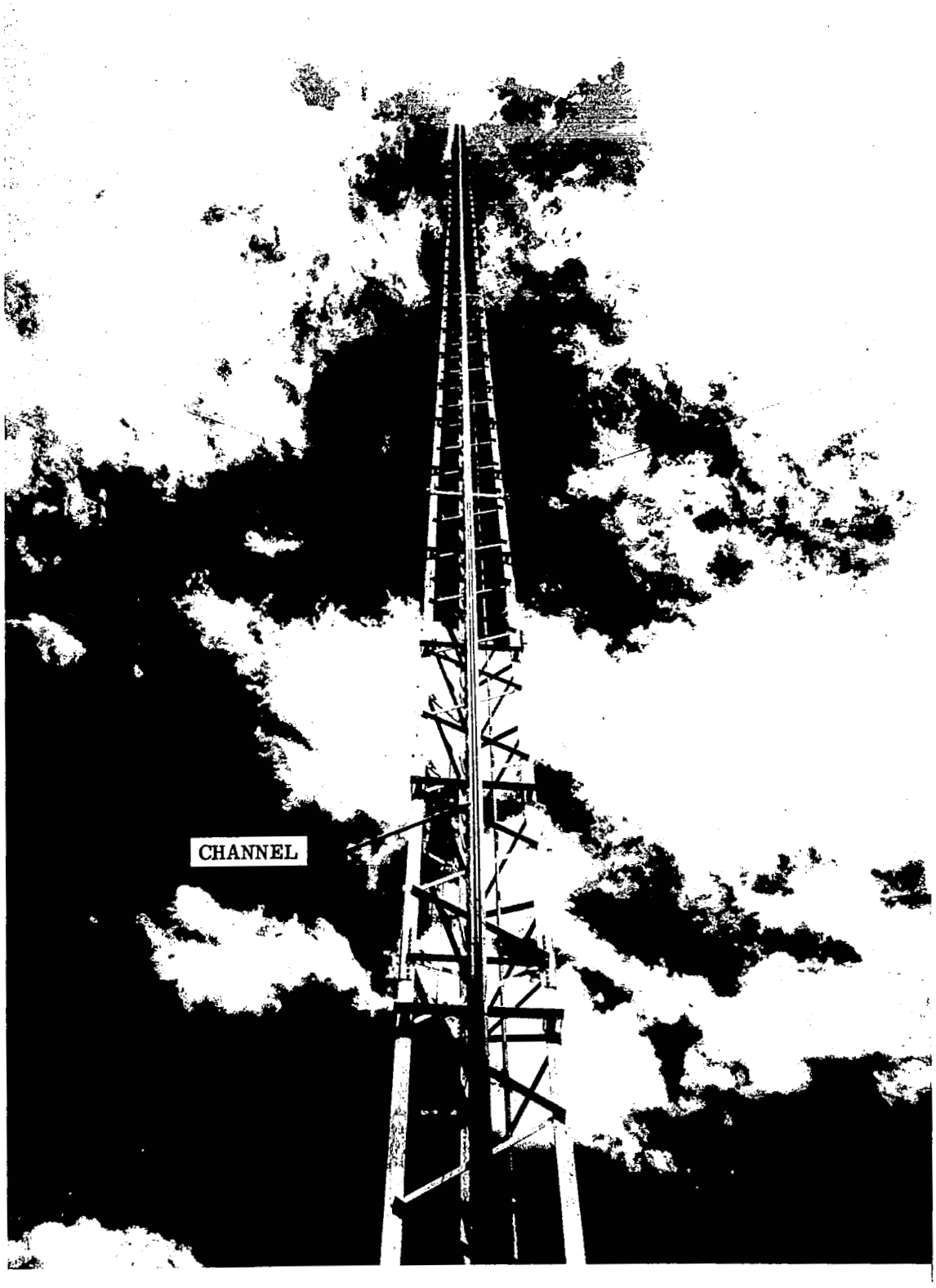

Figure 4. View of Channel on the 420-Foot Tower

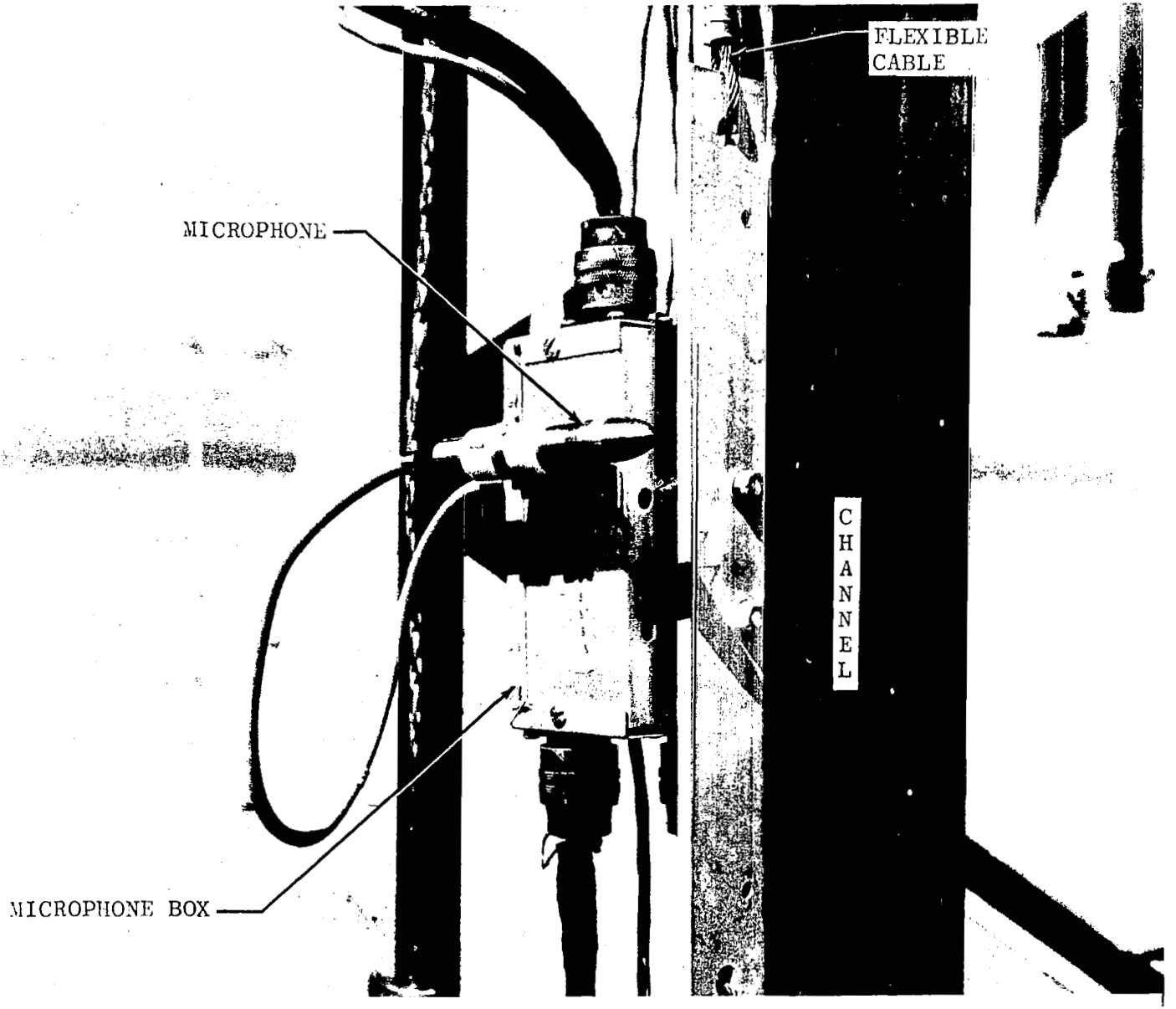

Figure 5. Typical Microphone Installation on Tower

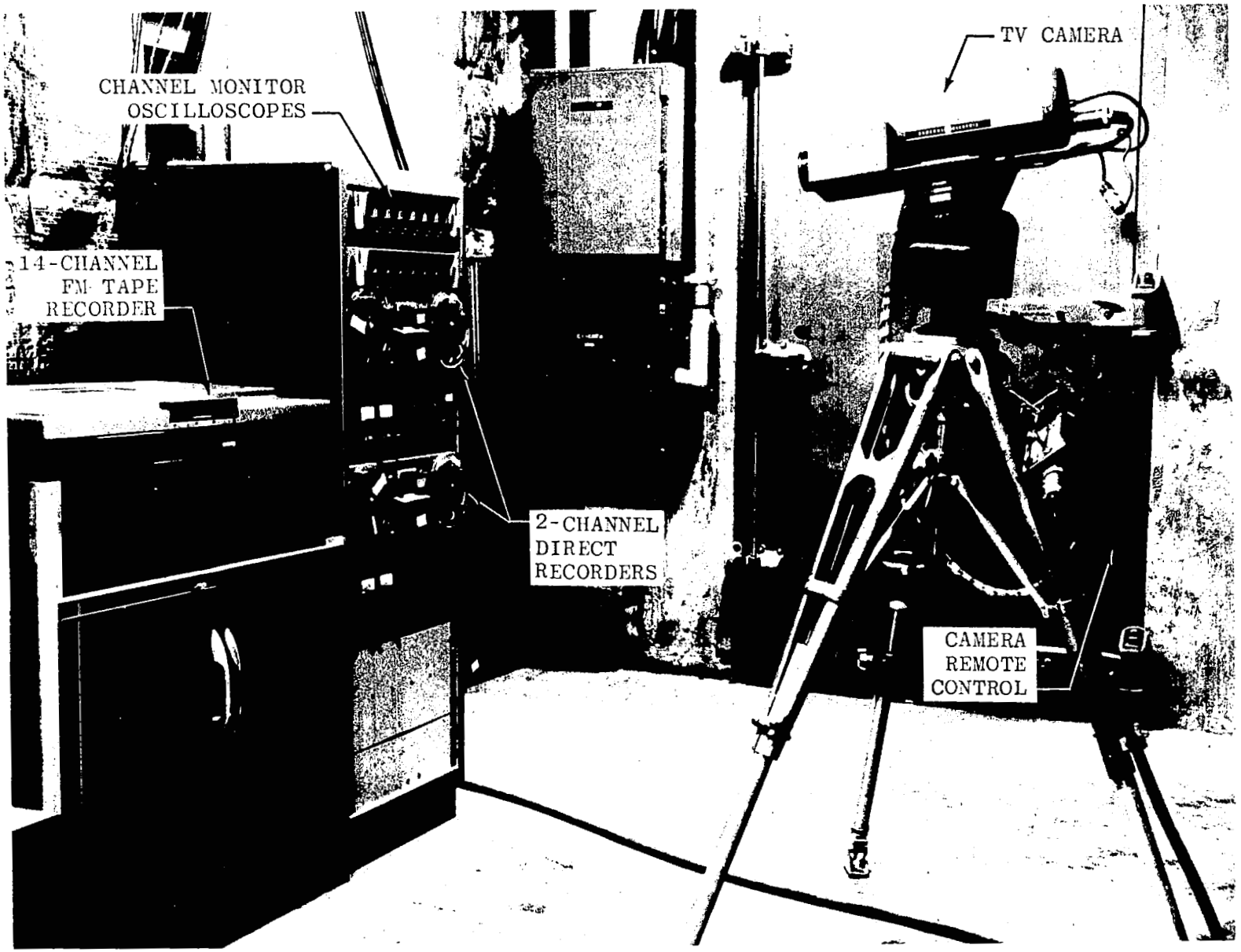

Figure 6. Tape Recorders and Remote TV Monitor in Test Cell C Basement

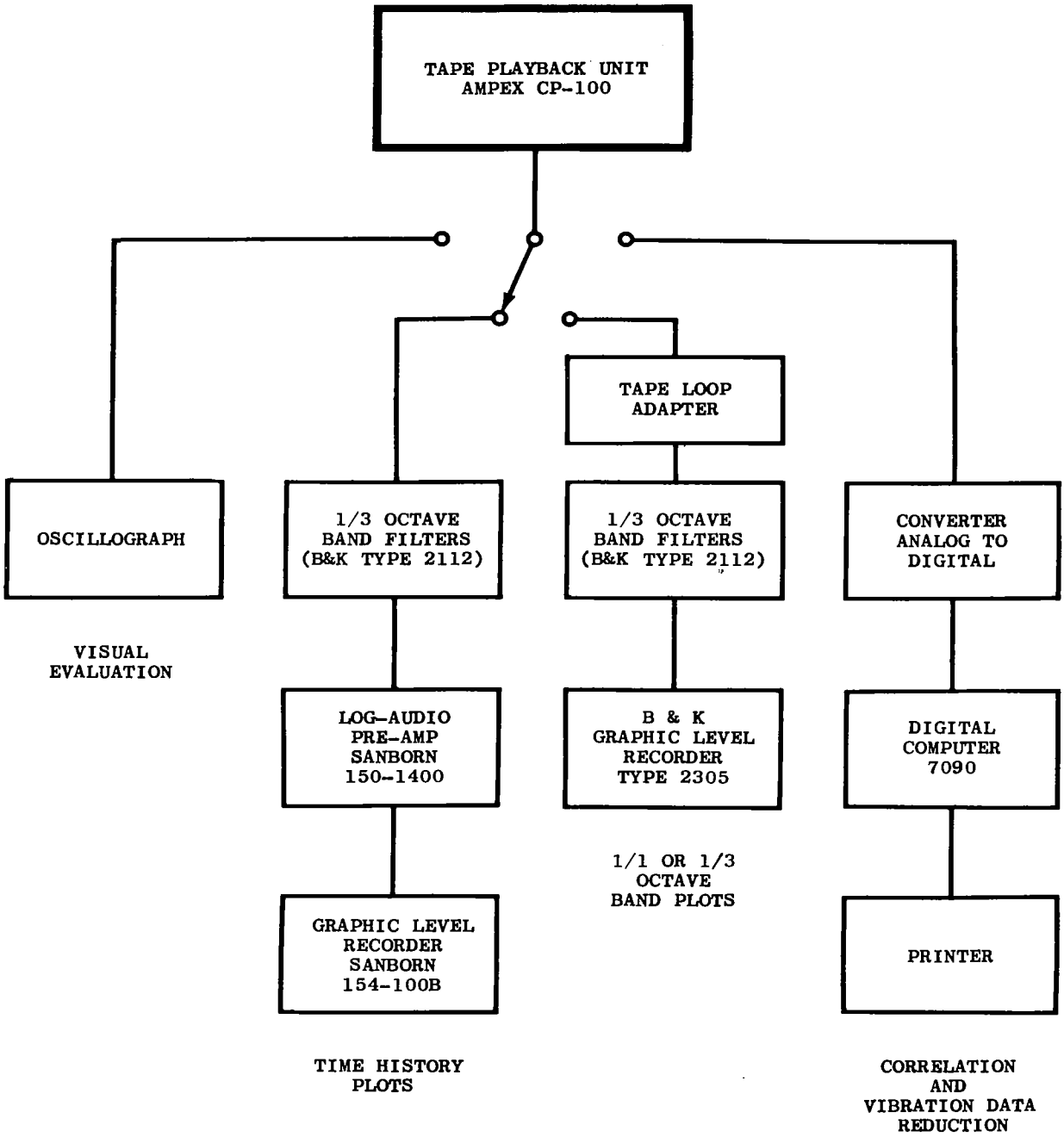

Figure 7. Block Diagram of Data Reduction System

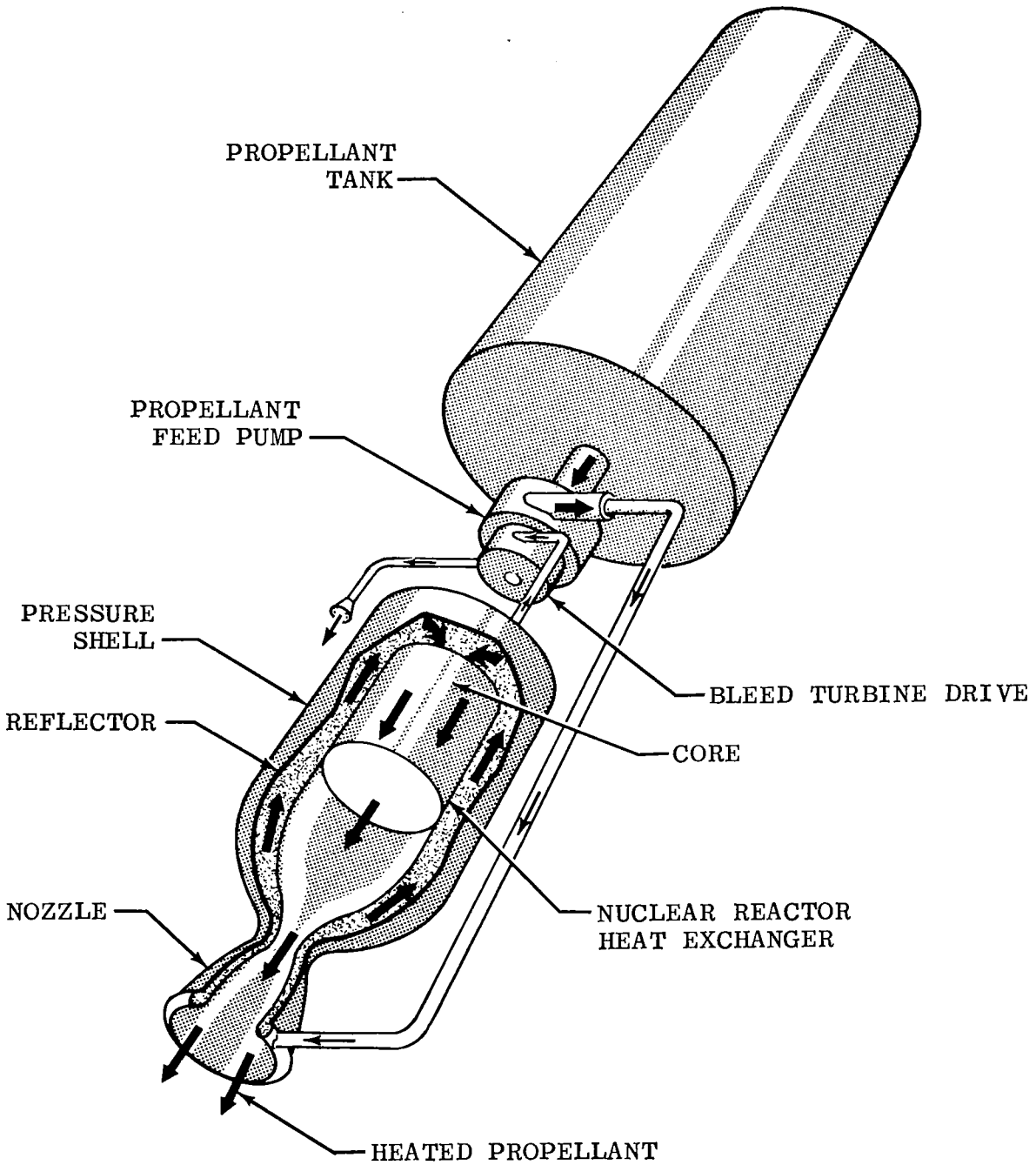

Figure 8. Schematic of Nuclear Rocket Propulsion System

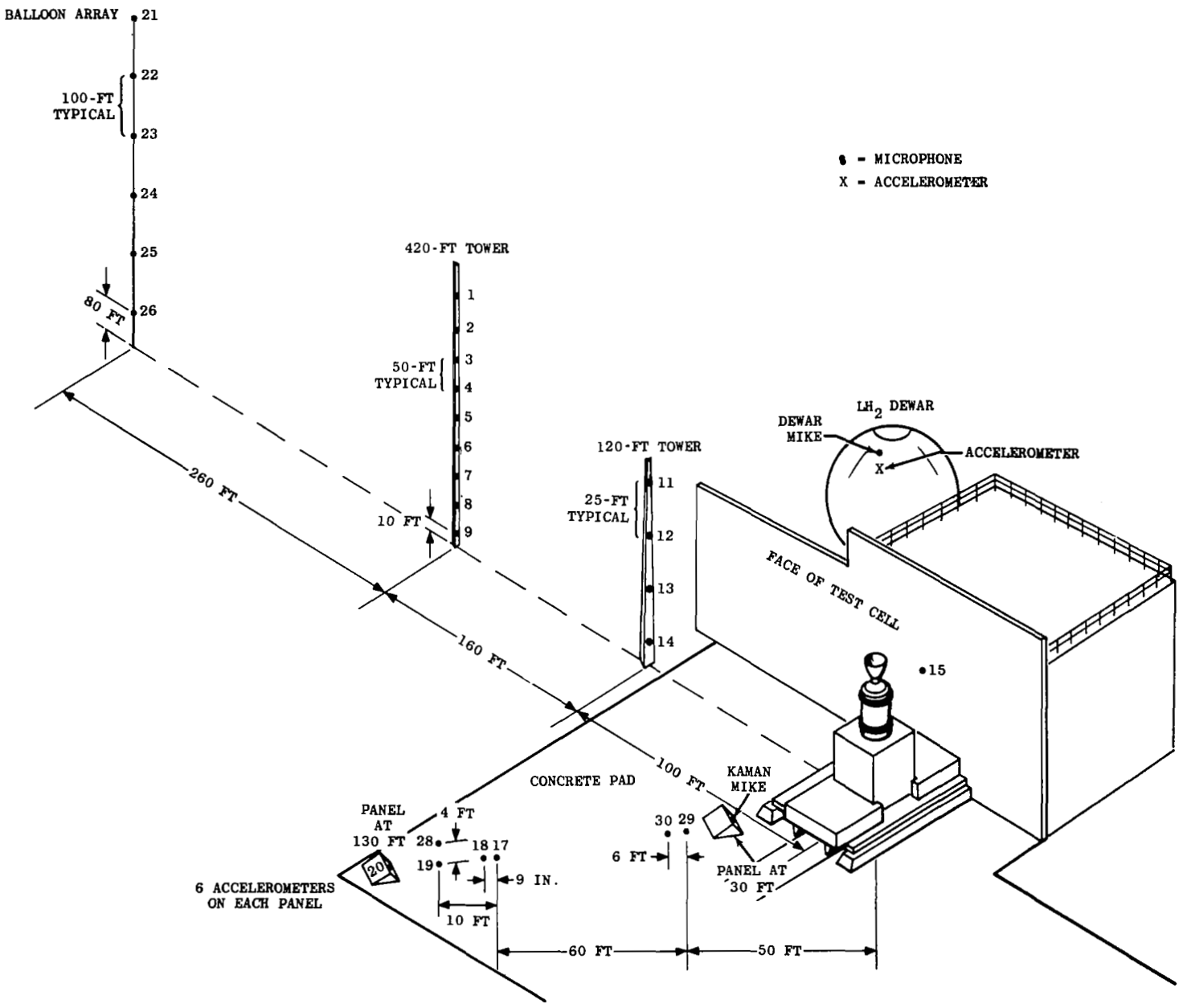

Figure 9. Geometrical Location of Sensors

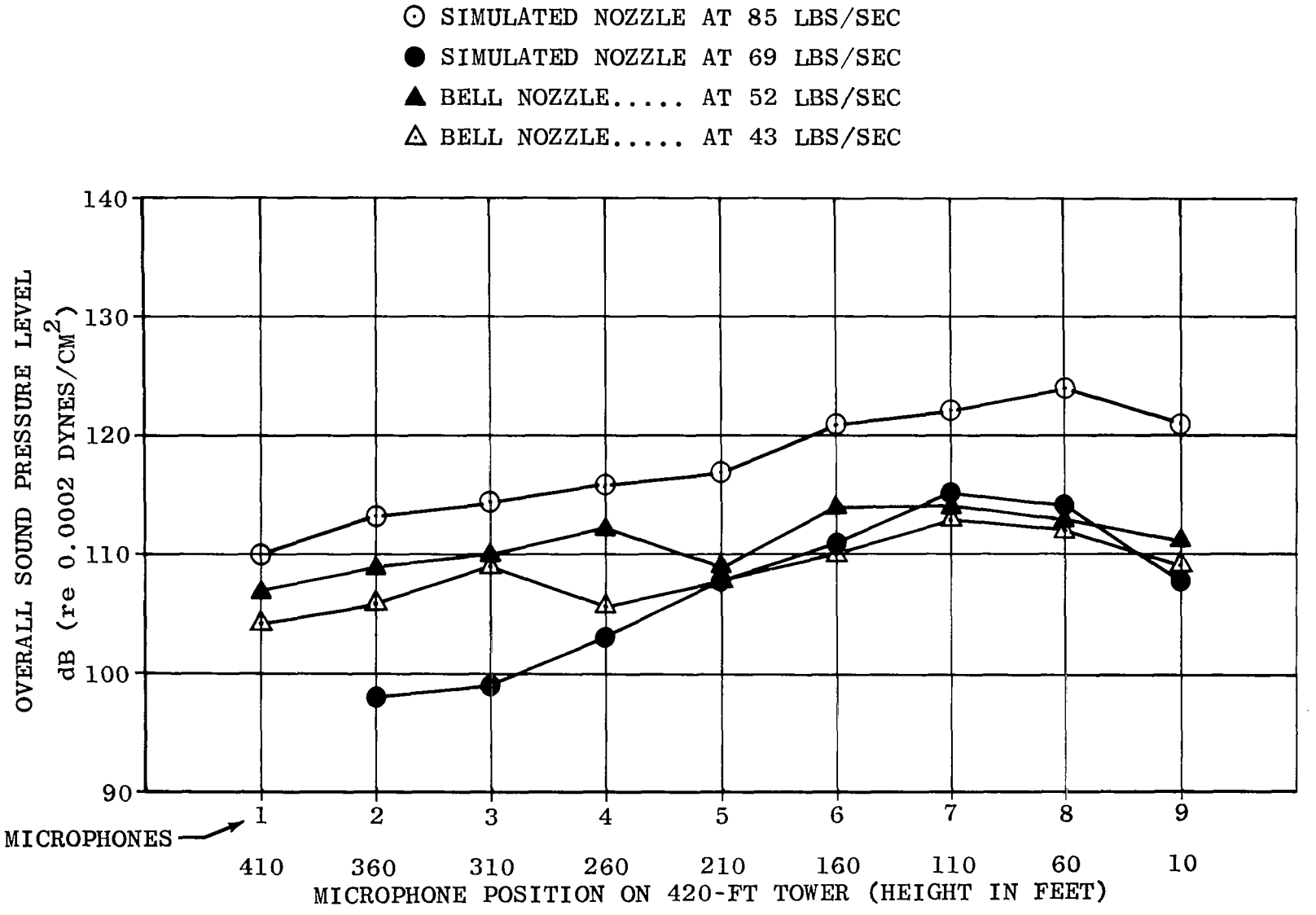

Figure 10. Comparison of Overall Sound Pressure Levels Versus Microphone Position for Gaseous Nitrogen Cold Flows

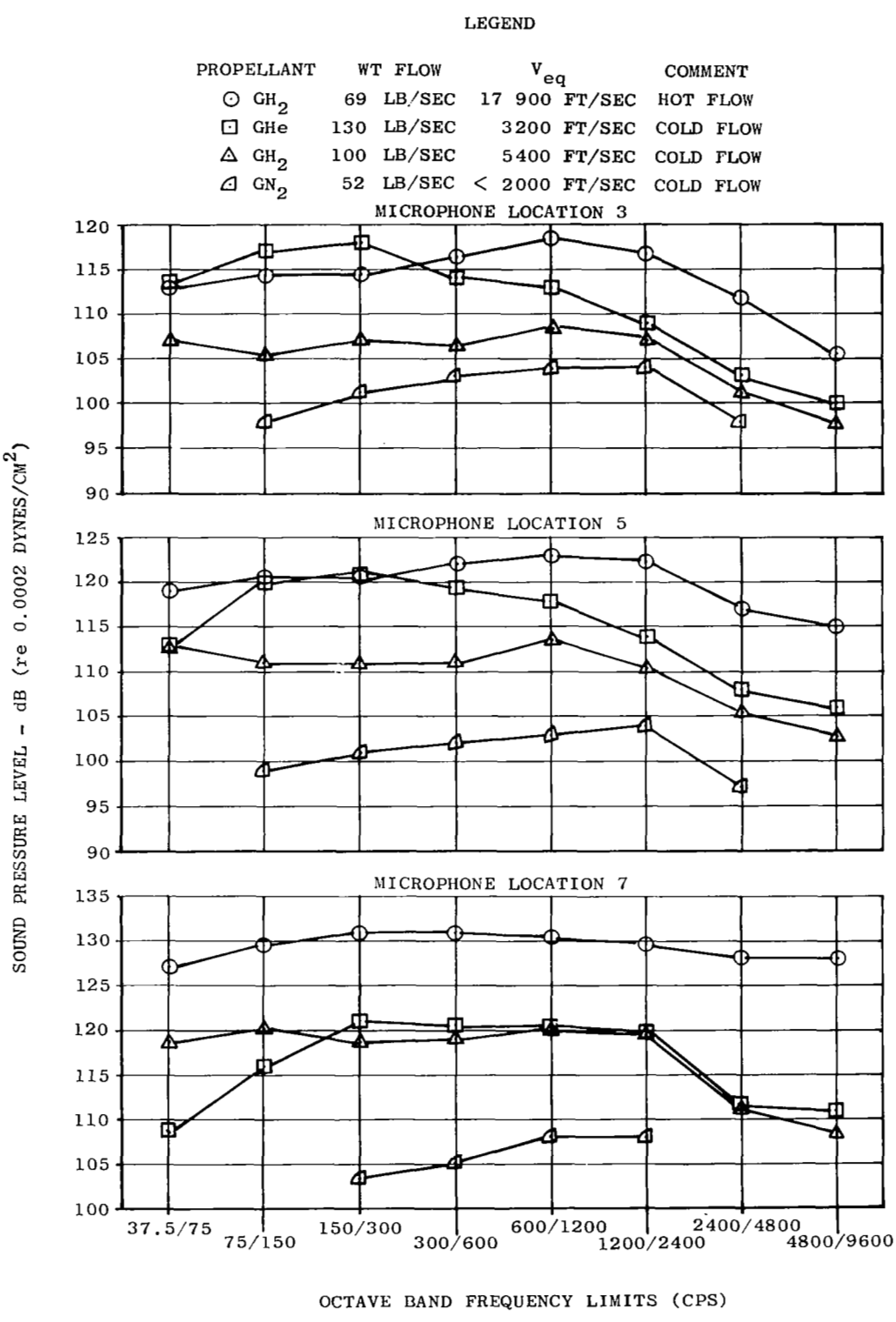

Figure 11. Octave Band Spectra Comparisons

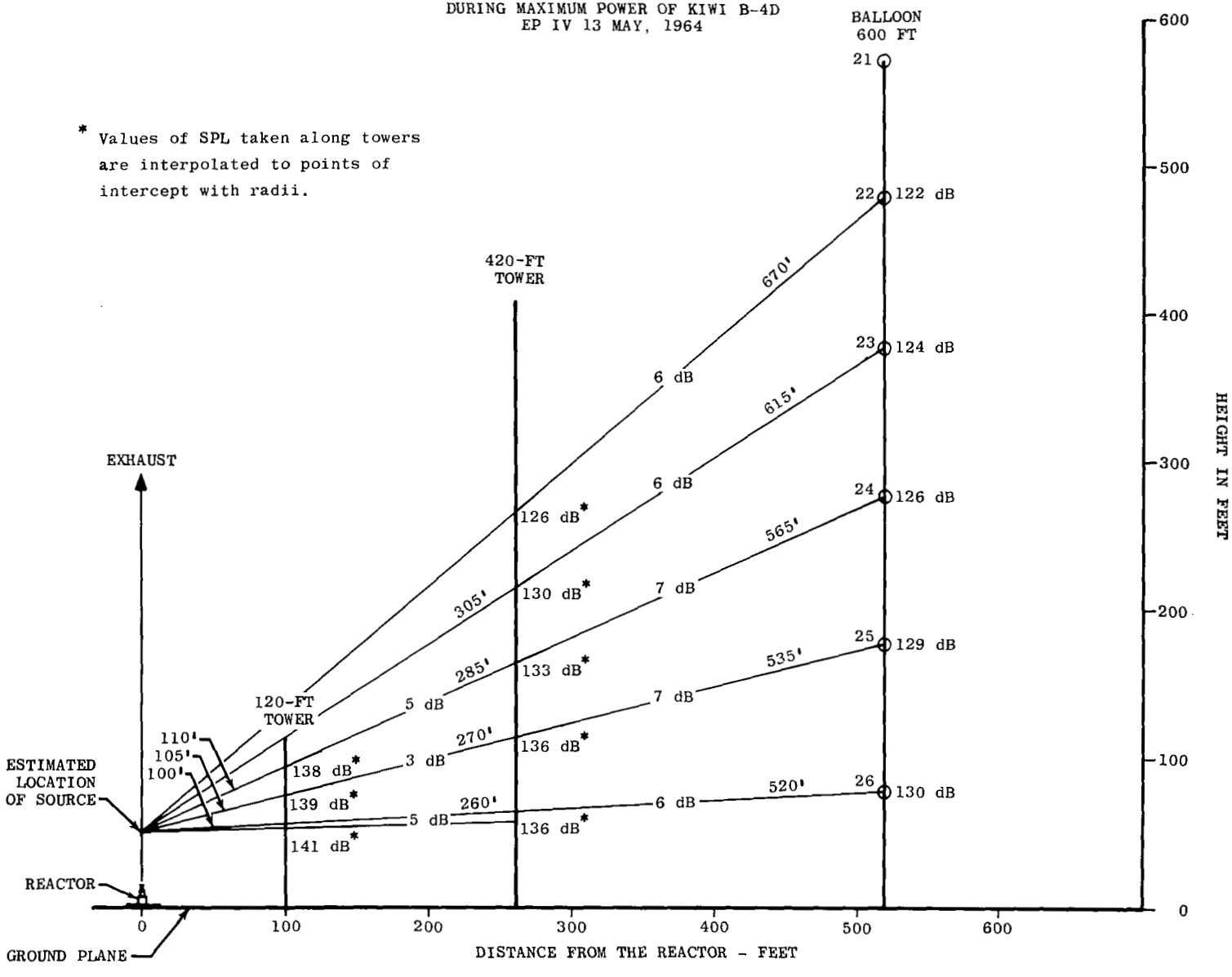

Figure 12. Comparison of Overall SPL's along Radii from the Reactor to the Balloon Microphones

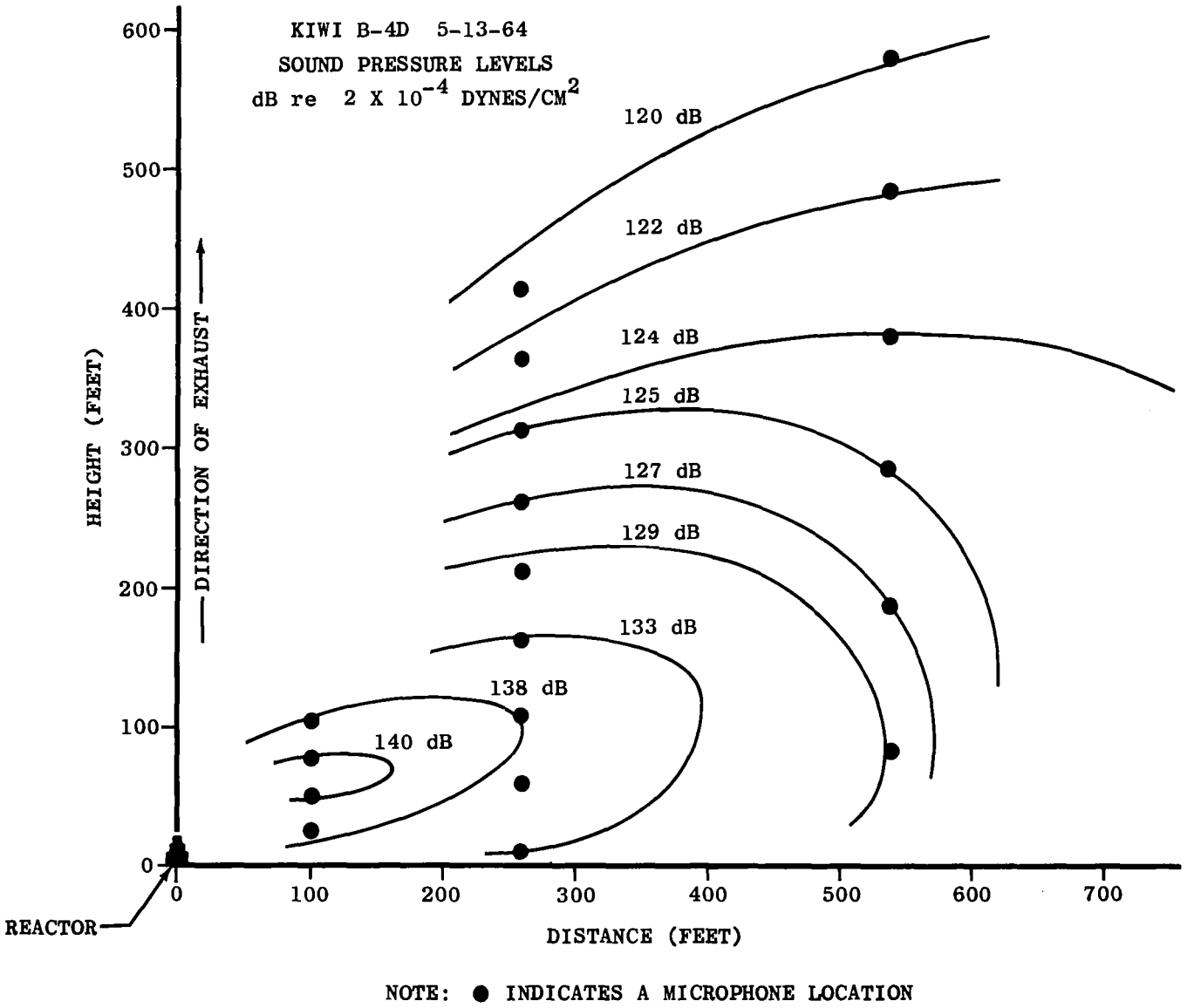

Figure 13a. Estimated Equal Sound Pressure Level--Overall SPL in dB

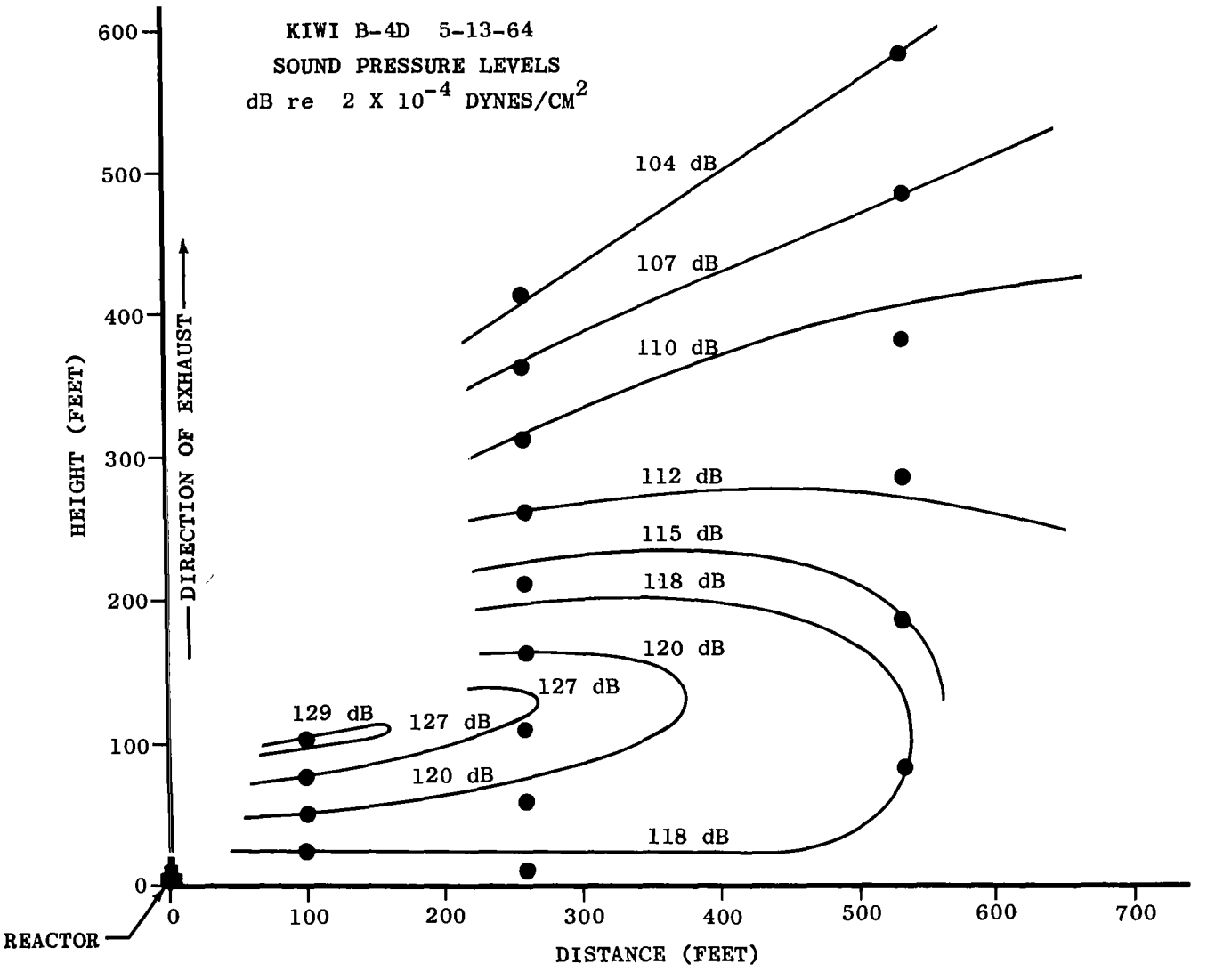

NOTE: ● INDICATES A MICROPHONE LOCATION

Figure 13b. Estimated Equal Sound Pressure Level--One-Third Octave Band: Center Frequency 100 cps

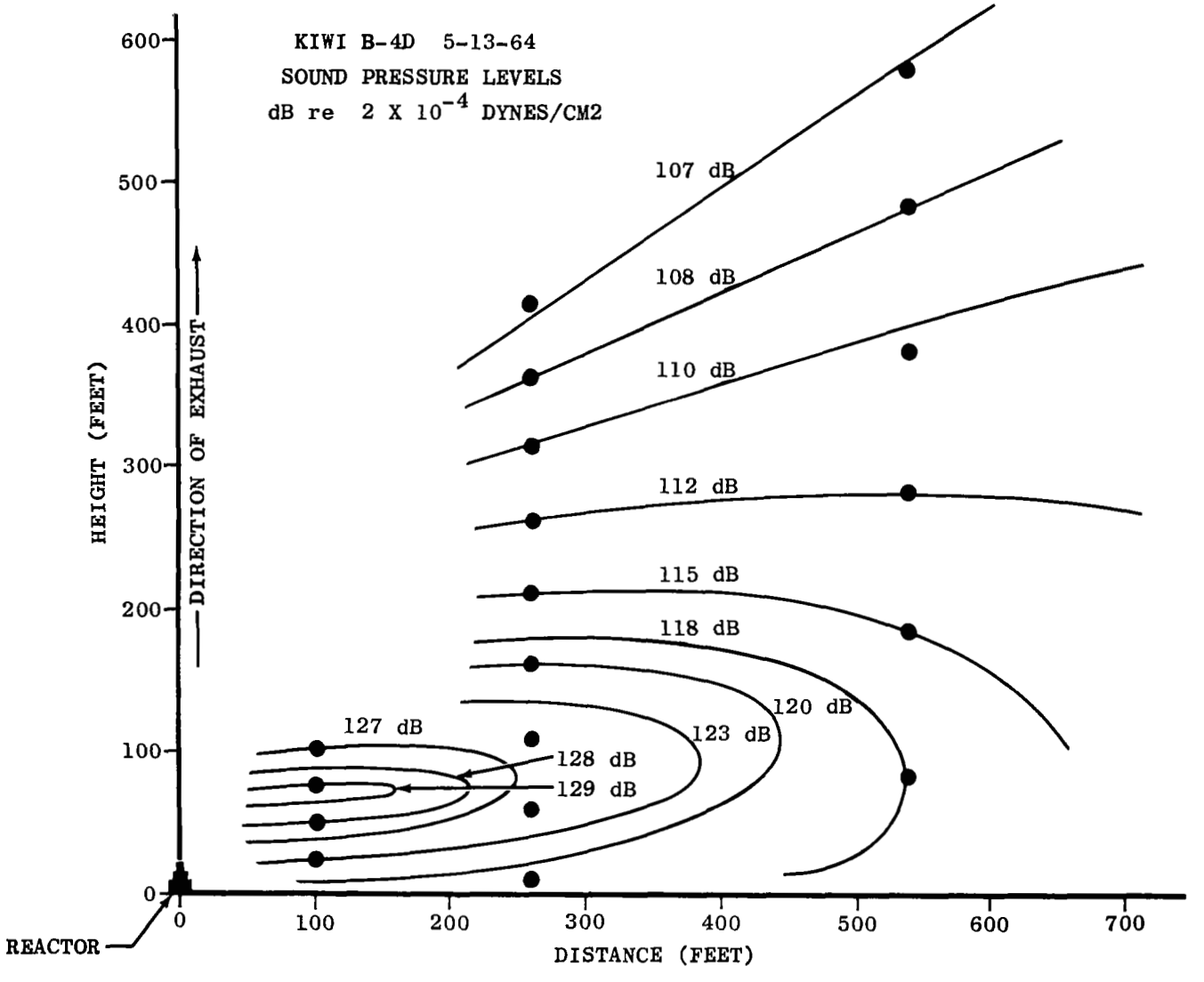

NOTE: ● INDICATES A MICROPHONE LOCATION

Figure 13c. Estimated Equal Sound Pressure Level--One-Third Octave Band: Center Frequency 250 cps

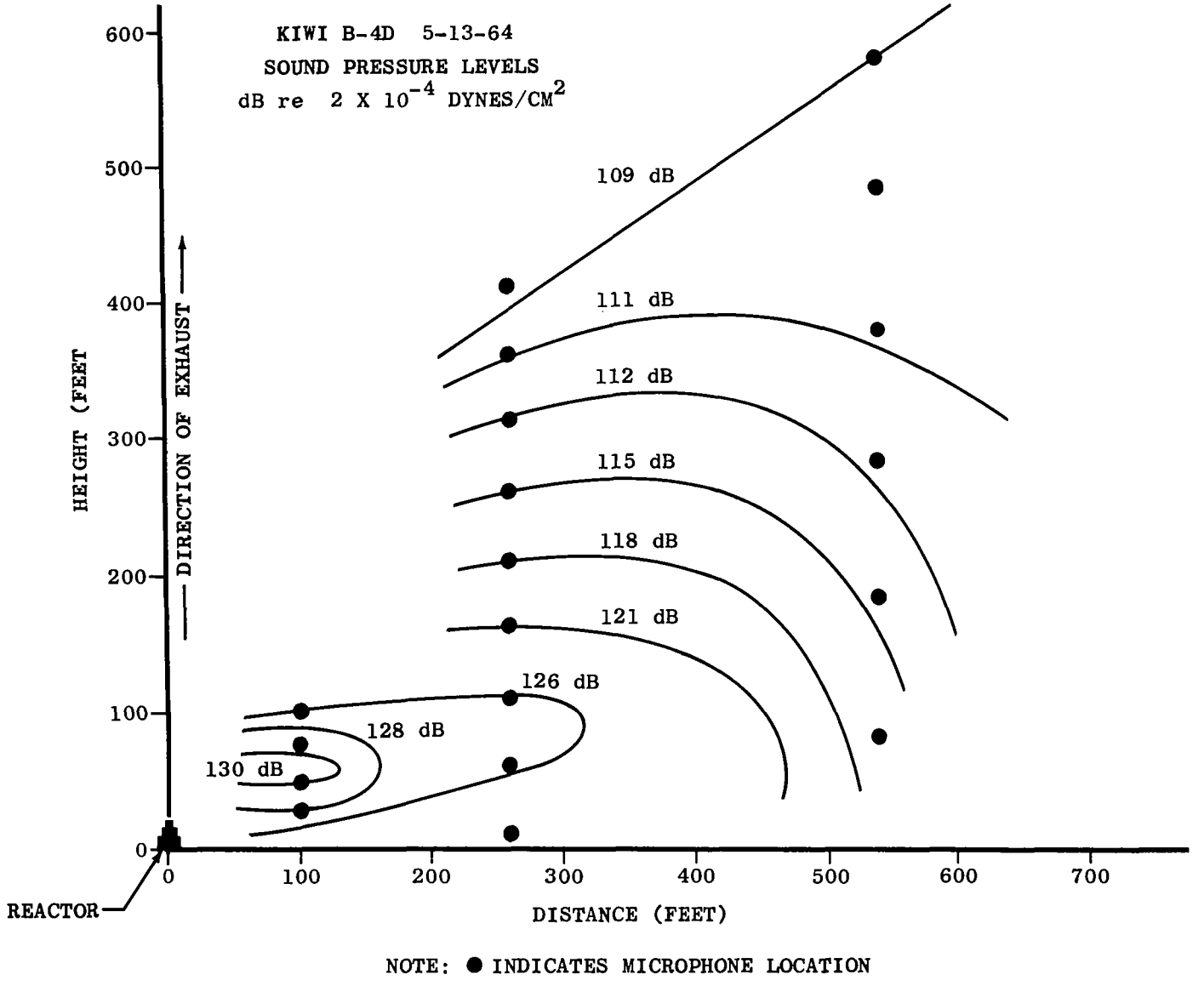

NOTE: ● INDICATES MICROPHONE LOCATION

Figure 13d. Estimated Equal Sound Pressure Level--One-Third Octave Band: Center Frequency 500 cps

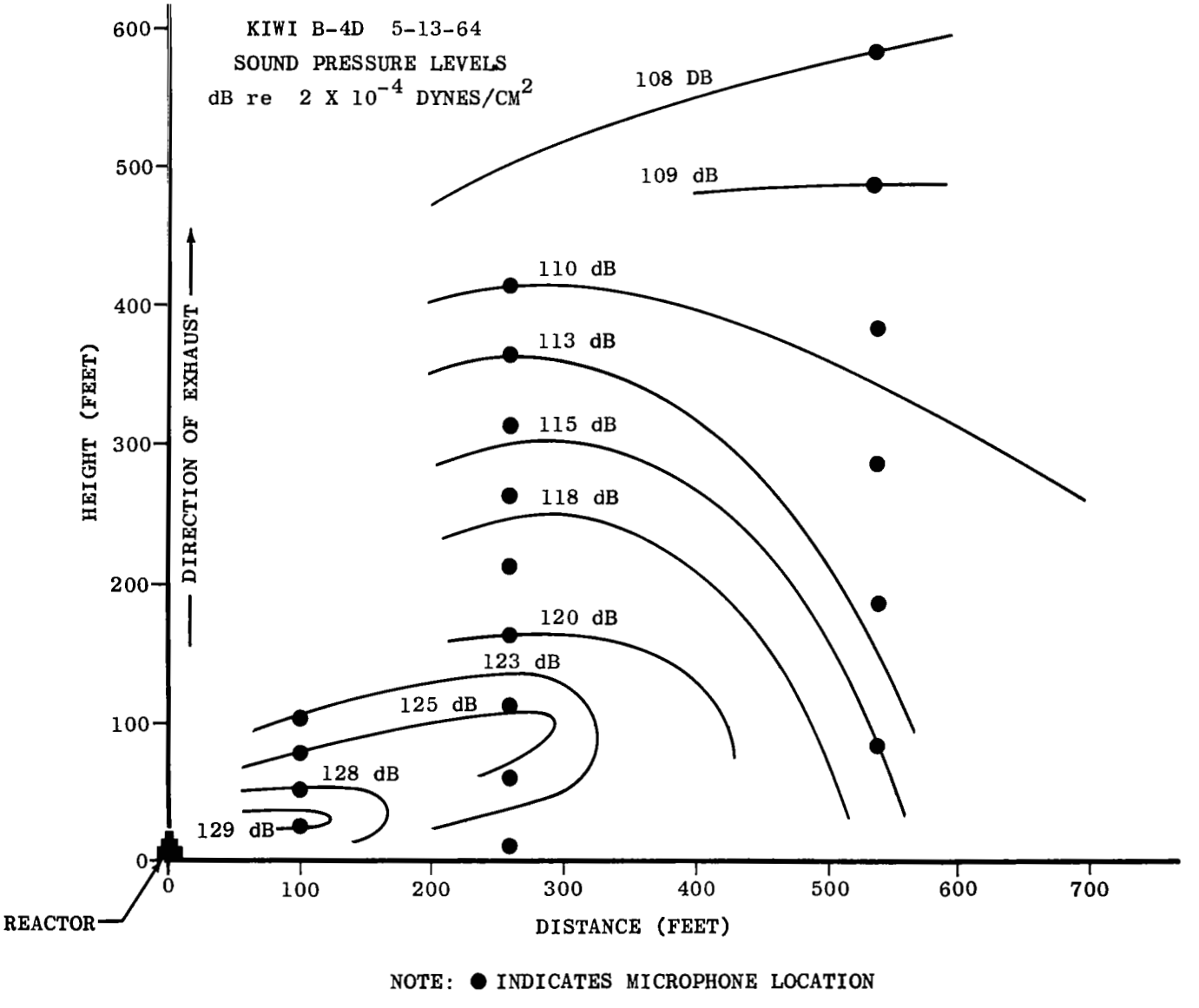

NOTE: ● INDICATES MICROPHONE LOCATION

Figure 13e. Estimated Equal Sound Pressure Level--One-Third Octave Band: Center Frequency 1000 cps

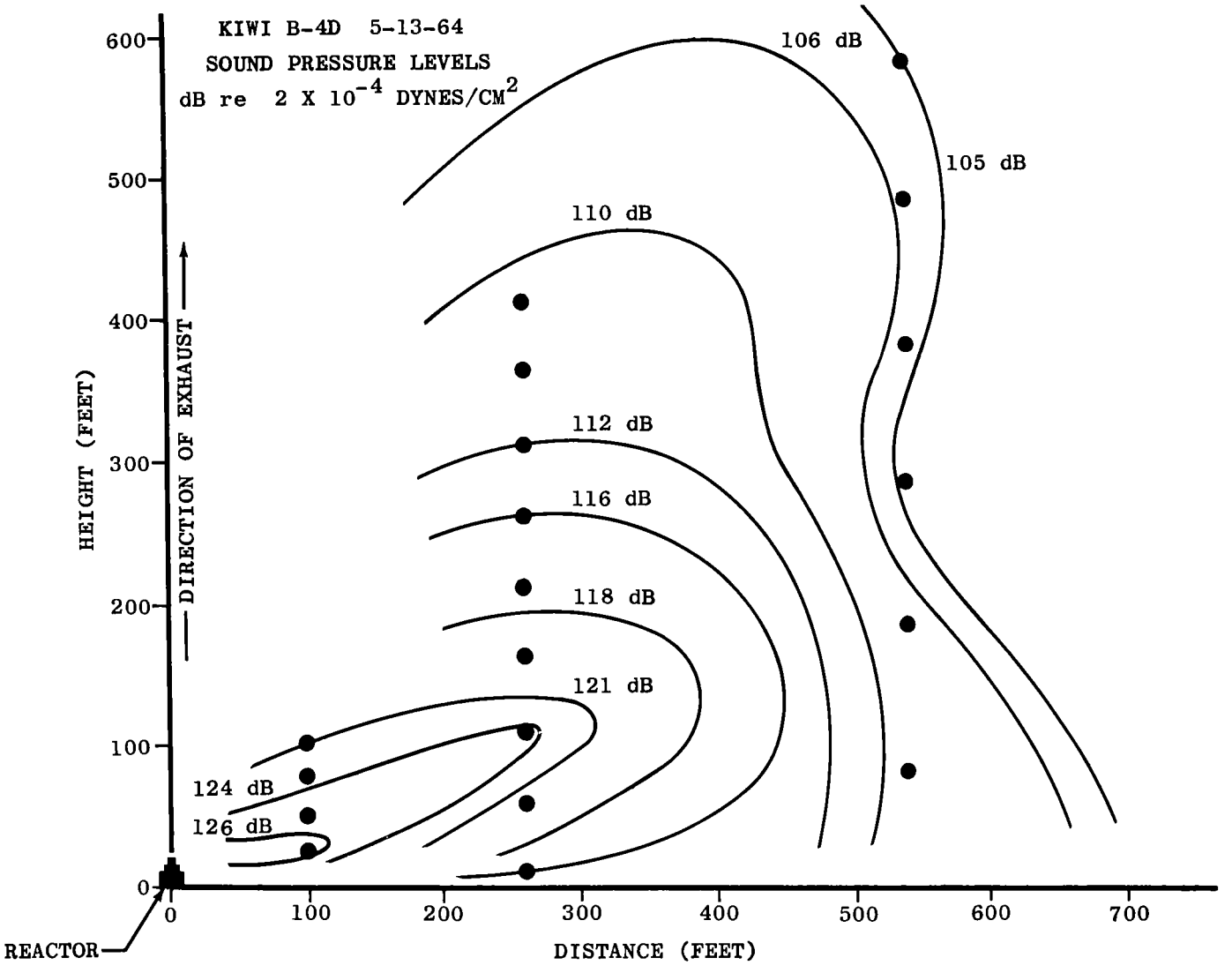

NOTE: ● INDICATES MICROPHONE LOCATION

Figure 13f. Estimated Equal Sound Pressure Level--One-Third Octave Band: Center Frequency 2000 cps

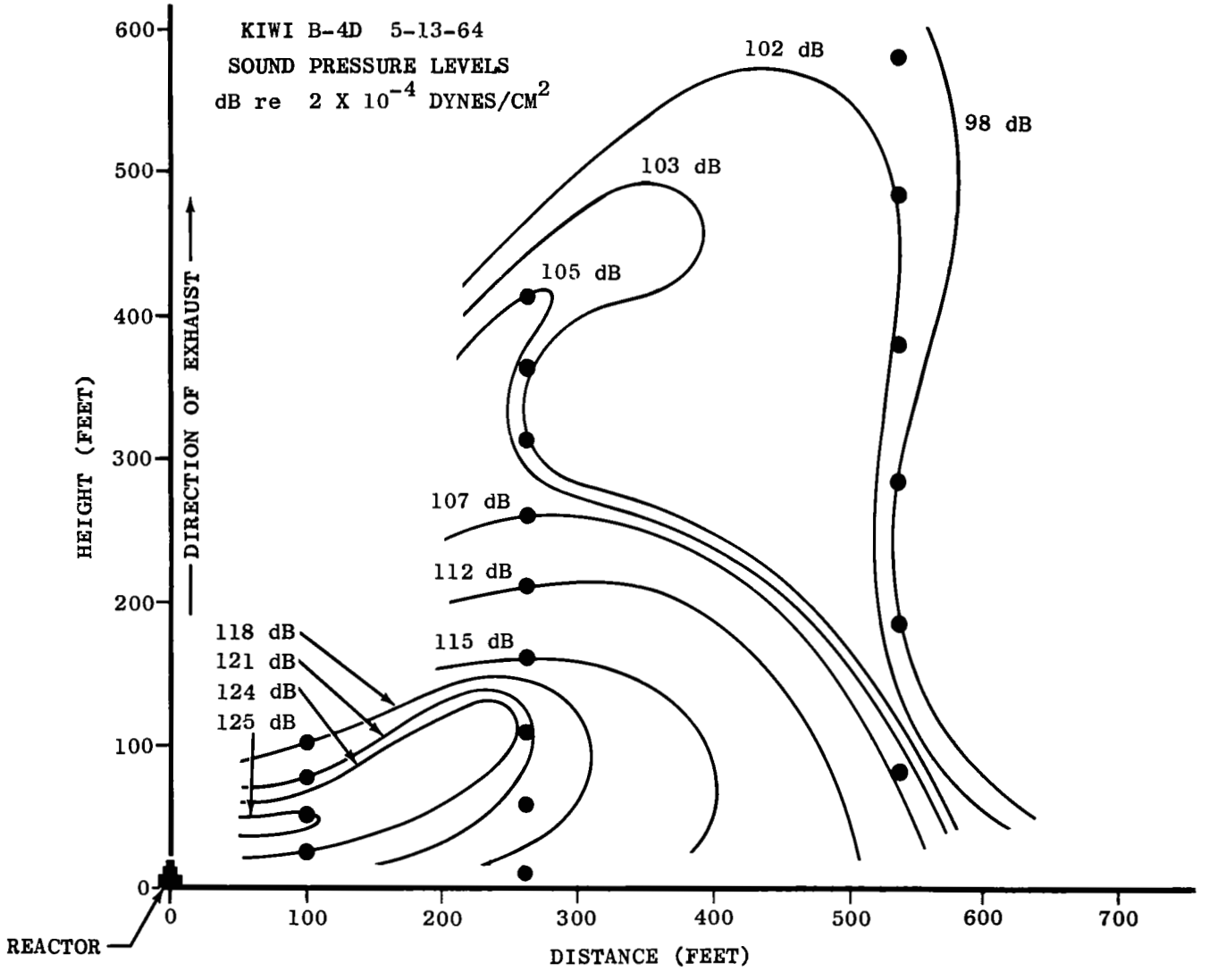

NOTE: ● INDICATES MICROPHONE LOCATION

Figure 13g. Estimated Equal Sound Pressure Level--One-Third Octave Band: Center Frequency 4000 cps

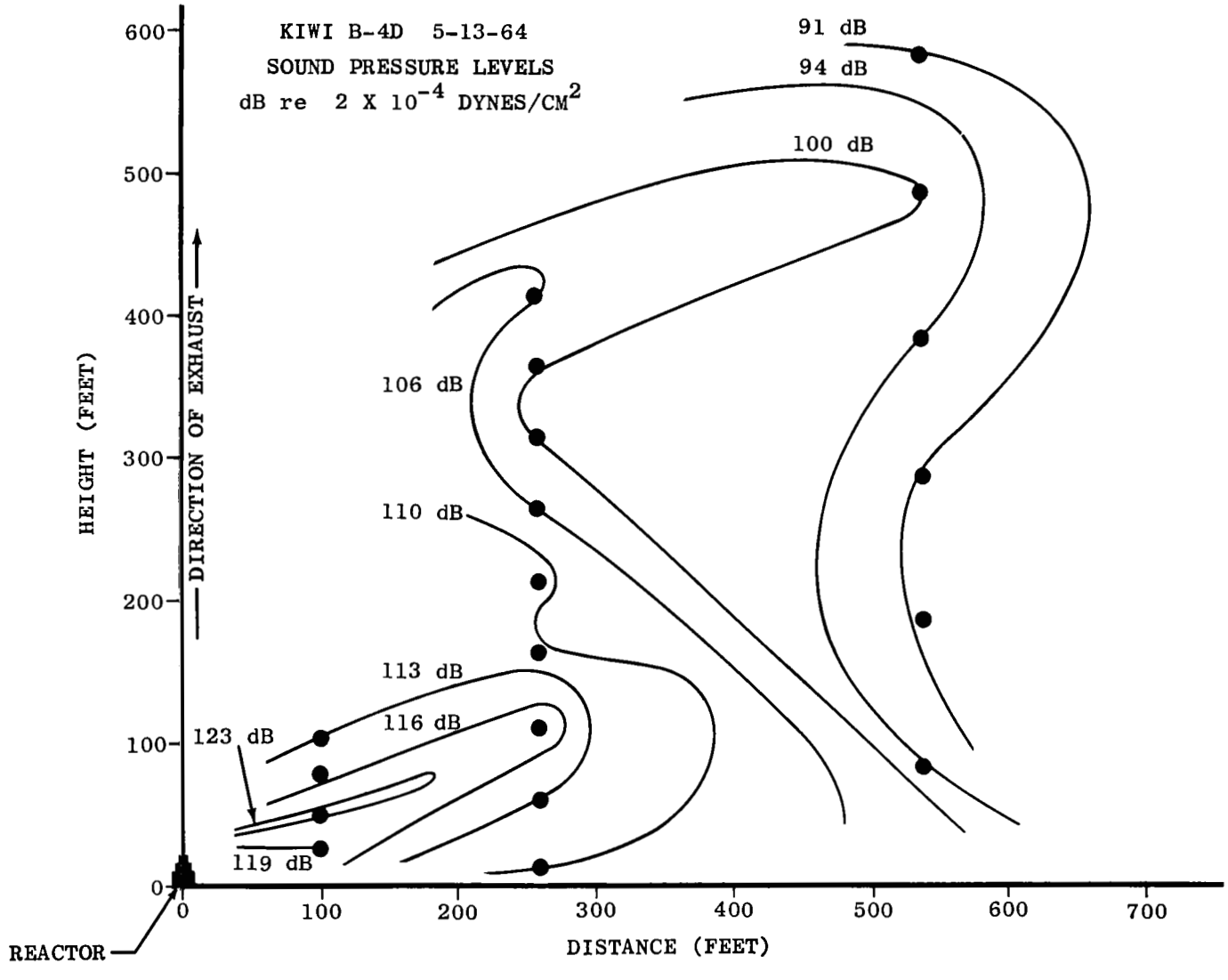

NOTE: ● INDICATES MICROPHONE LOCATION

Figure 13h. Estimated Equal Sound Pressure Level--One-Third Octave Band: Center Frequency 8000 cps

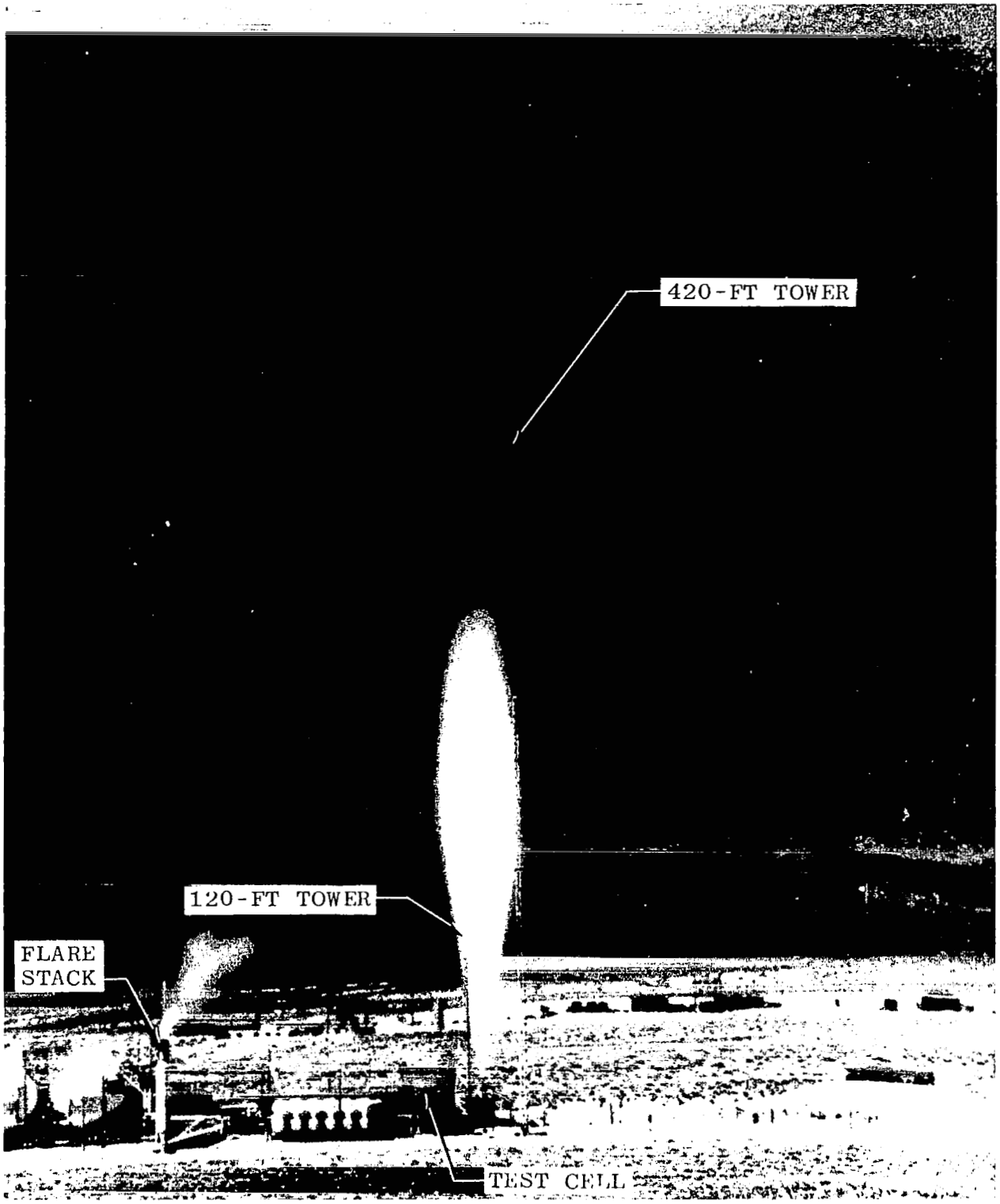

Figure 14. Infrared Photograph of KIWI B Exhaust at Full Power

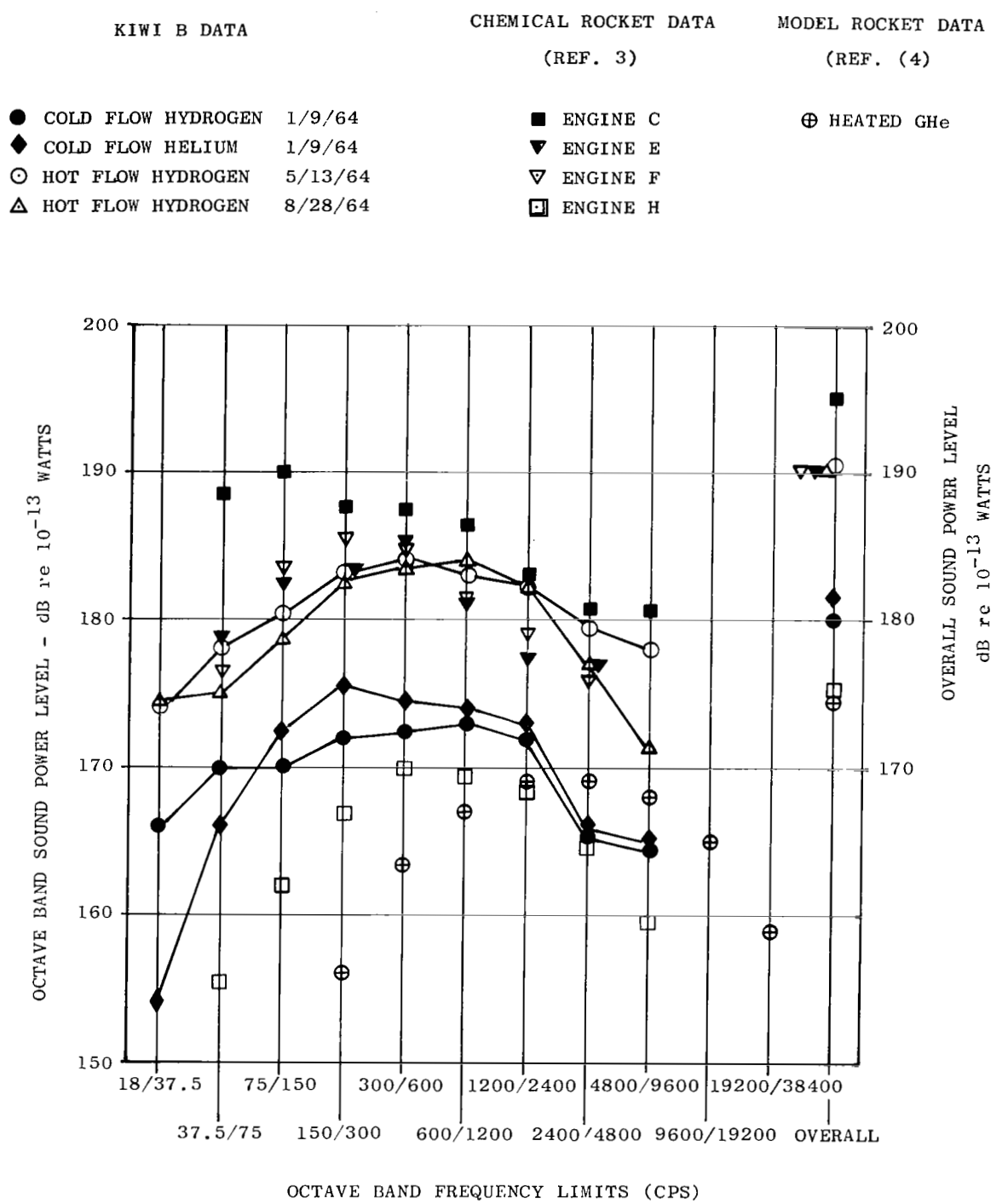

Figure 13. Comparison of Sound Power Levels for KIWI B and Chemical Rockets

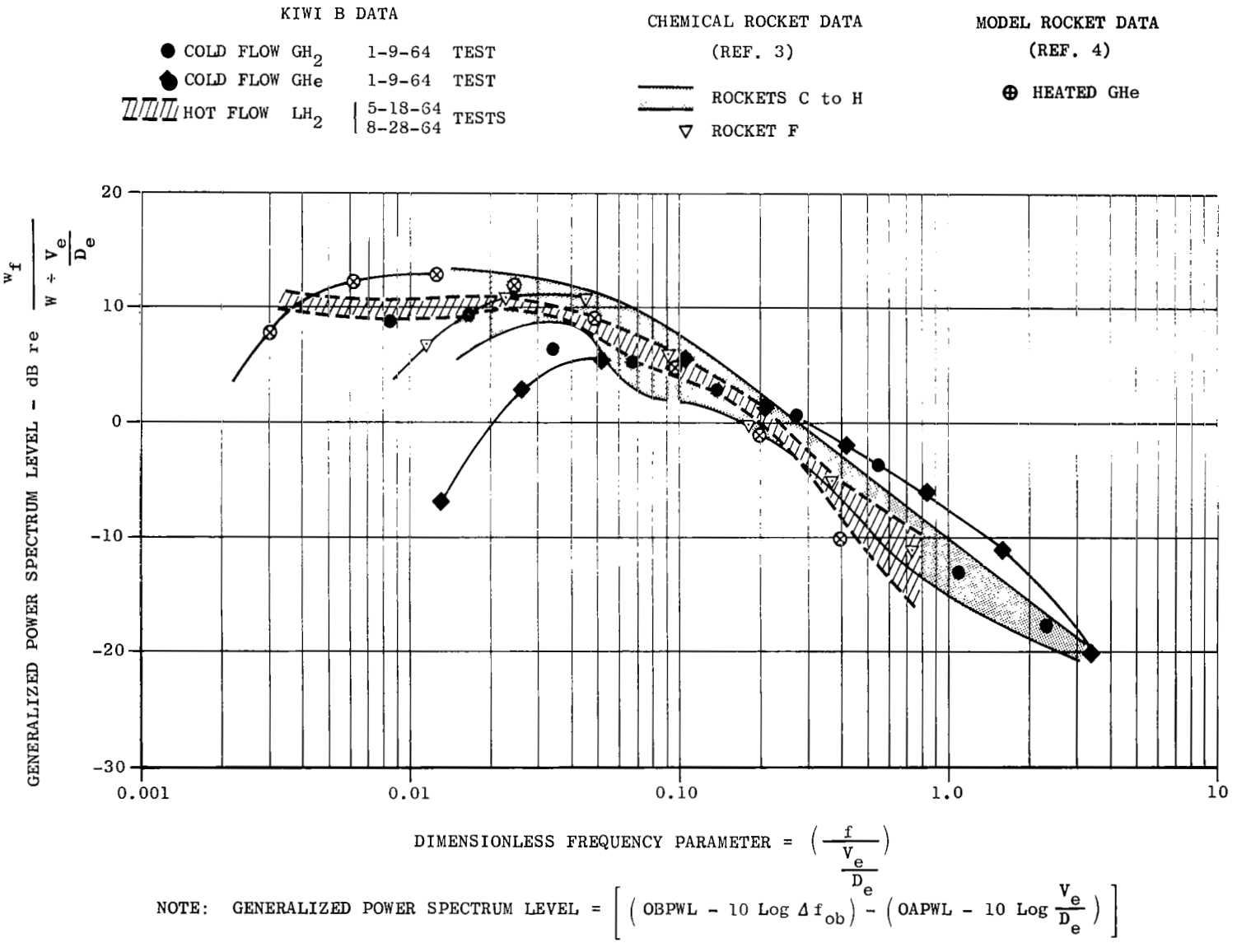

Figure 16. Generalized Sound Power Spectra of KIWI B and Chemical Rocket Noise

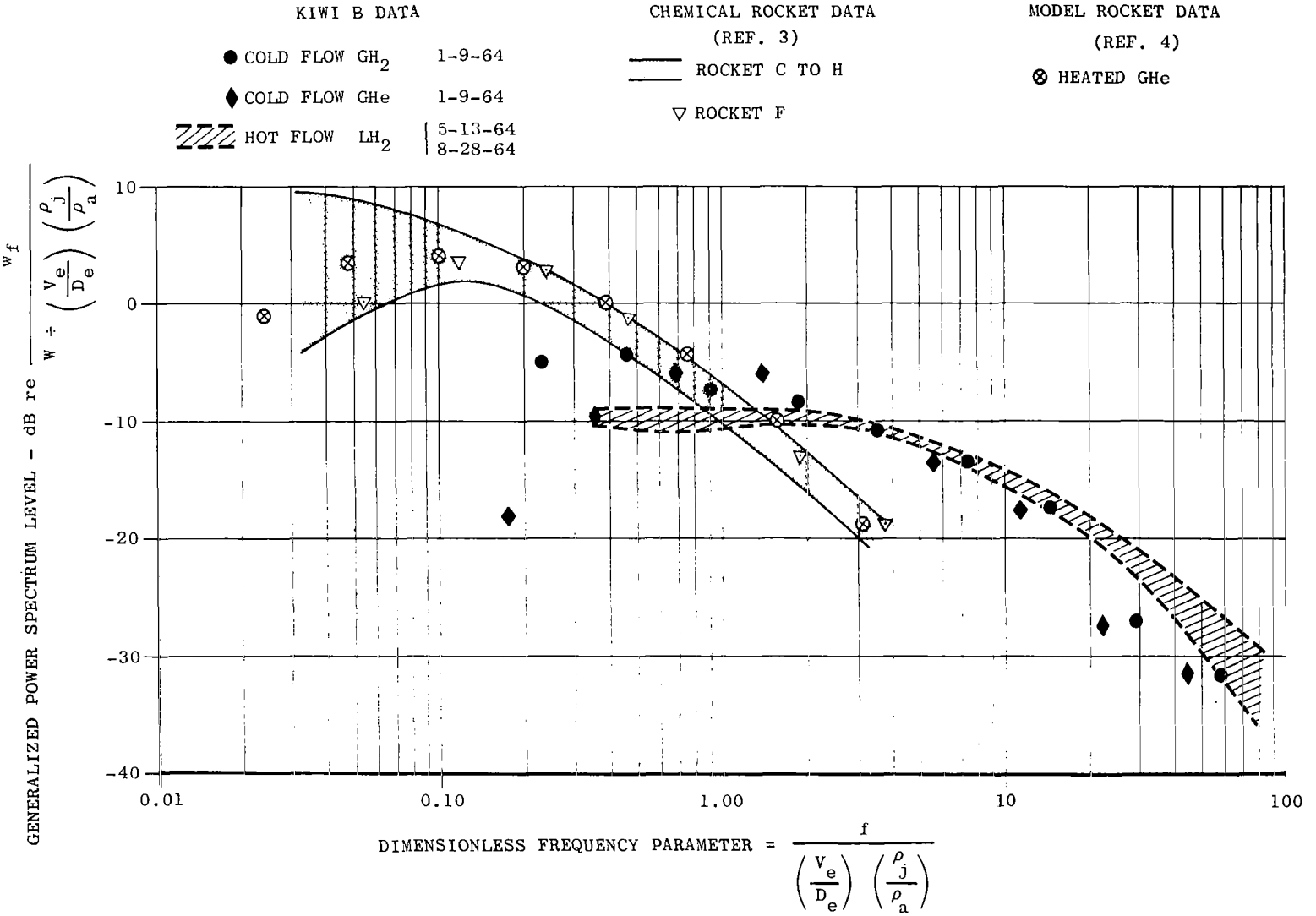

NOTE: GENERALIZED POWER SPECTRUM LEVEL = $\left\{\left(\text{OBPWL} - 10 \text{ Log } \Delta f_{ob}\right) - \left[\text{OAPWL} - 10 \text{ Log}\left(\frac{V_e}{D_e} \times \frac{\rho_j}{\rho_a}\right)\right]\right\}$

Figure 17. Generalized Sound Power Spectra of KIWI B and Chemical Rocket Noise (Effect of Density Ratio)

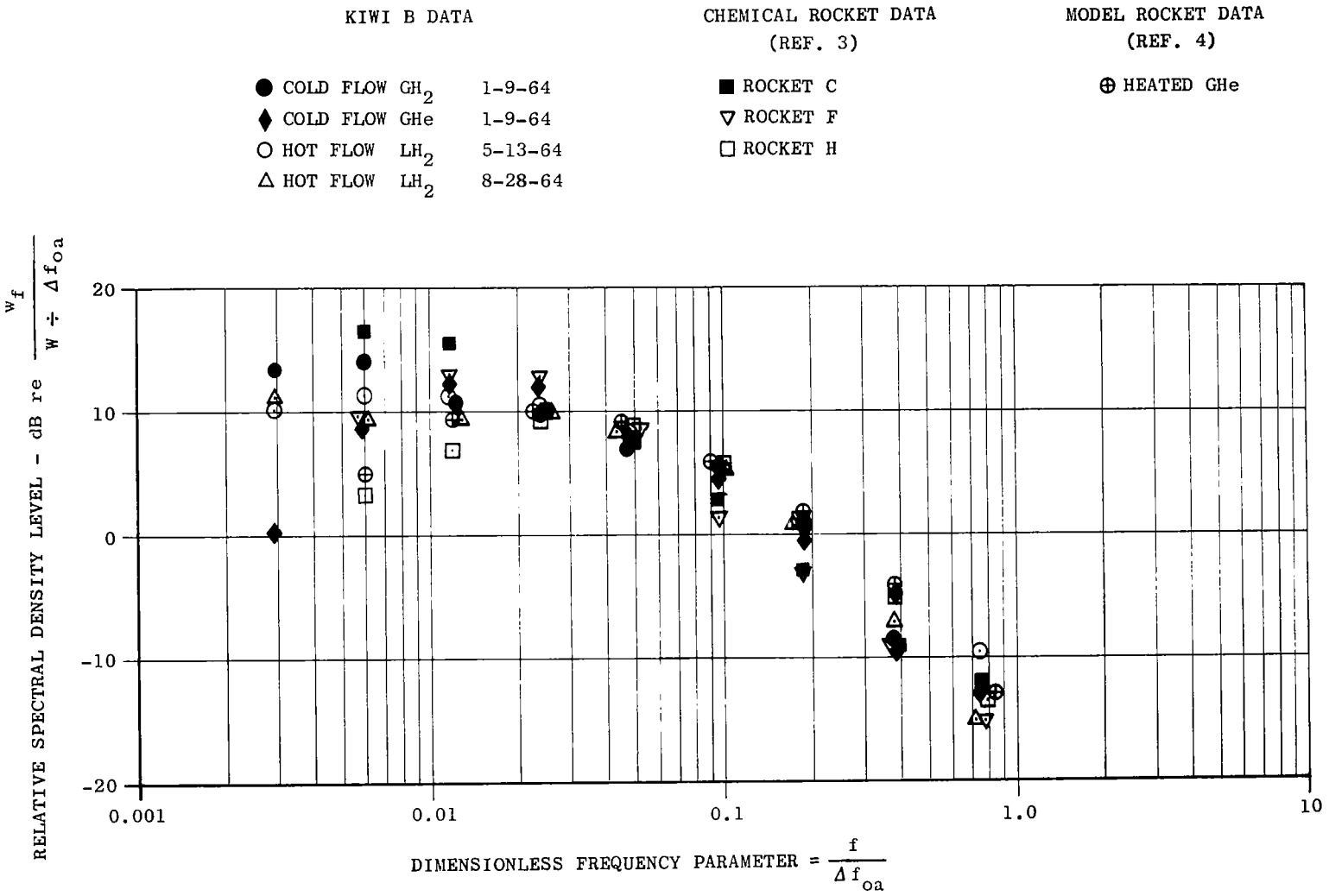

NOTE: RELATIVE SPECTRAL DENSITY LEVEL = $\left[\left(\text{OBPWL} - 10 \text{ Log } \Delta f_{ob} \right) - \left(\text{OAPWL} - 10 \text{ Log } \Delta f_{oa} \right) \right]$

Figure 18. Relative Spectral Density Levels for KIWI B and Chemical Rocket Noise

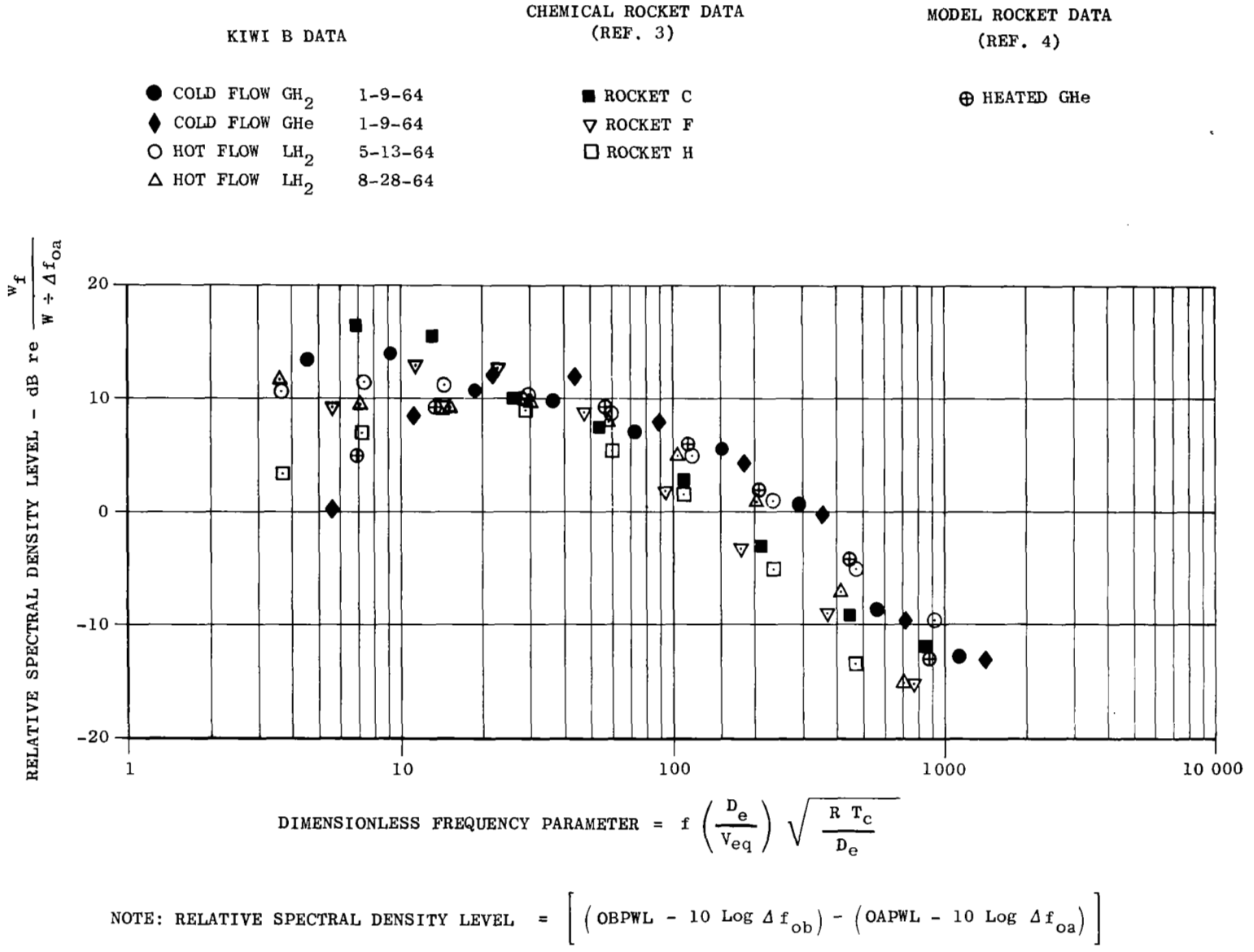

Figure 19. Generalized Sound Spectral Density for KIWI B and Chemical Rocket Noise (Effect of Exhaust Gas Parameters)

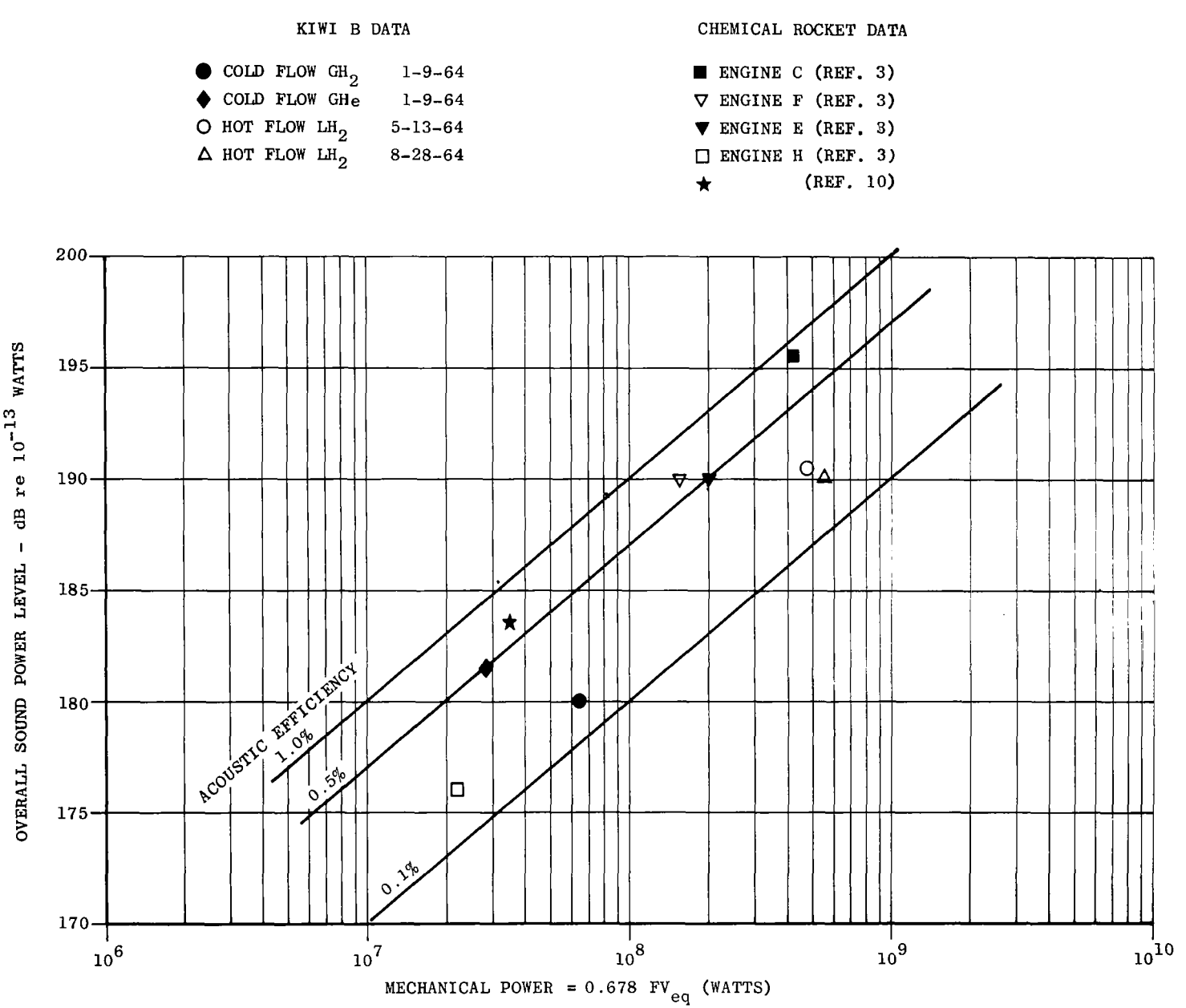

Figure 20. Relation of Radiated Sound Power to Exhaust Mechanical Power

420-FT TOWER DATA		WEIGHT FLOW LB/SEC	V_{eq} FT/SEC
● COLD FLOW GH_2	1-9-64	100	5400
⊙ HOT FLOW GH_2	5-13-64	69	17 900
△ HOT FLOW GH_2	8-28-64	69	19 500
◆ COLD FLOW GHe	1-9-64	130	3200

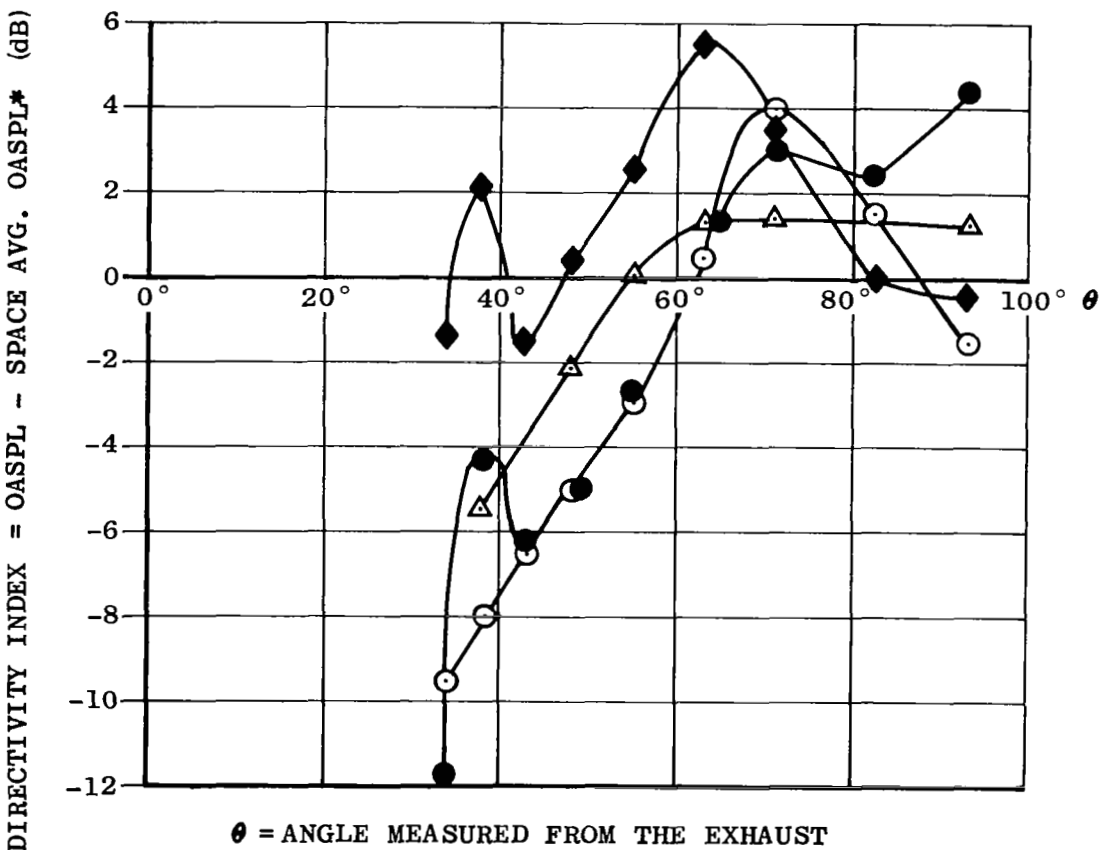

θ = ANGLE MEASURED FROM THE EXHAUST FLOW DIRECTION WITH THE ORIGIN AT THE CENTER OF THE NOZZLE EXIT

* AT 350-FT RADIUS FROM NOZZLE

Figure 21. Comparison of Acoustical Directivity Patterns for Hot and Cold Gas Flows

KIWI B-4D POWER RUN 5-13-64

△ 120-FT TOWER: SPACE AVG. OASPL = 140 dB @ 110-FT RADIUS

□ 420-FT TOWER: SPACE AVG. OASPL = 132 dB @ 350-FT RADIUS

⊙ BALLOON CABLE: SPACE AVG. OASPL = 125 dB @ 600-FT RADIUS

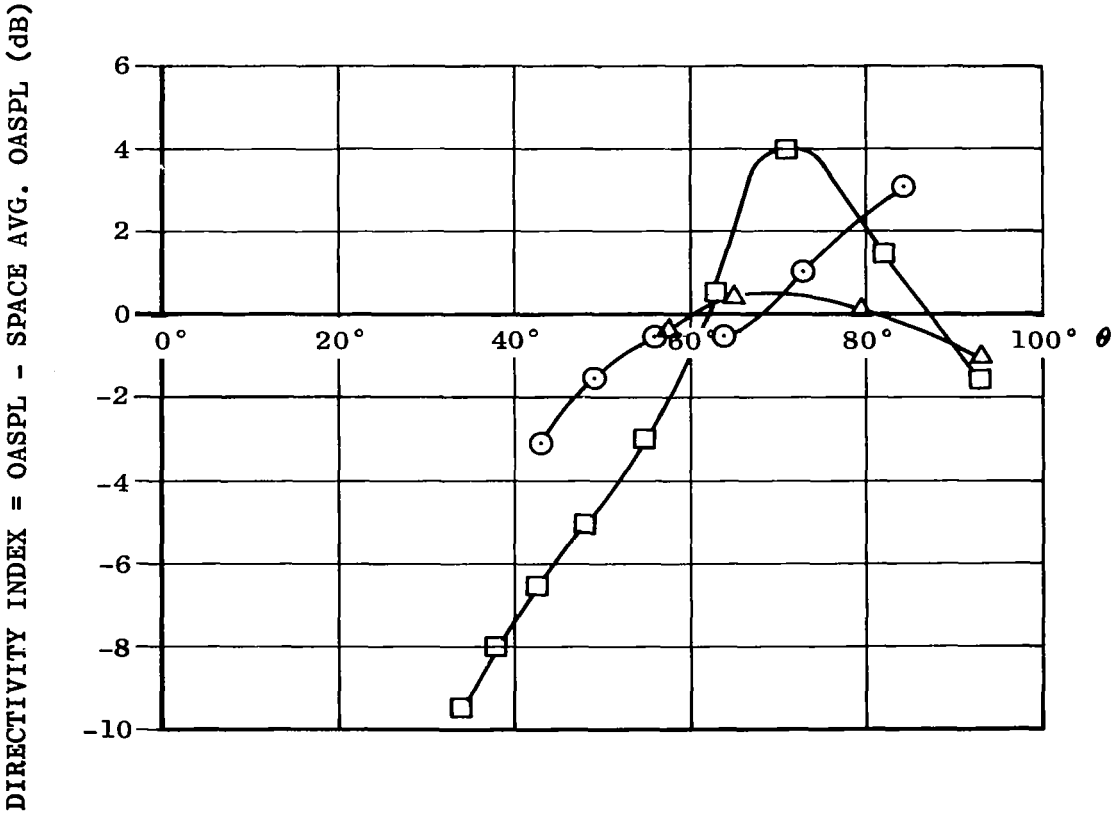

θ = ANGLE MEASURED FROM THE EXHAUST FLOW DIRECTION WITH THE ORIGIN AT THE CENTER OF THE NOZZLE EXIT

Figure 22. Comparison of Acoustical Directivity Patterns for Overall Sound Pressure Levels

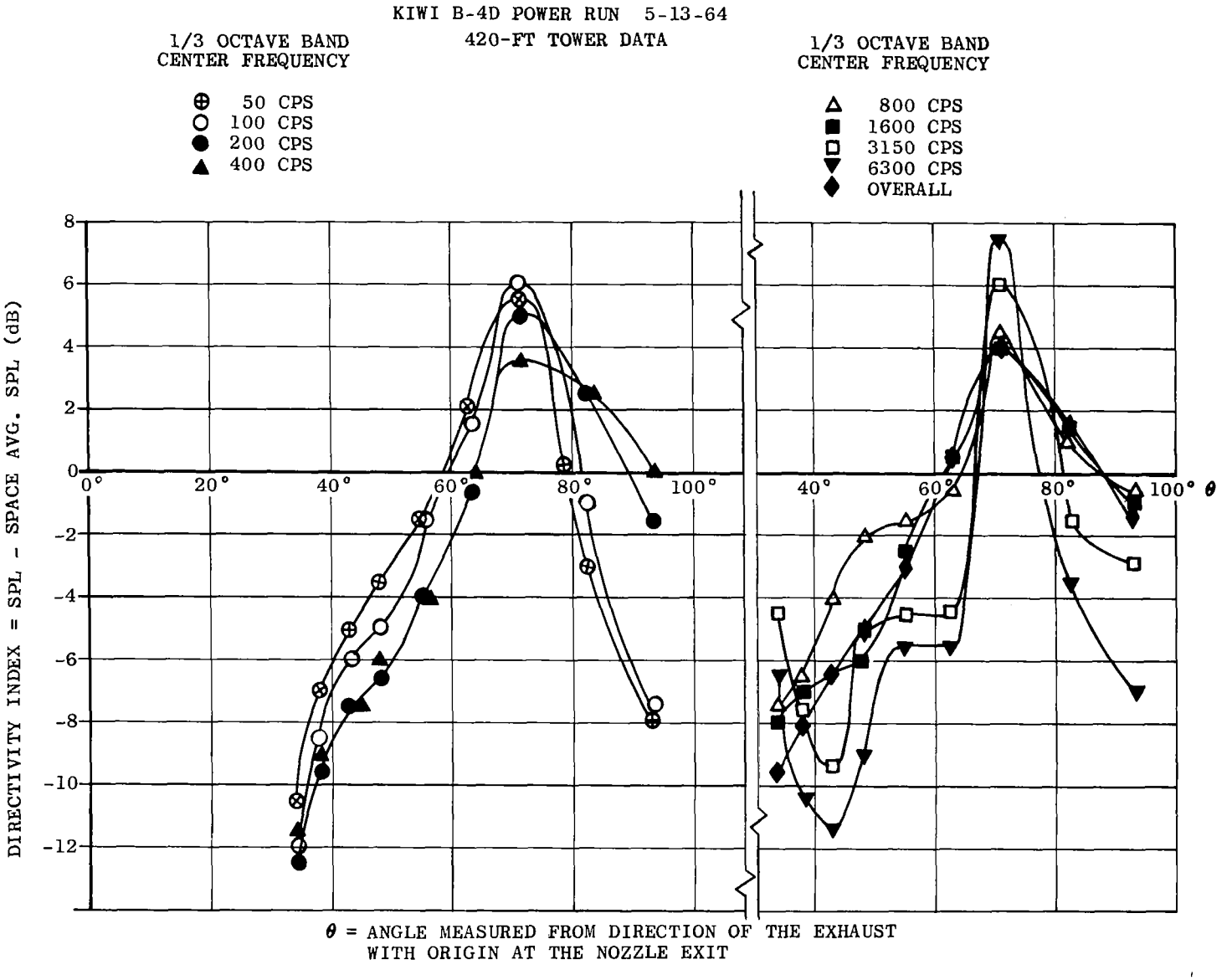

Figure 23. Acoustical Directivity Patterns in One-Third Octave Bands

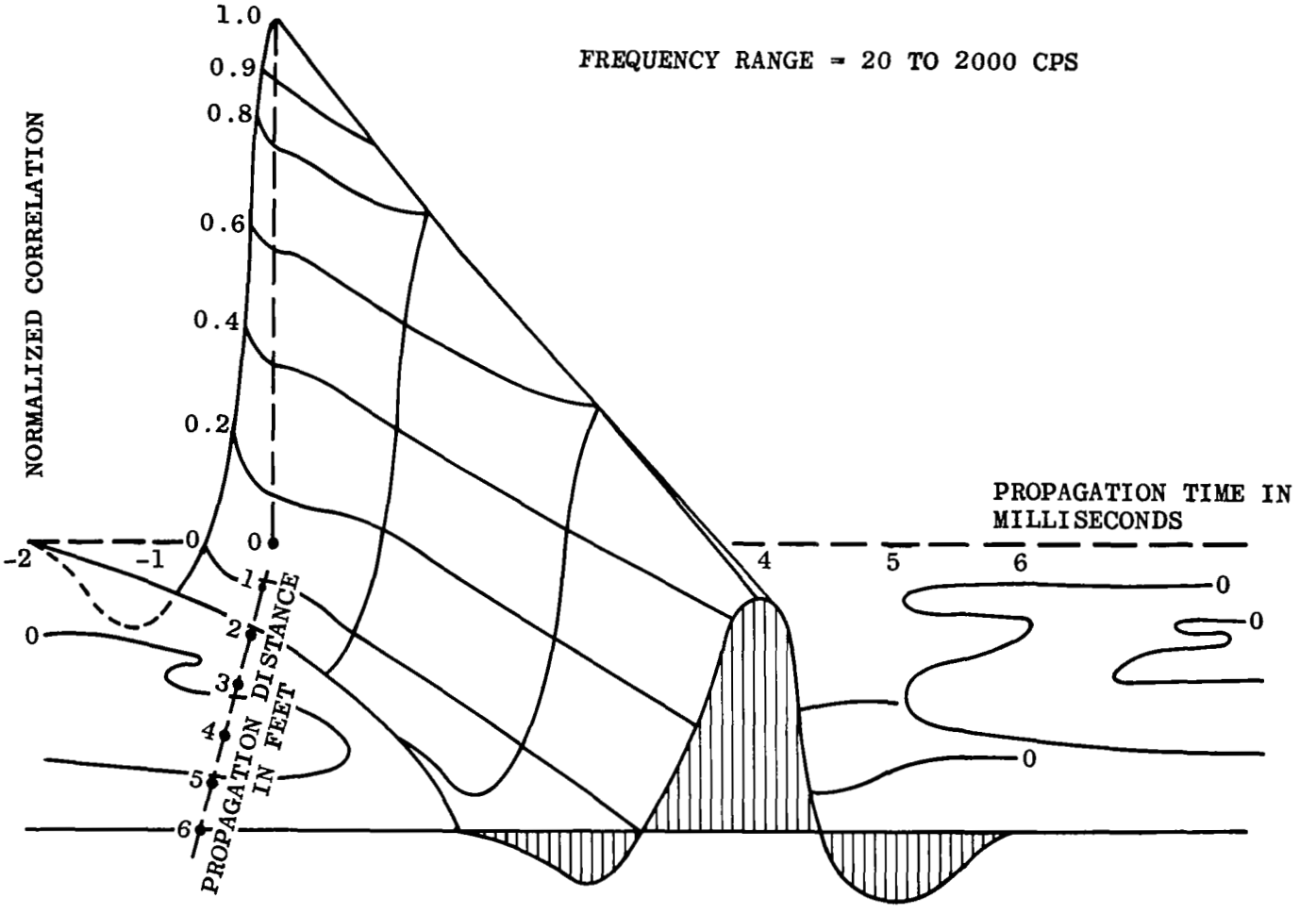

Figure 24. Representation of Space-Time Correlation of KIWI B Acoustic Field

NOTE: Microphone 17 was 110 feet from the reactor for both EP's. Separation distance for microphones 17, 18 and 19 were different for 5/13/64 and 8/28/64 EP's. (See Tables IV and V.)

SYMBOL	MICROPHONES UTILIZED	TEST DATE
○	17 x 17	5/13/64
■	17 x 18	8/28/64
□	17 x 18	5/13/64
◪	18 x 19	5/13/64
△	17 x 19	5/13/64
●	18 x 19	8/28/64
▲	17 x 19	8/28/64

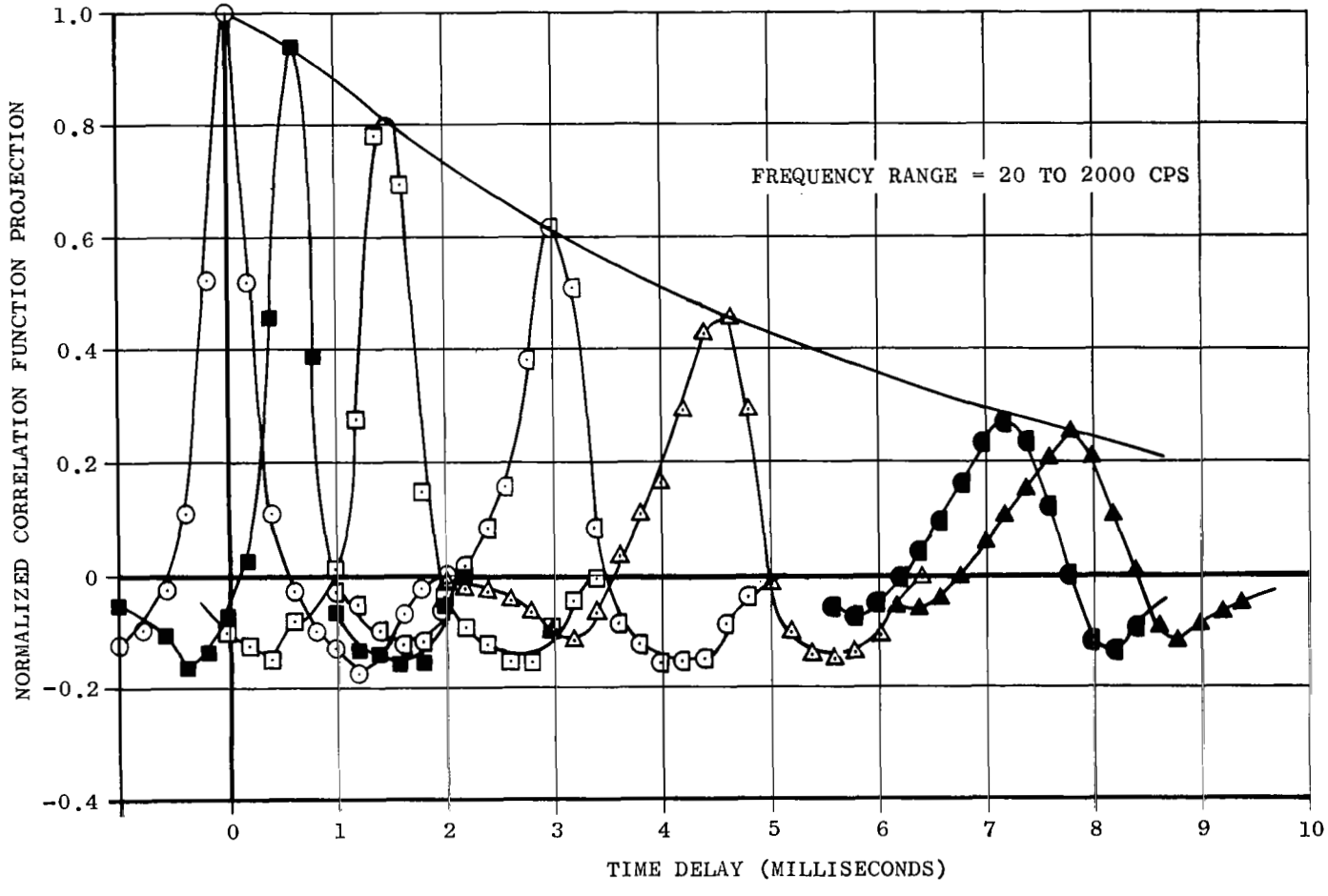

Figure 25. Projections of the Space-Time Correlations of the Acoustic Field for the KIWI B Engine

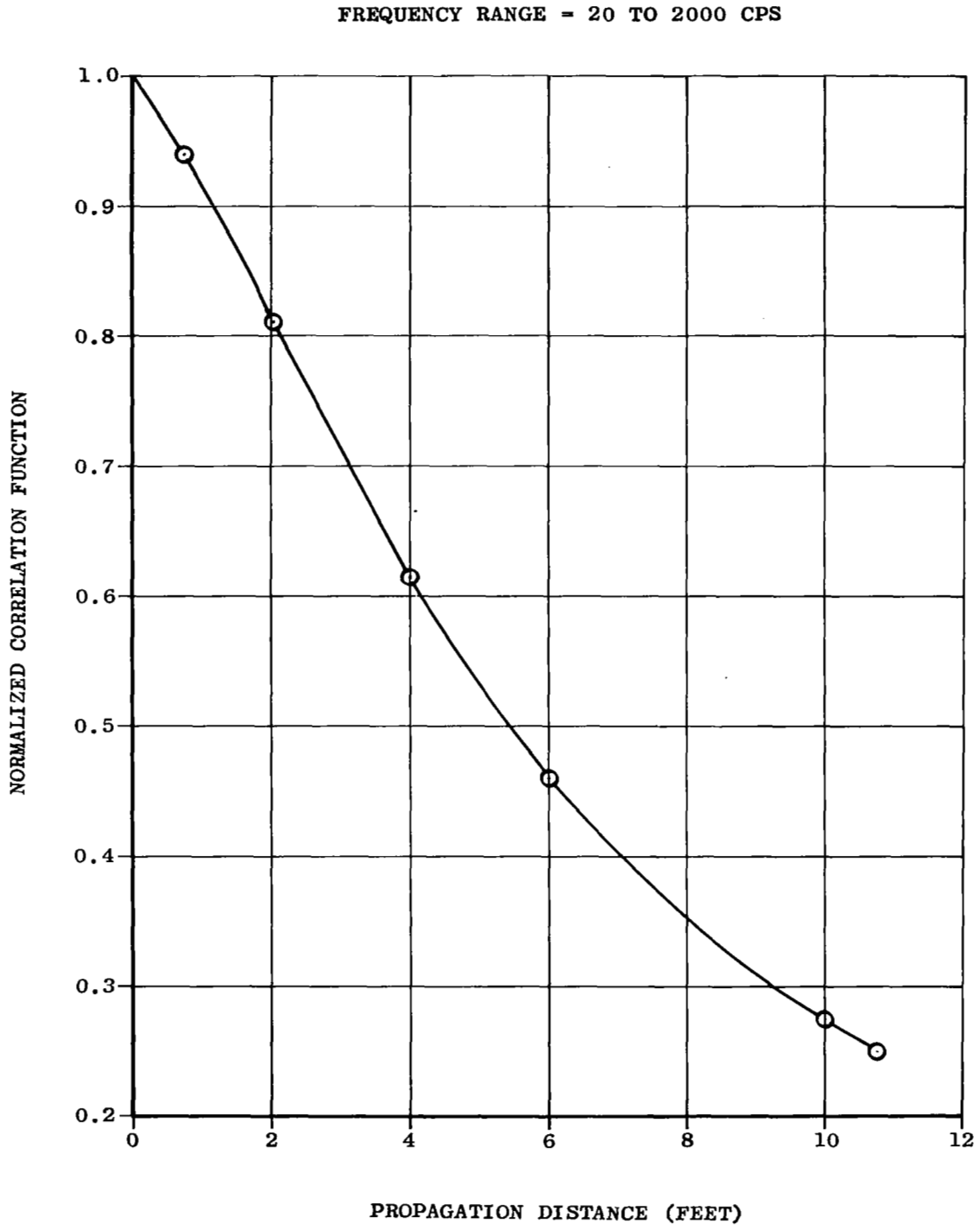

Figure 26. Variation of Peak Correlation Amplitude with Distance

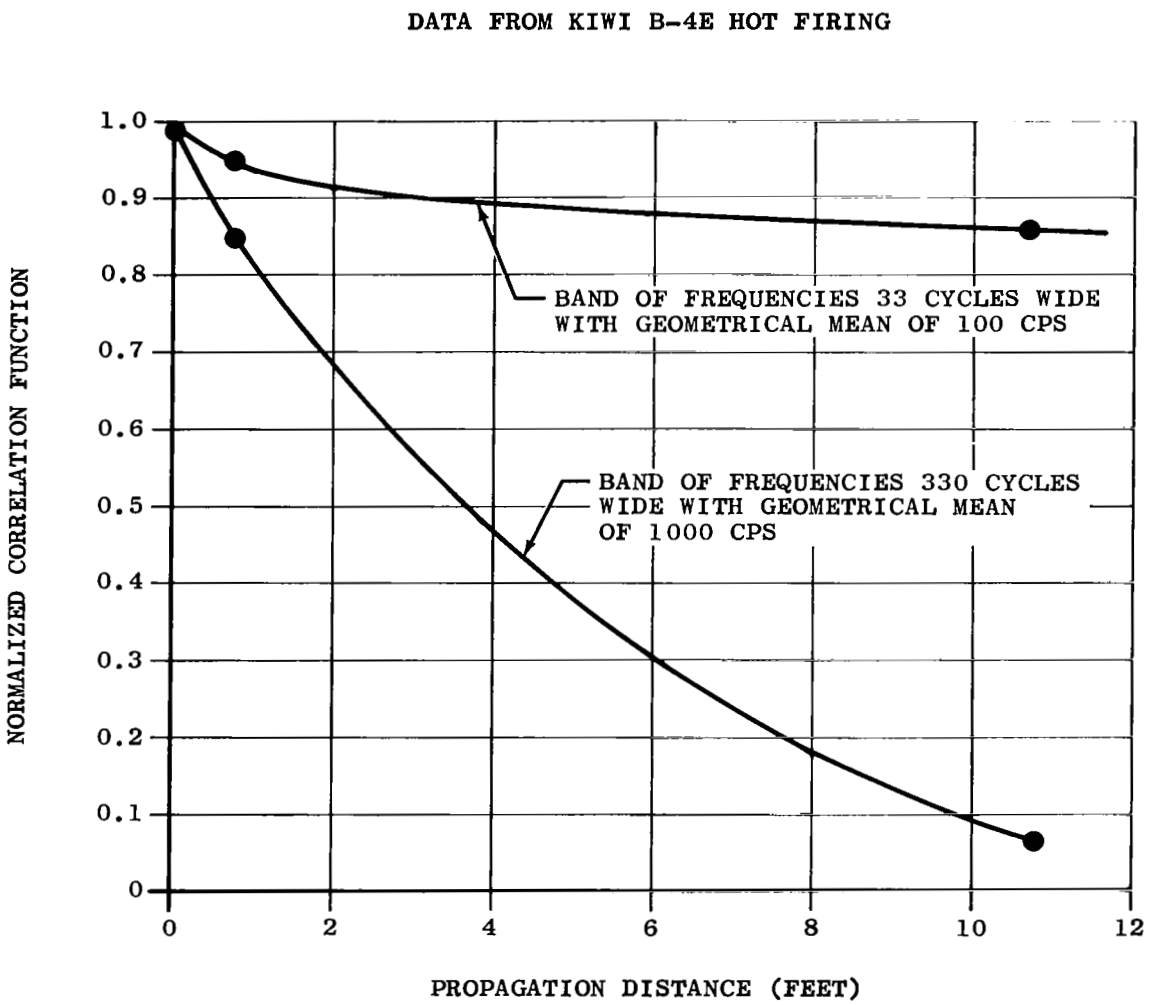

Figure 27. Comparison of Spatial Correlation Maxima for Low and High Frequencies

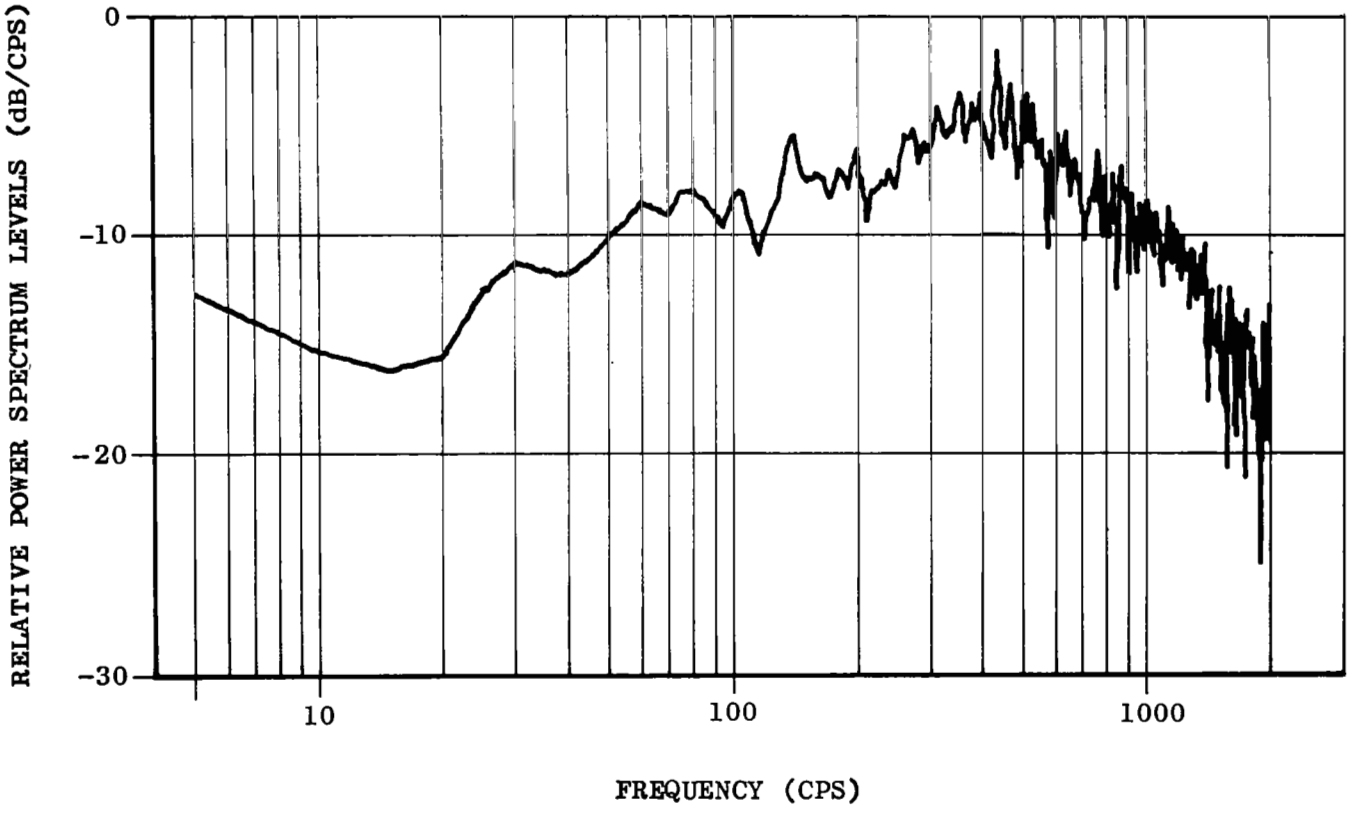

Figure 28. Typical Cross Power Spectrum Level Plot

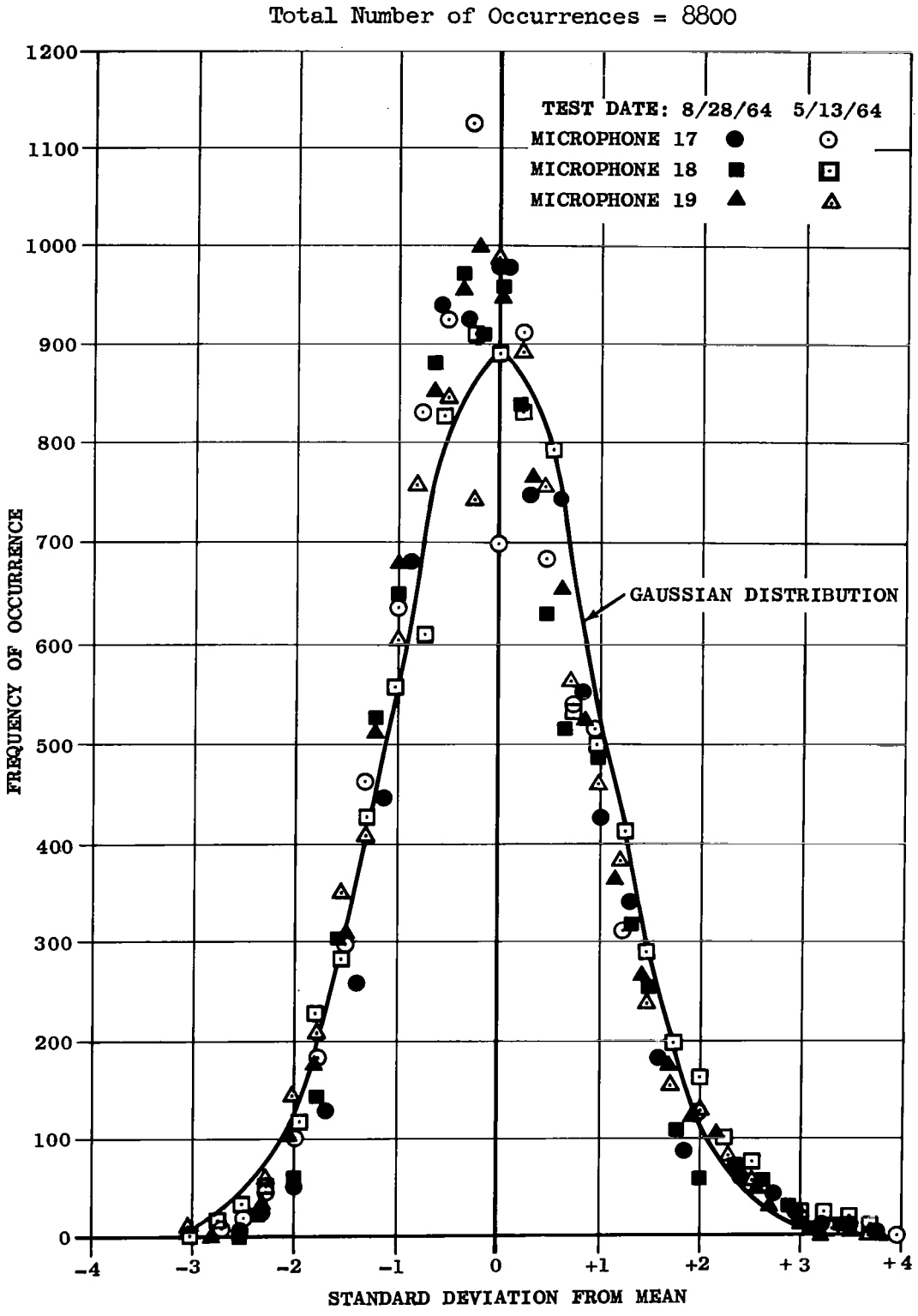

Figure 29. Distribution of Instantaneous Peak Pressures

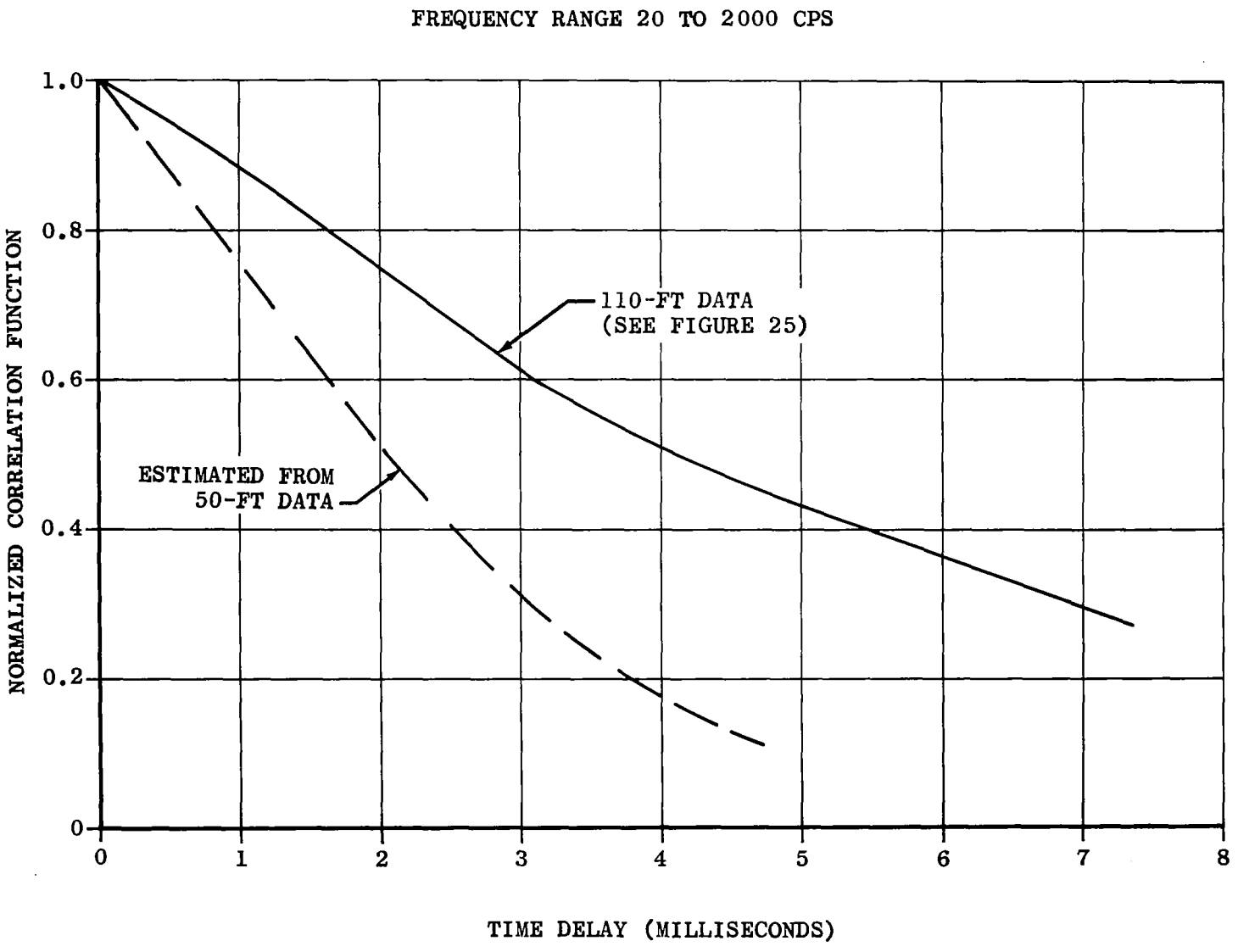

Figure 30. Comparisons of Projections of Space-Time Correlation at Two Distances From the Source

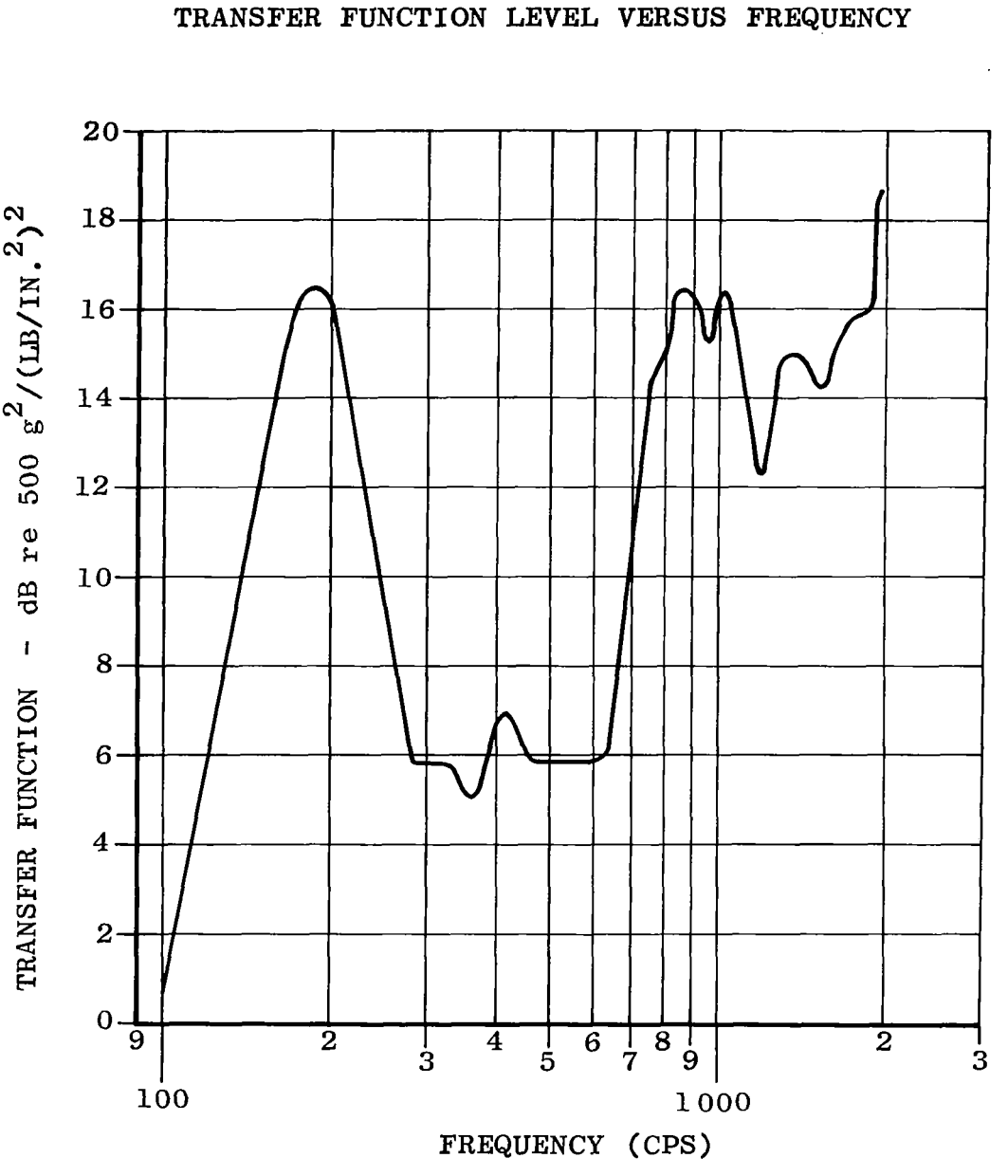

$$TF = 10 \log_{10}\left[\frac{\text{ACCELERATION OF DEWAR } (g^2/\text{CPS})}{\text{IMPINGING SOUND PRESSURE } \left[(\text{LB/IN.}^2)^2/\text{CPS}\right]}\right]$$

Figure 31. Plot of Transfer Function for Dewar During KIWI B 4D Power Run

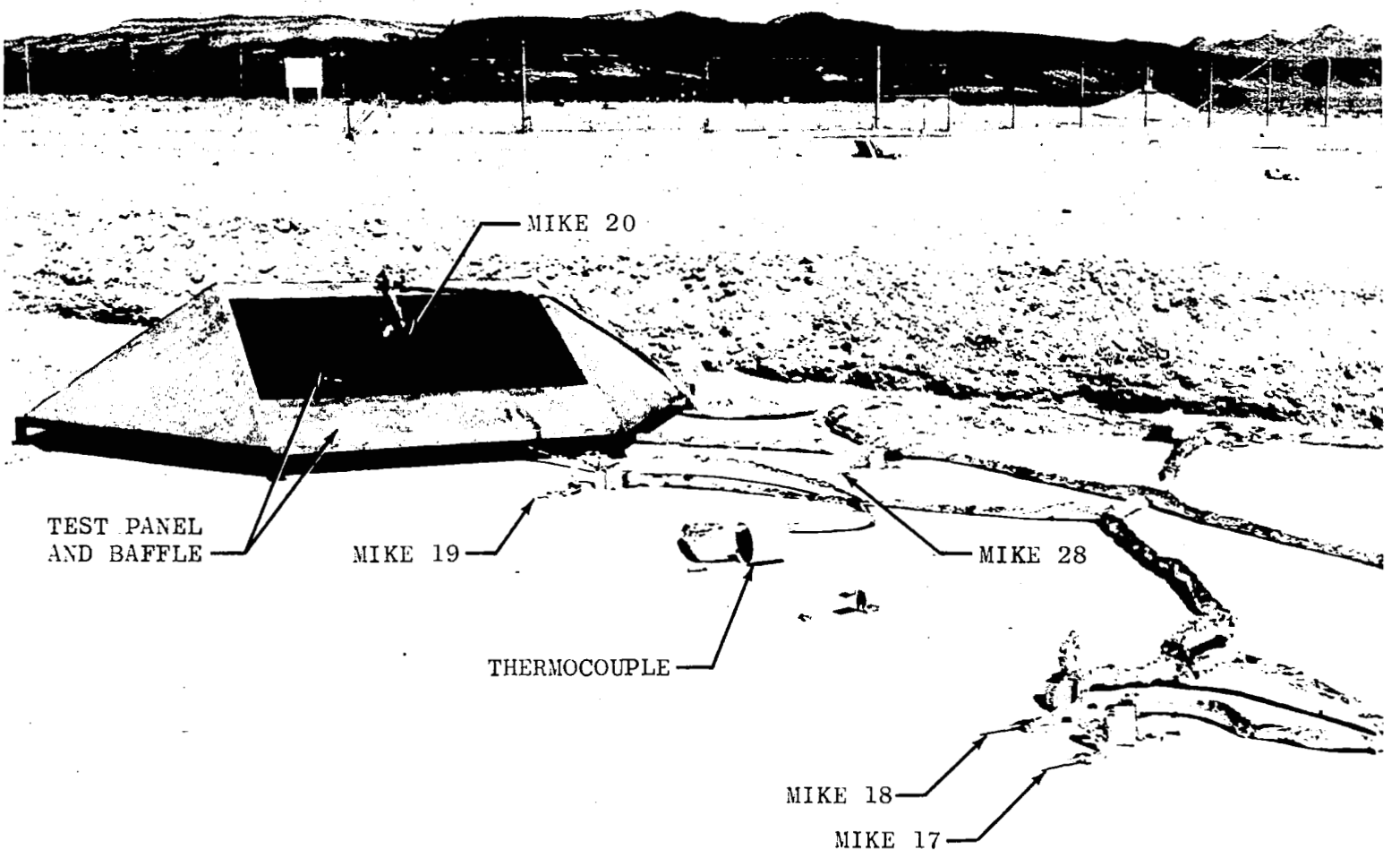

Figure 32. Detailed View of Installation of Correlation Microphones for EP V

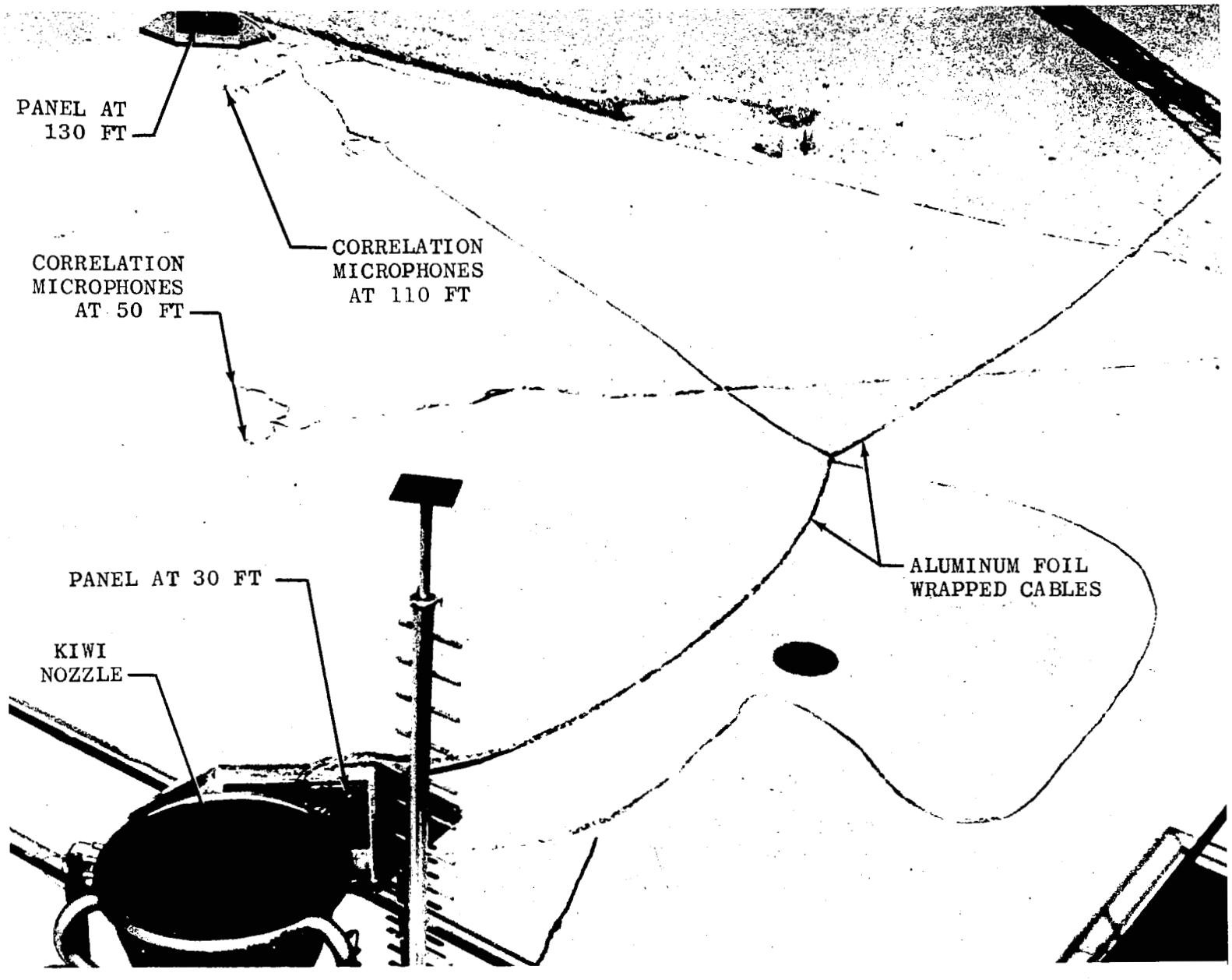

Figure 33. View of Near-Field Instrumentation EP V

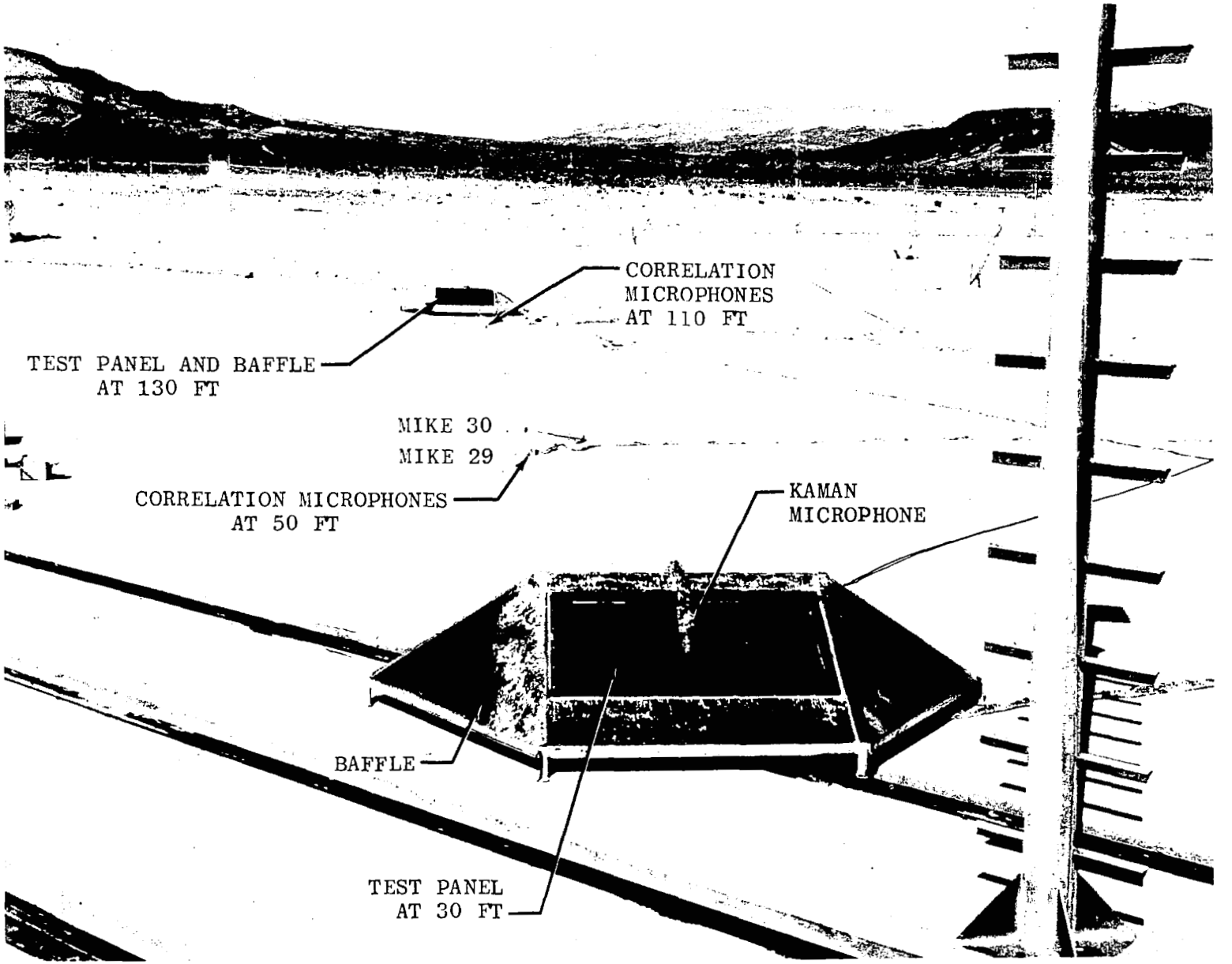

Figure 34. EP V Near-Field Instrumentation Viewed From Reactor

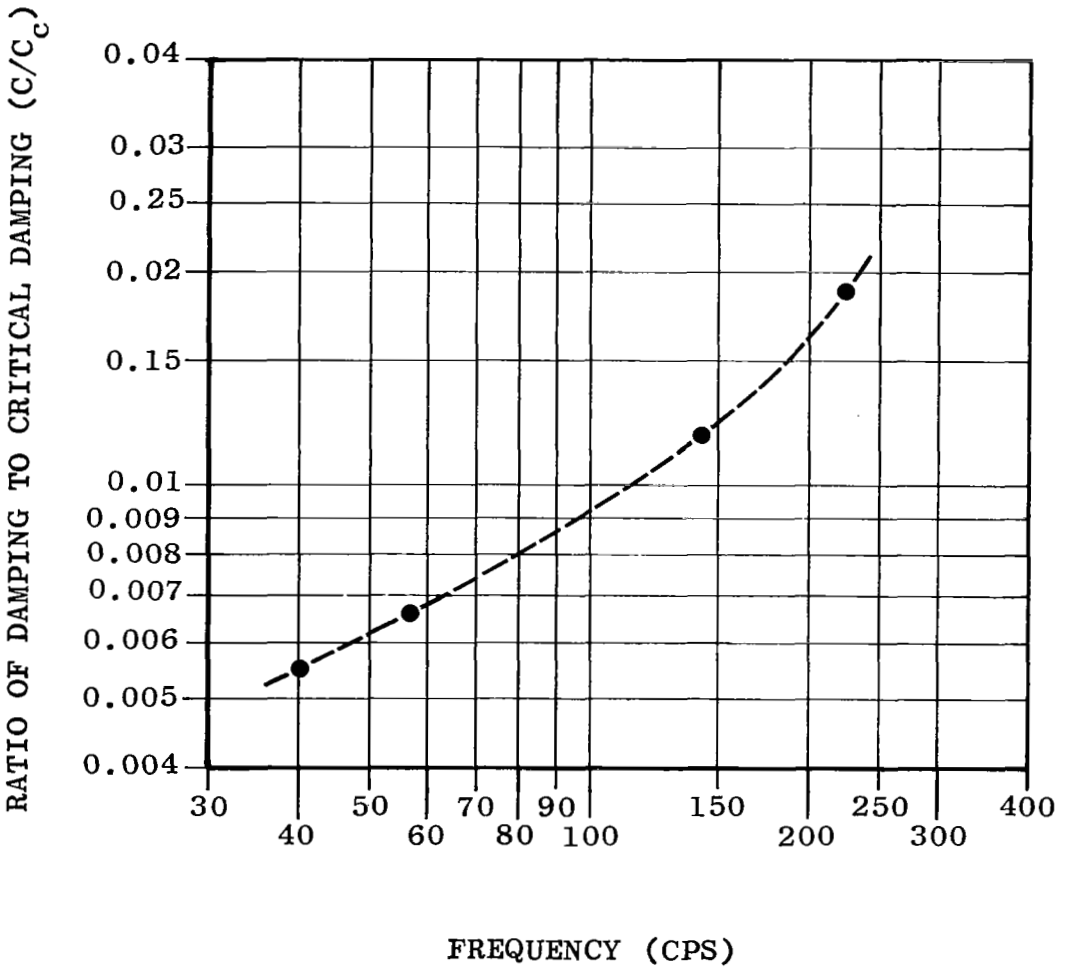

Figure 35. Measured Damping of KIWI B Test Panel

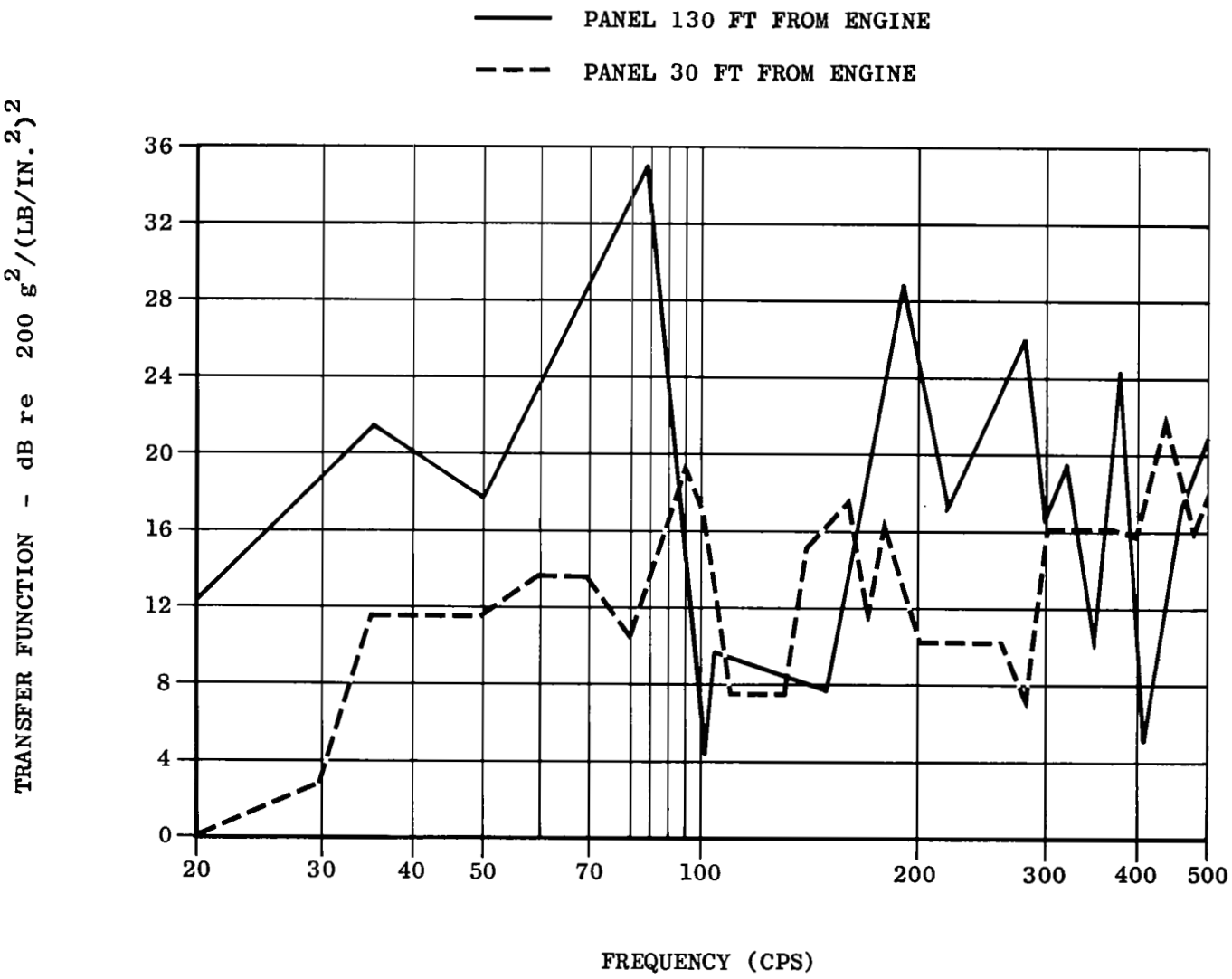

Figure 36. Power Transfer Function for Accelerometer 1 on KIWI B Test Panels

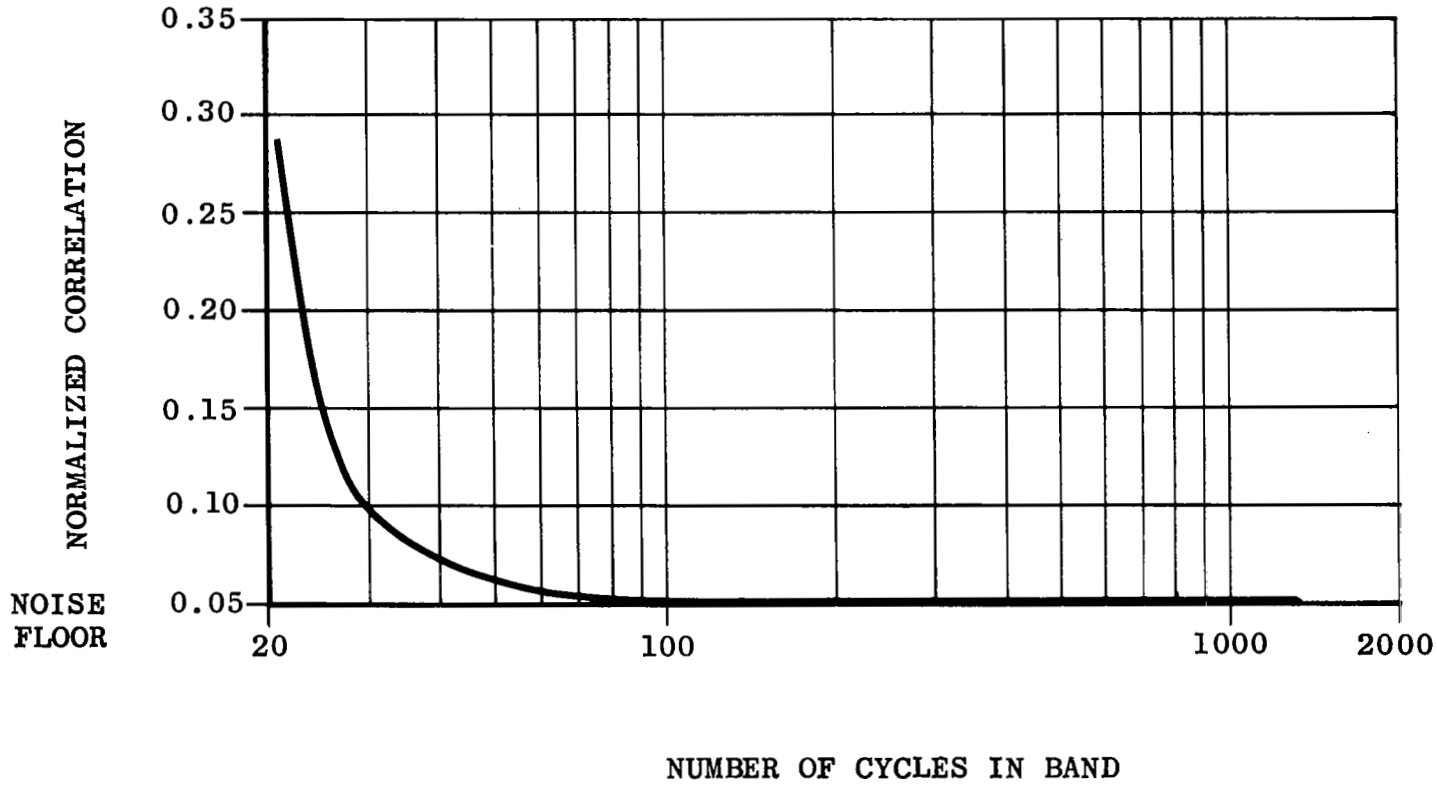

Figure 37. Effect of Filtering Uncorrelated Data for Cross-Correlation Calculations